**UNIVERSITÉ DU QUÉBEC À CHICOUTIMI**

THÈSE PRÉSENTÉE COMME EXIGENCE PARTIELLE
DU
DOCTORAT EN INGÉNIERIE

Par

**Jogendra Singh Thongam**

# Commande de haute performance sans capteur d'une machine asynchrone

**Juin 2006**

Bibliothèque Paul-Émile-Boulet

UQAC Université du Québec à Chicoutimi

# ***Mise en garde/Advice***

Afin de rendre accessible au plus grand nombre le résultat des travaux de recherche menés par ses étudiants gradués et dans l'esprit des règles qui régissent le dépôt et la diffusion des mémoires et thèses produits dans cette Institution, **l'Université du Québec à Chicoutimi (UQAC)** est fière de rendre accessible une version complète et gratuite de cette œuvre.

Motivated by a desire to make the results of its graduate students' research accessible to all, and in accordance with the rules governing the acceptation and diffusion of dissertations and theses in this Institution, the **Université du Québec à Chicoutimi (UQAC)** is proud to make a complete version of this work available at no cost to the reader.

L'auteur conserve néanmoins la propriété du droit d'auteur qui protège ce mémoire ou cette thèse. Ni le mémoire ou la thèse ni des extraits substantiels de ceux-ci ne peuvent être imprimés ou autrement reproduits sans son autorisation.

The author retains ownership of the copyright of this dissertation or thesis. Neither the dissertation or thesis, nor substantial extracts from it, may be printed or otherwise reproduced without the author's permission.

**THE UNIVERSITY OF QUEBEC AT CHICOUTIMI**

A THESIS SUBMITTED IN PARTIAL FULFILMENT OF
THE REQUIREMENTS FOR THE DEGREE
OF
DOCTOR OF PHYLOSOPHY

By

**Jogendra Singh Thongam**

# High Performance Sensorless Induction Motor Drive

**June 2006**

## Abstract

Induction machine, when driven by a field oriented controller behaves like a separately excited dc machine, where torque and flux are naturally decoupled and are controlled independently; and this control strategy allows high performance to be achieved from it. However, conventional vector controlled induction motor drive has the disadvantage of requiring speed sensor which increases the cost and complexity of the drive system. Moreover, drive performance is affected by rotor resistance, whose unknown variation during the operation causes incorrect decoupling of flux and torque which leads to deterioration of drive performance. This thesis focusses on the development of a high performance sensorless induction motor drive. Control of the drive is done in rotor flux coordinates which allows natural decoupling of flux and torque producing components of stator current space vector. Sensorless control of the drive system is achieved by developing rotor flux and speed estimation algorithms using only the measurable stator terminal quantities: the current and voltage. The state and parameter estimation problem is looked into as a question of proper mathematical modeling of the machine in an appropriate reference frame, which along with proper choice of states, enables us to develop an estimation algorithm capable of accurate estimation.

In this work a two pronged approach is adopted to achieve the research objective. First approach is based on the fact that dynamics of rotor speed is much slower than that of electrical states of the machine. Hence, the time derivative of rotor speed can be conveniently equated to zero in the machine model used for implementing the estimation

algorithm. To this end, a new quantity, which is a function of rotor flux and speed is defined, introducing which a new motor model is derived. First of all, a novel speed estimation algorithm for indirect vector controlled induction motor drive is developed based on observing the newly defined quantity mentioned above. This algorithm uses rotor flux obtained from the reference flux for speed computation. However, the speed estimation accuracy decreases as speed decreases. To overcome this problem, a rotor flux observer, based on the voltage model of the machine is used along with the observer of the new quantity and satisfactory results are obtained. Finally, a new rotor flux estimation algorithm for speed sensorless induction motor drive is developed based on a modified Blaschke equation and on observing the newly defined quantity mentioned above.

In the second approach, the mathematical model of the machine used for developing estimation algorithm takes into account the coupling between the mechanical and the electric modes of the drive, which is true for small sized machines. Speed and rotor resistance are estimated simultaneously using a reduced order Kalman filter without injecting any external signal. Satisfactory results are obtained during both transient and steady state conditions. The simultaneous estimation of speed and rotor resistance was considered impossible for a long time by many researchers working in the area of drive control. Therefore, what has been achieved in this work constitutes a major contribution to the domain of variable speed induction motor drive.

# Résumé

Une machine asynchrone pilotée par un contrôleur vectoriel se comporte comme une machine à courant continu à excitation séparée, où le couple et le flux sont découplés et contrôlés indépendamment, permettant ainsi d'obtenir une bonne précision de régulation et de hautes performances dynamiques. Cependant, la commande vectorielle présente l'inconvénient de nécessiter l'emploi d'un capteur de vitesse; ce qui impose un surcoût et augmente la complexité des montages. De plus cette commande fait intervenir la résistance du rotor, et la variation de ce paramètre pourrait fausser le découplage entre le flux et le couple et, par le fait même, entraînerait la détérioration des performances.

L'objectif de cette thèse est la mise en oeuvre d'une commande de haute performance et sans capteur pour une machine asynchrone. La commande est réalisée dans un système de coordonnées lié au vecteur flux rotorique. Pour un fonctionnement sans capteur, la vitesse et le flux rotorique sont estimés à partir seulement des grandeurs statoriques mesurables : courants et tensions. Le problème de l'estimation simultanée des états et des paramètres est résolu en recourant à un modèle mathématique de la machine établi dans un référentiel approprié. Ceci nous a permis de mettre en œuvre un algorithme inédit d'estimation capable d'obtenir des estimés exacts.

Pour l'atteinte des objectifs recherchés, deux approches ont été utilisées. La première est basée sur le fait que la dynamique du mode mécanique est beaucoup moins rapide que celle des modes électriques. En d'autres termes, la vitesse mécanique varie beaucoup moins vite que les états électriques de la machine. Le taux de variation de la vitesse peut

donc être considéré nul lors de l'élaboration du modèle de la machine utilisé pour la mise en œuvre de l'algorithme d'estimation. Ceci a permis d'obtenir une nouvelle variable qui est fonction du flux rotorique et de la vitesse de rotation et une nouvelle formulation des équations régissant le fonctionnement de la machine. Tout d'abord, nous avons mis au point un algorithme d'estimation de la vitesse pour un contrôleur vectoriel indirect en observant la nouvelle variable ci-haut mentionnée et en utilisant la commande de flux. Il s'est avéré que les résultats ne sont pas satisfaisants dans le domaine des vitesses réduites. Pour palier à ce problème, nous avons utilisé, conjointement avec l'observateur de la nouvelle variable, un estimateur de flux établi à partir du modèle tension de la machine; et les résultats obtenus sont très concluants. Finalement, nous avons mis au point un autre estimateur inédit de le flux en utilisant une nouvelle formulation des équations de Blaschke conjointement avec l'observateur de la nouvelle variable.

La deuxième approche tient compte du couplage entre le mode mécanique et les modes électriques; ce qui est en réalité vrai pour les machines de petites puissances. La vitesse de rotation et la résistance du rotor sont estimées simultanément, sans l'injection d'aucun signal externe, en utilisant le filtre de Kalman d'ordre réduit. Les résultats obtenus s'avèrent très satisfaisants tant en régime transitoire qu'en régime permanent. L'estimation simultanée de la vitesse et de la résistance du rotor a longtemps été considérée impossible par plusieurs chercheurs oeuvrant dans le domaine des entraînements régulés. Ce que nous avons réalisé constitue donc une contribution majeure au domaine des entraînements à vitesse variable par machines asynchrones.

## Acknowledgements

I would like to express my sincere thanks to my supervisor, Professor Mohand A. Ouhrouche for his invaluable guidance and support during each stage of my doctoral research. I also would like to express my appreciation to all my collegues in the EMIC Lab for their cooperation and encouragements. Finally, I would like to record my deep gratitude to my family members for their consistent encouragement, support and understanding throughout the years of my PhD study.

# Table of Contents

## List of Symbols and Abbreviations

**Bold** typeface is used for representing quantities in matrix form.

| | | |
|---|---|---|
| $\boldsymbol{A}$ | system matrix | |
| $\boldsymbol{B}$ | input matrix | |
| $\boldsymbol{C}$ | output matrix | |
| F | damping coefficient | N.m.s |
| $f$ | stator frequency | Hz |
| $\boldsymbol{G}$ | Gopinath's observer gain matrix | |
| $I, i, \boldsymbol{i}$ | current | A |
| $j$ | $\sqrt{-1}$ | |
| $\Im$ | imaginary part of a complex number | |
| $J$ | inertia | $Kg.m^2$ |
| k | discrete time step | |
| $\boldsymbol{K}$ | Kalman gain matrix | |
| $K_b$ | fan/blower or centrifugal pump load constant | $N.m.s^2/rad^2$ |
| $K_v$ | viscous friction constant | N.m.s/rad |
| $L$ | inductance | H |
| $p$ | number of pole pairs | |
| $R$ | resistance | Ω |
| $s$ | per unit slip | |
| $s$ | Laplace operator | |

| | | |
|---|---|---|
| $T_{em}$ | torque | N.m |
| $T$ | sampling period | s |
| $V, v, \boldsymbol{v}$ | voltage | V |
| $\boldsymbol{x}$ | state vector | |
| $\boldsymbol{y}$ | output vector | |
| $\boldsymbol{Z}$ | a newly defined quantity | |
| $\rho, \varepsilon, \xi, \theta$ | angle of rotor flux, rotor, stator current and arbitrary reference frame | rad |
| $\omega_e, \omega, \omega_{sl}$ | synchronous, rotor and slip frequency | rad/s |
| $\omega_m$ | mechanical rotor speed | rad/s |
| $\psi, \boldsymbol{\psi}, \boldsymbol{\Psi}$ | flux | Wb |
| $\sigma$ | leakage factor | |
| $\tau$ | time constant | s |

**Subscripts**

| | |
|---|---|
| *a, b, c* | three-phase parameters |
| *d, q* | direct and quadrature components |
| *L* | load parameter |
| *l* | leakage |
| *m* | magnetizing |

| | |
|---|---|
| $r$ | rotor |
| $s$ | stator |
| $\alpha$, $\beta$ | components of stationary stator reference frame |

**Superscripts**

| | |
|---|---|
| c | conjugate of a complex vector |
| * | reference |
| $T$ | transpose |
| s | stationary frame |
| ^ | estimated quantity |
| ~ | error |
| → | space vector |

**Abbreviations**

| | |
|---|---|
| DSP | digital signal processor |
| DTC | direct torque control |
| EKF | extended kalman filter |
| FLC | feedback linearized control |
| FOC | field oriented control |
| MRAS | model reference adaptive system |
| VC | vector control |

# List of Figures

# List of Tables

# CHAPTER 1

# INTRODUCTION

## 1.1 Background

Induction machine, a work horse of industry was traditionally used in fixed speed applications because it represents a highly nonlinear, interacting, multivariable control plant requiring complex control algorithms. Consequently, when variable speed was required, dc machine appeared to be the appropriate electromechanical device where torque and flux are naturally decoupled and can be controlled independently. With the advancement of power electronics and Digital Signal Processor (DSP) technology, advanced control techniques for induction machine which were once thought impractical can now be implemented in real-time. Induction machines offer many advantages over other machines. They are more rugged, compact, cheap and reliable in comparison to other machines used in similar applications. It is due to this reason that they can be found in a wide range of the industrial drive applications. Field oriented control (FOC) or Vector control (VC) proposed by Blaschke [1] and Hasse [2] has become an industry standard for control of induction machines in high performance drive applications. Control of induction motor using the principle of field orientation gives control characteristics similar to that of a separately

excited dc machine. Orientation is possible along mutual flux or stator flux or the rotor flux; however, orientation of the stator current space vector with respect to the rotor flux alone gives natural decoupling between the torque and flux producing components of the stator current space vector. VC induction motor drive outperforms the dc drive because of higher transient current capability, increased speed range and lower rotor inertia. It is due to this reason that modern high performance drive application is moving towards using induction machine as the drive element.

## 1.2 Research Problem

Sensors widely used in electric drives degrade the reliability of the system especially in hostile environments and require special attention to electrical noise. Moreover, it is difficult to mount sensors in certain applications in addition to extra expenses involved. Therefore, a lot of researches are underway to develop accurate speed estimation techniques. With sensorless vector control we have a decoupled control structure similar to that of a separately excited dc motor retaining the inherent ruggedness of the induction motor at the same time. Speed sensorless control technique first appeared in 1975 [3]. Several review and comparison papers are available on sensorless control techniques [4-7]. The commonly used methods for speed estimation are Model Reference Adaptive System (MRAS) [8-11], Neural Networks [12-19], Extended Kalman Filter (EKF) [20-25] and Nonlinear Observer [26-29]. Techniques for high performance induction motor control implementation require

precise knowledge of machine parameters, and the rotor resistance being the most important of them. The commonly used methods for rotor resistance or rotor time constant estimation are MRAS [30-32], EKF [33-38] and Neural Networks [39-42]. Further, a high performance sensorless induction motor drive requires speed estimation in addition to estimating machine parameters most important of which is the rotor resistance which varies during the operation of the motor. Very few works have been reported on simultaneous estimation of speed and rotor resistance [43-47].

## 1.3 Objective

The objective of this doctoral research is to realize a high performance sensorless vector controlled induction motor drive. This drive system should not require a mechanical speed sensor and is desired to be robust against rotor resistance variation. The estimation algorithm is desired to be capable of simultaneous estimation of speed and rotor resistance under both transient and steady state conditions without requiring any external signal to be injected if possible.

## 1.4 Methodology

In this thesis, the state and parameter estimation of induction machine is looked into as a question of proper mathematical modeling of the machine in an appropriate reference frame

and with proper choice of states. This allows development of accurate estimation algorithm.

The fact that the rotor resistance dynamics is much slower than that of speed and electrical states of the machine is exploited while developing estimation algorithm in some parts of the thesis. Assumption is made in some parts of the work that rotor speed dynamics is much slower than that of electrical states.

The performance of the whole vector controlled drive systems incorporating the estimation algorithms are verified using SIMULINK. Finally, real-time digital simulations are carried out in order to ascertain the performance of the developed schemes.

### 1.5 Overview of the Thesis

This thesis is presented in seven chapters. After introduction in Chapter1, and a general discussion on the induction machine model in Chapter 2, a brief account of commonly used induction motor drive control methods are given in Chapter 3. In Chapter 4 a new induction machine model is derived after introducing a newly defined quantity. Sensorless control of induction motor drives presented in this chapter are achieved by developing new rotor flux and speed estimation algorithms based on observing the newly defined quantity.

A new Sensorless induction motor drive robust against rotor resistance variation is presented in Chapter 5 where simultaneous estimation of speed and rotor resistance is discussed. The simultaneous estimation presented in this thesis is achieved without injecting

any external signal. Chapter 6 presents results of real-time digital simulation. Finally, conclusion and scope for future work is given in Chapter 7.

# CHAPTER 2

# INDUCTION MACHINE MODELLING

## 2.1 Introduction

In this chapter, the induction motor modeling is discussed. The chapter starts with the introduction of the reference frames. Then, the co-ordinate transformations (Clarke and Park Transformations) are introduced. An induction machine model based on an induction machine equivalent circuit in a synchronously rotating arbitrary reference frame *d-q* is presented. Then, machine model in stationary stator reference frame $\alpha - \beta$ is given.

## 2.2 Reference Frames

Modelling of induction motor is the first and essential step for its identification and control. The mathematical model of the machine should on one hand have such a structure so as to completely describe the characteristics of the machine and on the other hand be convenient to use it for implementing estimation algorithms.

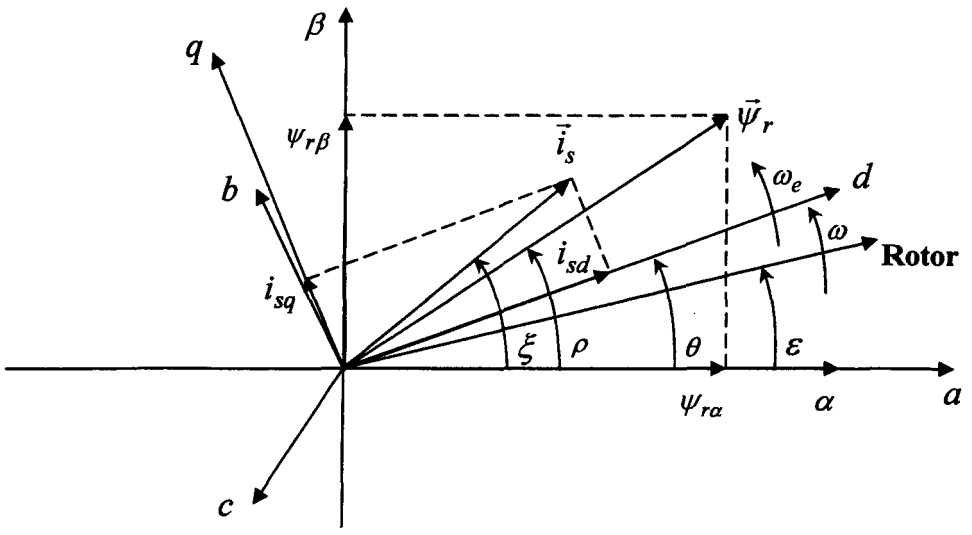


**Figure 2.1** Reference frames and representation of stator current and rotor flux as space vectors.

In the development of an induction machine model, a three-phase machine with symmetrical windings is assumed. Figure 2.1 shows the reference frames and representation of stator current and rotor flux as space vectors. In the figure, a, b and c are respectively the axes of the stator winding a, b and c. $\alpha-\beta$ axis is the axis of the fixed stator reference frame, where $\alpha$ has been considered to be coincident with stator winding axis 'a'. *d-q* is an arbitrary reference frame rotating with a speed $\omega_e$.

## 2.3 Clarke Transformation

The transformation from three-phase stationary reference frame *a-b-c* into two-phase arbitrary stationary reference frame *d-q* (i.e. for $\omega_e = 0$) commonly known as Clarke Transformation is given as:

$$\begin{bmatrix} i_{sd}^s \\ i_{sq}^s \end{bmatrix} = k \begin{bmatrix} \cos(\theta) & \cos\left(\theta - \frac{2\pi}{3}\right) & \cos\left(\theta + \frac{2\pi}{3}\right) \\ -\sin(\theta) & -\sin\left(\theta - \frac{2\pi}{3}\right) & -\sin\left(\theta + \frac{2\pi}{3}\right) \end{bmatrix} \begin{bmatrix} i_{sa} \\ i_{sb} \\ i_{sc} \end{bmatrix} \tag{2.1}$$

where the scaling factor $k$ depends upon the convention used. For power invariant form $k = \sqrt{\frac{2}{3}}$, and for the classical non-power-invariant form $k = \frac{2}{3}$.

The reverse transformation from 2-phase to 3-phase (reverse Clark Transformation) is given below:

$$\begin{bmatrix} i_{sa} \\ i_{sb} \\ i_{sc} \end{bmatrix} = \sqrt{\frac{2}{3}} \begin{bmatrix} \cos(\theta) & -\sin(\theta) \\ \cos\left(\theta - \frac{2\pi}{3}\right) & -\sin\left(\theta - \frac{2\pi}{3}\right) \\ \cos\left(\theta + \frac{2\pi}{3}\right) & -\sin\left(\theta + \frac{2\pi}{3}\right) \end{bmatrix} \begin{bmatrix} i_{sd}^s \\ i_{sq}^s \end{bmatrix} \tag{2.2}$$

We have considered current as the variable. The voltage and flux linkages can also be transformed by similar equations. Assuming that *d-axis* is aligned with the *a-axis* then the transformation simplifies to

$$\begin{bmatrix} i_{s\alpha} \\ i_{s\beta} \end{bmatrix} = k \begin{bmatrix} 1 & -\frac{1}{2} & -\frac{1}{2} \\ 0 & \frac{\sqrt{3}}{2} & -\frac{\sqrt{3}}{2} \end{bmatrix} \begin{bmatrix} i_{sa} \\ i_{sb} \\ i_{sc} \end{bmatrix} \tag{2.3}$$

$$\text{and} \begin{bmatrix} i_{sa} \\ i_{sb} \\ i_{sc} \end{bmatrix} = \begin{bmatrix} 1 & 0 \\ -\frac{1}{2} & \frac{\sqrt{3}}{2} \\ -\frac{1}{2} & -\frac{\sqrt{3}}{2} \end{bmatrix} \begin{bmatrix} i_{s\alpha} \\ i_{s\beta} \end{bmatrix} \tag{2.4}$$

$$\text{here} \begin{bmatrix} i_{sd}^{s} \\ i_{sq}^{s} \end{bmatrix} = \begin{bmatrix} i_{s\alpha} \\ i_{s\beta} \end{bmatrix}$$

## 2.4 Park Transformation

The conversion from the *a-b-c* frame to the fixed frame $\alpha - \beta$ gives values in a stationary reference frame fixed to the stator. It is often useful to model the machine in an alternative reference frame, usually rotating at synchronous speed. The transformation from the stationary frame to any frame *d-q* rotating at an angular speed $\omega_e$, also known as the Park Transformation is given as [48]:

$$\begin{bmatrix} i_{sd} \\ i_{sq} \end{bmatrix} = \begin{bmatrix} \cos\theta & \sin\theta \\ -\sin\theta & \cos\theta \end{bmatrix} \begin{bmatrix} i_{s\alpha} \\ i_{s\beta} \end{bmatrix} \tag{2.5}$$

where $\theta$ is the angle between the arbitrary synchronously rotating reference frame $d$-axis and the stationary frame $\alpha$-axis. The reverse transformation from the synchronous frame to the stationary frame (reverse Park Transformation) is given by

$$\begin{bmatrix} i_{s\alpha} \\ i_{s\beta} \end{bmatrix} = \begin{bmatrix} \cos\theta & -\sin\theta \\ \sin\theta & \cos\theta \end{bmatrix} \begin{bmatrix} i_{sd} \\ i_{sq} \end{bmatrix} \tag{2.6}$$

## 2.5 Space Vector Representation of Induction Machine

Space vector representation of induction machine is given in this section. The machine model is represented in a rotating as well as fixed reference frames.

### 2.5.1 Induction Machine Model in Rotating Reference Frame

The induction motor model in an arbitrary reference frame $d$-$q$, rotating with a synchronous speed $\omega_e$ using complex vector notation is given as [49]:

$$\vec{v}_s e^{-j\theta} = R_s \vec{i}_s e^{-j\theta} + \frac{d\vec{\psi}_s e^{-j\theta}}{dt} + j\omega_e \vec{\psi}_s e^{-j\theta} \tag{2.7}$$

$$0 = R_r \vec{i}_r e^{j(\varepsilon-\theta)} + \frac{d\vec{\psi}_r e^{j(\varepsilon-\theta)}}{dt} + j(\omega_e - \omega)\vec{\psi}_r e^{j(\varepsilon-\theta)} \tag{2.8}$$

where $\vec{v}_s$, $\vec{i}_s$ and $\vec{\psi}_s$ are respectively the stator voltage, current and flux space vectors in stator reference frame; and $\vec{i}_r$ and $\vec{\psi}_r$ are respectively the rotor current and flux in rotor reference frame. The stator and rotor fluxes are given below:

$$\vec{\psi}_s e^{-j\theta} = L_s \vec{i}_s e^{-j\theta} + L_m \vec{i}_r e^{j(\varepsilon-\theta)} \tag{2.9}$$

$$\vec{\psi}_r e^{j(\varepsilon-\theta)} = L_r \vec{i}_r e^{j(\varepsilon-\theta)} + L_m \vec{i}_s e^{-j\theta} \tag{2.10}$$

The electromechanical equation is given by

$$J\frac{d\omega}{dt} = pT_{em} - pT_L - F\omega \tag{2.11}$$

The electromagnetic torque is given by

$$T_{em} = \frac{3}{2} pL_m \Im\left[\vec{i}_s e^{-j\theta}\left(\vec{i}_r e^{j(\varepsilon-\theta)}\right)^{\mathbb{C}}\right] \tag{2.12}$$

The imaginary part of the bracket is equivalent to the vector products of the two currents. The equation of electromagnetic torque can also be given by

$$T_{em} = \frac{3}{2} p\left[\left(\vec{\psi}_s e^{-j\theta}\right) \times \left(\vec{i}_s e^{-j\theta}\right)\right] = \frac{3}{2} p \frac{L_m}{L_r}\left[\left(\vec{\psi}_r e^{j(\varepsilon-\theta)}\right) \times \left(\vec{i}_s e^{-j\theta}\right)\right] \qquad (2.13)$$

### 2.5.2 Induction Machine Model in Fixed Stator Reference Frame

Equating $\theta$ and $\omega_e$ to zero we get the motor model in stationary stator reference frame $\alpha - \beta$ as given below:

$$\vec{v}_s = R_s \vec{i}_s + \frac{d\vec{\psi}_s}{dt} \qquad (2.14)$$

$$0 = R_r \vec{i}_r e^{j\varepsilon} + \frac{d\vec{\psi}_r e^{j\varepsilon}}{dt} - j\omega \vec{\psi}_r e^{j\varepsilon} \qquad (2.15)$$

The electromechanical equation is given by

$$J\frac{d\omega}{dt} = pT_e - pT_L - F\omega = \frac{3}{2} p^2 L_m \Im\left[\vec{i}_s \left(\vec{i}_r e^{j\varepsilon}\right)^{\mathbb{C}}\right] - pT_L - F\omega$$

$$= \frac{3}{2} p^2 \left[\vec{\psi}_s \times \vec{i}_s\right] - pT_L - F\omega = \frac{3}{2} p^2 \frac{L_m}{L_r}\left[\left(\vec{\psi}_r e^{j\varepsilon}\right) \times \vec{i}_s\right] - pT_L - F\omega \qquad (2.16)$$

## 2.6 Two-phase Induction Machine Model

Two-phase representation of three-phase induction machine is very useful in designing control and estimation algorithms. In the following sections two-phase models of the machine in rotating and fixed reference frames are discussed.

### 2.6.1 Two-phase Machine Model in Rotating Reference Frame

The induction motor model in an arbitrary reference frame *d-q* rotating with a speed $\omega_e$ can be obtained from (2.7)-(2.8) as

$$v_{sd} = R_s i_{sd} + \frac{d}{dt}\psi_{sd} - \omega_e \psi_{sq} \tag{2.17}$$

$$v_{sq} = R_s i_{sq} + \frac{d}{dt}\psi_{sq} + \omega_e \psi_{sd} \tag{2.18}$$

$$0 = R_r i_{rd} + \frac{d}{dt}\psi_{rd} - (\omega_e - \omega)\psi_{rq} \tag{2.19}$$

$$0 = R_r i_{rq} + \frac{d}{dt}\psi_{rq} + (\omega_e - \omega)\psi_{rd} \tag{2.20}$$

where $\vec{v}_s e^{-j\theta} = v_{sd} + jv_{sq}$, $\vec{\psi}_s e^{-j\theta} = \psi_{sd} + j\psi_{sq}$, $\vec{i}_r e^{j(\varepsilon-\theta)} = i_{rd} + ji_{rq}$ and $\vec{\psi}_r e^{j(\varepsilon-\theta)} = \psi_{rd} + j\psi_{rq}$.

The equivalent circuits of the machine in the arbitrary rotating reference frame *d-q* are shown in Figure 2.2 [50].

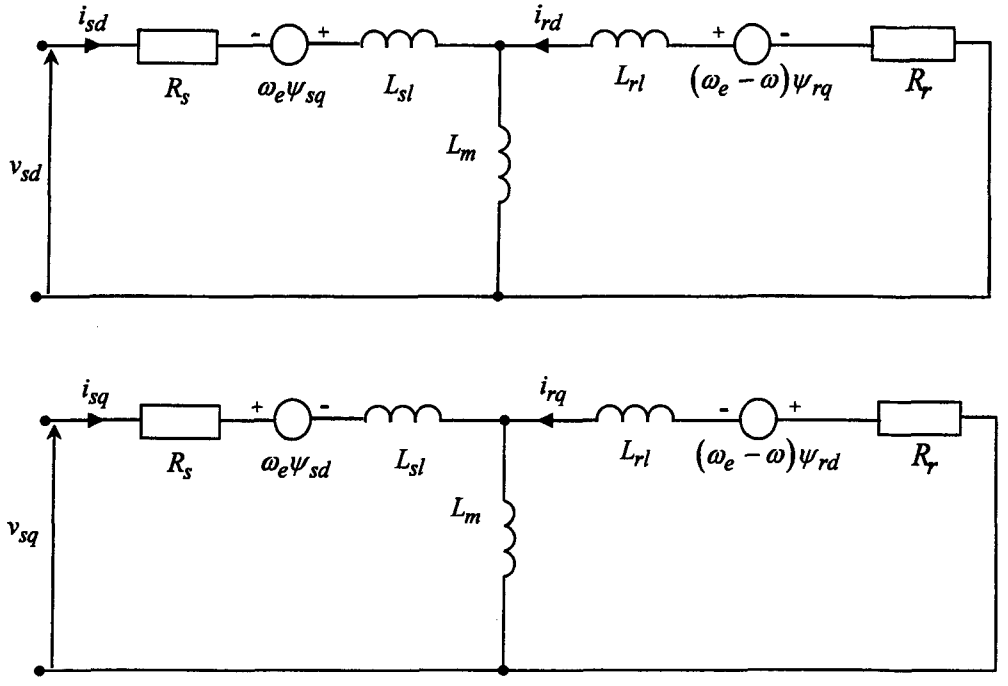


**Figure 2.2** Equivalent circuit of Induction Machine in *d-q* reference frame

Eliminating the stator flux and rotor current and introducing the electro-mechanical equation of drive, the model of induction machine drive in *d-q* reference frame may be written as given by equation (2.21).

$$\frac{d}{dt}\begin{bmatrix} i_{sd} \\ i_{sq} \\ \psi_{rd} \\ \psi_{rq} \\ \omega \end{bmatrix} = \begin{bmatrix} -\left(\frac{R_s}{\sigma L_s}+\frac{1-\sigma}{\sigma\tau_r}\right)i_{sd} + \omega_e i_{sq} + \frac{L_m}{\sigma L_s L_r \tau_r}\psi_{rd} + \frac{L_m\omega}{\sigma L_s L_r}\psi_{rq} \\ -\omega_e i_{sd} - \left(\frac{R_s}{\sigma L_s}+\frac{1-\sigma}{\sigma\tau_r}\right)i_{sq} - \frac{L_m\omega}{\sigma L_s L_r}\psi_{rd} + \frac{L_m}{\sigma L_s L_r \tau_r}\psi_{rq} \\ \frac{L_m}{\tau_r}i_{sd} - \frac{1}{\tau_r}\psi_{rd} + (\omega_e-\omega)\psi_{rq} \\ \frac{L_m}{\tau_r}i_{sq} - (\omega_e-\omega)\psi_{rd} - \frac{1}{\tau_r}\psi_{rq} \\ \frac{3p^2 L_m}{2JL_r}\left(i_{sq}\psi_{rd} - i_{sd}\psi_{rq}\right) - \frac{F}{J}\omega - \frac{p}{J}T_l \end{bmatrix} + \begin{bmatrix} \frac{1}{\sigma L_s}v_{sd} \\ \frac{1}{\sigma L_s}v_{sq} \\ 0 \\ 0 \\ 0 \end{bmatrix} \quad (2.21)$$

where $\sigma = \left(1 - L_m^2 / L_s L_r\right)$ is the leakage coefficient.

### 2.6.2 Two-phase Machine Model in Fixed Stator Reference Frame

The induction motor drive model in stationary stator reference frame $\alpha - \beta$, can be obtained by equating $\omega_e$ to zero as given below:

$$\frac{d}{dt}\begin{bmatrix} i_{s\alpha} \\ i_{s\beta} \\ \psi_{r\alpha} \\ \psi_{r\beta} \\ \omega \end{bmatrix} = \begin{bmatrix} -\left(\frac{R_s}{\sigma L_s}+\frac{R_r(1-\sigma)}{\sigma L_r}\right)i_{s\alpha} + \frac{R_r L_m}{\sigma L_s L_r^2}\psi_{r\alpha} + \frac{L_m\omega}{\sigma L_s L_r}\psi_{r\beta} \\ -\left(\frac{R_s}{\sigma L_s}+\frac{R_r(1-\sigma)}{\sigma L_r}\right)i_{s\beta} - \frac{L_m\omega}{\sigma L_s L_r}\psi_{r\alpha} + \frac{R_r L_m}{\sigma L_s L_r^2}\psi_{r\beta} \\ \frac{R_r L_m}{L_r}i_{s\alpha} - \frac{R_r}{L_r}\psi_{r\alpha} - \omega\psi_{r\beta} \\ \frac{R_r L_m}{L_r}i_{s\beta} + \omega\psi_{r\alpha} - \frac{R_r}{L_r}\psi_{r\beta} \\ \frac{3p^2 L_m}{2JL_r}\left(i_{s\beta}\psi_{r\alpha} - i_{s\alpha}\psi_{r\beta}\right) - \frac{F}{J}\omega - \frac{p}{J}T_l \end{bmatrix} + \frac{1}{\sigma L_s}\begin{bmatrix} v_{s\alpha} \\ v_{s\beta} \\ 0 \\ 0 \\ 0 \end{bmatrix} \quad (2\text{-}22)$$

## 2.7 Conclusion

Modeling of induction motor is the first and essential step for its identification and control. The mathematical model of the machine should on one hand have such a structure so as to completely describe the characteristics of the machine and on the other hand be convenient to use it for implementing estimation algorithms. In this chapter, the induction motor modeling is discussed. The chapter starts with the introduction of the reference frames. Then, the co-ordinate transformations (Clarke and Park Transformations) are introduced. An induction machine model based on an induction machine equivalent circuit in a synchronously rotating arbitrary reference frame *d-q* is presented. Then, machine model in stationary stator reference frame $\alpha - \beta$ is derived.

# CHAPTER 3

# INDUCTION MOTOR CONTROL

## 3.1 Introduction

Induction machine occupies an important position in industry due to its various advantages over other machines as regards to price, size, robustness etc. However, it was traditionally used in fixed speed applications because it represents a highly nonlinear, interacting, multivariable control plant requiring complex control algorithms. It is essentially a constant-speed machine as long as it is connected to a constant voltage and constant frequency power supply. In this case the operating speed is very close to the synchronous speed, and changes in the torque makes small changes in the speed. It is suitable for use in constant-speed drive systems, while for variable speed applications the controllers used are more complicated than the traditional dc motor speed controllers. However, with the advancement of power electronics and digital signal processing technology advanced control techniques for induction motor which were once thought to be impractical can now be implemented easily. There are various methods for controlling the speed of an induction machine. Some of the important methods are briefly discussed in this chapter.

### 3.2 Induction Motor Control Techniques

The speed of induction machine can be defined as

$$\omega = (1\text{-s})\,\omega_e \tag{3.1}$$

where $\omega_e$ is the synchronous angular speed and $s = \frac{\omega_e - \omega}{\omega_e}$ is the slip.

In the past, according to equation (3.1), there were two general categories of induction machine control methods. One is to change the slip; the second is to change the synchronous angular frequency. However, the control techniques based on changing slip or synchronous angular frequency are suitable only for limited speed range applications [51-52]. The advent of static power converters has allowed the use of more sophisticated control techniques which allow operation of induction machine over a wide speed range in all four quadrants [50]. The following section describes some of the commonly used control techniques.

#### 3.2.1 Scalar Control

Scalar control is based on the steady state model of the machine. The control is due to the magnitude variation of the control variables only, and disregards the coupling effect in the machine. For example, the voltage of a machine can be controlled to control the flux, and frequency or slip can be controlled to control torque. However, flux and torque are also

functions of frequency and voltage respectively. This method is simple and robust; however, it has poor dynamic performance.

Under steady state condition the machine equation is as given below:

$$\vec{v}_s = R_s\vec{i}_s + j\omega_e\vec{\psi}_s \tag{3.2}$$

$$0 = R_r\vec{i}_r + j(\omega_e - \omega)\vec{\psi}_r \tag{3.3}$$

From (3.3) we have

$$\vec{\psi}_r = j\frac{R_r}{s\omega_e}\vec{i}_r \tag{3.4}$$

$$\text{or,}\quad \vec{i}_r = -j\frac{s\omega_e}{R_r}\vec{\psi}_r \tag{3.5}$$

From (2.10) we have

$$\vec{i}_s e^{-j\theta} = \frac{\vec{\psi}_r e^{j(\varepsilon-\theta)}}{L_m} - \frac{L_r}{L_m}\vec{i}_r e^{j(\varepsilon-\theta)} \tag{3.6}$$

The electromagnetic torque is given by

$$T_{em} = \frac{3pL_m}{2L_r}\left(\vec{\psi}_r e^{j(\varepsilon-\theta)}\right)\times\left(\vec{i}_s e^{-j\theta}\right) \tag{3.7}$$

Substituting the stator current in (3.7) with that of (3.6), we have

$$T_{em} = -\frac{3p}{2}\left(\vec{\psi}_r e^{j(\varepsilon-\theta)}\right)\times\left(\vec{i}_r e^{j(\varepsilon-\theta)}\right) \tag{3.8}$$

Replacing the rotor current with that in (3.5) we have

$$T_{em} = \frac{3ps\omega_e}{2R_r}{\psi_r}^2 \tag{3.9}$$

Equation (3.9) shows that at constant flux the torque is proportional to the slip, or at constant slip the electromagnetic torque is proportional to square of the flux. Two commonly used scalar control methods are discussed in this section.

#### 3.2.1.1 Volts/Hertz Control

A simple and common open-loop volts/hertz speed control method for an induction motor is shown in Figure 3.1. In this controller, the scalar quantities which are controlled

are the magnitude of the applied voltage and its frequency. The scheme is defined as the volts/hertz control because the voltage command $V_s^*$ is generated directly from the frequency command through a *V/f* function generator.

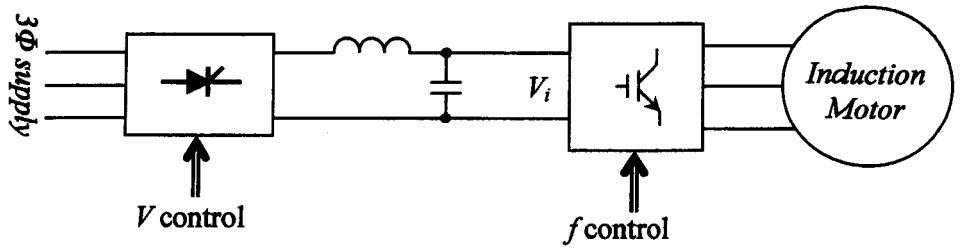


**Figure 3.1** Open-loop Voltage & Frequency Controller

Figure 3.1 shows the block diagram of an open-loop speed controller in which the supply frequency of the induction motor is varied. In order to achieve maximum torque sensitivity to rotor speed ($T\alpha|\psi_m|^2\,\omega_{sl}$), it is necessary to maintain rated air gap flux. In steady state, air gap flux can be given as [50]:

$$j\omega_e\psi_m = V_s - I_s(R_s + j\omega_e L_{\sigma s}) \tag{3.10}$$

At higher frequencies the stator voltage drop is negligible and the air gap flux can be approximated as:

$$j\omega_e \psi_m = V_s \tag{3.11}$$

Thus, in order to maintain a constant air gap flux the ratio of applied voltage to frequency must be constant. As the approximation is valid only at high frequencies (above 25% rated), the stator voltage drop will become significant and both flux and torque will be reduced at low frequencies. Therefore, an extra boost voltage $V_{boost}$ is added to the command voltage in order to make rated air gap flux and full torque available down to zero speed. However, at speeds higher than the base value *V/f* reduces as voltage remain constant at rated value while frequency increases which causes flux to reduce. The machine is said to be operating in the field weakening region.

With open-loop voltage control, the ac line voltage fluctuation and impedance drop will cause fluctuation in the air gap flux. This fluctuation can be prevented by providing closed-loop voltage control. With open-loop speed control, if the load torque is increased, the slip will increased within the stability limit and a balance will be maintained between the developed torque and the load torque. However, the rotor speed will tend to drift with the variation in load torque. If the open-loop speed drift is not allowable a closed-loop speed control can be provided. The speed loop error signal provides the frequency command.

During steady state operation, if the command frequency is step increased, the slip will exceed that of breakdown torque and the machine will become unstable. Similar instability will occur if the frequency is step decreased. This problem can be overcome with slip regulation which ensures that the slip frequency doesn't exceed the breakdown torque. In this control scheme, the error of the speed control loop generates the slip command through

a proportional-integral (PI) controller and limiter. The slip is added with the speed signal to generate the frequency command. The frequency command also generates the voltage command through a volts/hertz function generator which incorporates the low-frequency stator drop compensation. Since the slip is proportional to developed torque, the scheme can be considered as torque control within a speed control loop. The control is shown in Figure 3.2. With a step speed command, the machine accelerates freely with a slip limit that corresponds to maximum torque and then settles down to the slip value at steady state dictated by the load torque.

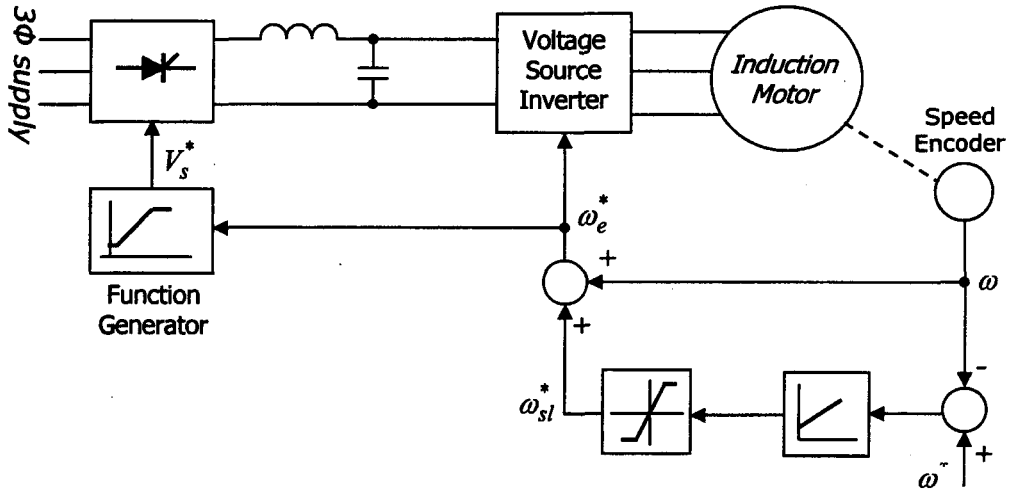


**Figure 3.2** Close loop speed control with volts/hertz control and slip regulation

The problem can be overcome by introducing a current limit control into the *V/f* scheme, which controls the rate of increase of frequency such that the machine current is not exceeded. The volts/hertz control scheme has the disadvantage that air gap flux may drift,

and as a result the torque sensitivity with slip or stator current will vary and cause lower operating frequency. In order to obtain better control of flux, a volts/hertz control technique based on the above closed-loop speed control can be implemented [50].

### 3.2.1.2 Current/Slip Regulation

A speed control method using a current/slip scheme is shown in Figure 3.3. In this controller the scalar quantities which are controlled are the magnitude of the stator current and its frequency. The scheme requires speed feedback in order to control slip and cannot operate in the open loop manner of the *V/f* scheme.

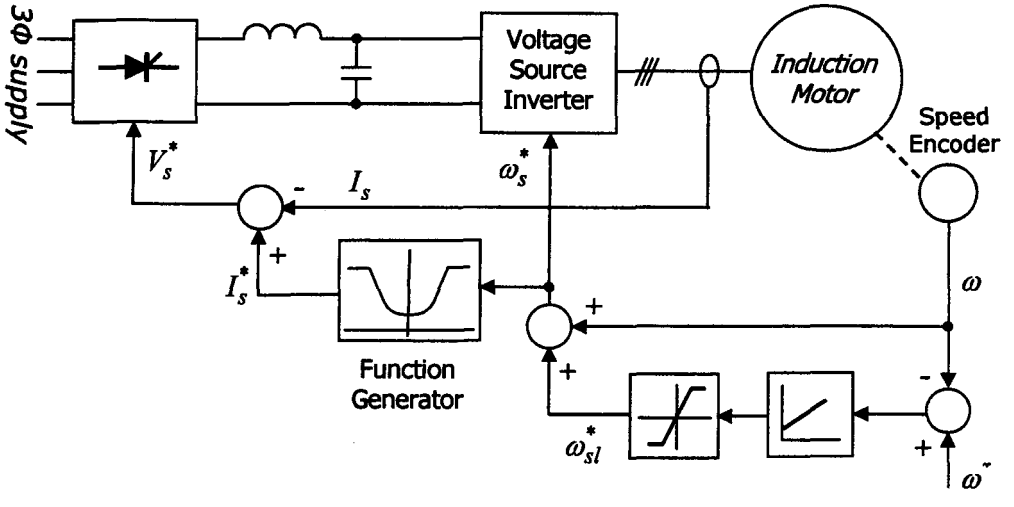


**Figure 3.3** Current/slip scalar control scheme

In this scheme the torque command is given to the drive as either a current command or a slip command. The current/slip relationship is then utilised to calculate the slip or current command. As with the *V/f* controller, the current slip relationship is maintained such that the flux in the machine is controlled. Field weakening operation is possible by altering the current/slip relationship above base speed such that the flux is reduced. The current/slip regulation scheme offers better dynamic performance than the volts/hertz scheme with the disadvantage of requiring both speed and current transducers.

### 3.2.2 Vector Control

The scalar control is somewhat simple to implement, but the inherent coupling effect (i.e., both torque and flux are functions of voltage or current and frequency) gives sluggish response and system is prone to instability because of a high-order (fifth-order) system effect [50]. For example, if the torque is increased by increasing the slip (i.e., the frequency), the flux tend to decrease. The flux variation in such system is always sluggish. The decrease in flux is then compensated by the sluggish flux control loop feeding in additional voltage. This temporary dipping of flux reduces the torque sensitivity with slip and lengthens response time. Therefore, high performance induction motor drives use vector or field oriented control (FOC) [1, 2] or direct torque and flux control (DTFC) [54] or feedback linearized control (FLC) [55].

Vector control is a very widely used control method for high performance induction motor drive applications. It implies independent (decoupled) control of flux and torque components of stator current through a coordinated change in supply voltage amplitude, phase and frequency. As the flux is controlled to be at the desired level, its constancy produces a fast torque response and finally a fast speed (or position) response. Flux level control is also essential to avoid magnetic saturation (and heavy core loss) and reduce the core losses. There are three distinct flux space vectors in the induction machine viz. $\vec{\psi}_m$-air gap flux vector, $\vec{\psi}_s$-stator flux vector and $\vec{\psi}_r$-rotor flux vector. Vector control can be performed with respect to any of these flux space phasors by attaching the reference system d-axis to the respective flux space vector direction and by keeping its amplitude under surveillance. However, orientation with respect to rotor flux alone gives natural decoupling between flux producing and torque producing components of stator current space vector [56]. Rotor FOC will be discussed in this section.

The FOC consists of controlling the stator current represented by a vector. Control is based on projections which transform a three phase time and speed dependent system into a two co-ordinate (d-q co-ordinate) time invariant system. These projections lead to a structure similar to that of a dc machine control. This requires information regarding the magnitude and position of rotor flux vector. In the induction motor magnetizing current is analogous to the main field flux of the dc machine and is controlled by $i_{sd}$, the direct component of the stator current. The quadrature component $i_{sq}$ is analogous to the armature current of the dc machine and it can be rapidly varied by an appropriate change in

stator current to give a fast response to a sudden torque demand. It also controls the angular velocity of rotor flux vector. In steady state operation with sinusoidal currents, the stator current vector and magnetizing current vector rotate in synchronism. Hence $i_{sd}$ and $i_{sq}$ are constant dc quantities and a steady torque is developed.

The technique of Vector Control has established itself as the standard technique for high performance control of induction machine drives. Vector control is classified into direct and indirect depending upon the method of obtaining the rotor flux position. Direct FOC usually indicates that the rotor flux is directly evaluated, either by using direct flux measurement, with Hall Effect transducers or search coil installed in the machine, or utilizing a flux observer. Indirect FOC on the other hand, usually implies that the instantaneous slip frequency is calculated from the two axis currents. As the slip frequency gives the speed of the rotor flux relative to the rotor mechanical speed, the slip is then integrated and added to the measured mechanical position. This gives a more accurate estimate of the flux position at low speeds and allows operation of the machine throughout the entire speed range. The two methods are discussed below.

#### 3.2.2.1 Indirect Vector Control

In rotor flux orientation the rotor flux vector is aligned with d-axis of synchronously rotating reference frame *d-q*. Therefore, $\omega_e$ is the synchronous speed of rotor flux space

vector. The $q$ axis rotor flux $\psi_{rq}$ is zero, and

$$\psi_r = \psi_{rd} \tag{3.12}$$

From equation (2.21) the rotor dynamics are given by the following equations:

$$\frac{d\psi_r}{dt} = \frac{L_m}{\tau_r} i_{sd} - \frac{1}{\tau_r}\psi_r \tag{3.13}$$

$$\frac{d\omega}{dt} = \frac{3p^2 L_m}{2JL_r}\left(\psi_r i_{sq}\right) - \frac{F}{J}\omega - \frac{p}{J}T_l \tag{3.14}$$

$$T_{em} = \frac{3pL_m\psi_r}{2L_r} i_{sq} \tag{3.15}$$

$$\rho = \int \omega_e dt = \int\left(\omega + \frac{R_r L_m i_{sq}}{L_r \psi_r}\right)dt \tag{3.16}$$

The rotor flux magnitude is related to the direct axis stator current by a first order differential equation so it can be controlled by controlling the direct axis stator current. Under steady state operation rotor flux is constant, so (3.13) becomes

$$\psi_r = L_m i_{sd} \tag{3.17}$$

Indirect vector control can be implemented using the following equations:

$$i_{sd}^{*} = \frac{\psi_r^{*}}{L_m} \tag{3.18}$$

$$i_{sq}^{*} = \frac{1}{p}\frac{L_r}{L_m}\frac{T_{em}^{*}}{\psi_r^{*}} \tag{3.19}$$

$$\omega_{sl}^{*} = \frac{R_r L_m i_{sq}^{*}}{L_r \psi_r^{*}} \tag{3.20}$$

$$\rho^{*} = \int \omega_e^{*} dt = \int \left(\omega + \omega_{sl}^{*}\right) dt \tag{3.21}$$

The principal scheme of the Indirect Vector Control is shown in figure 3.4 in which the function blocks $F_1$ and $F_2$ are presented by the equations (3.18) and (3.19) respectively.

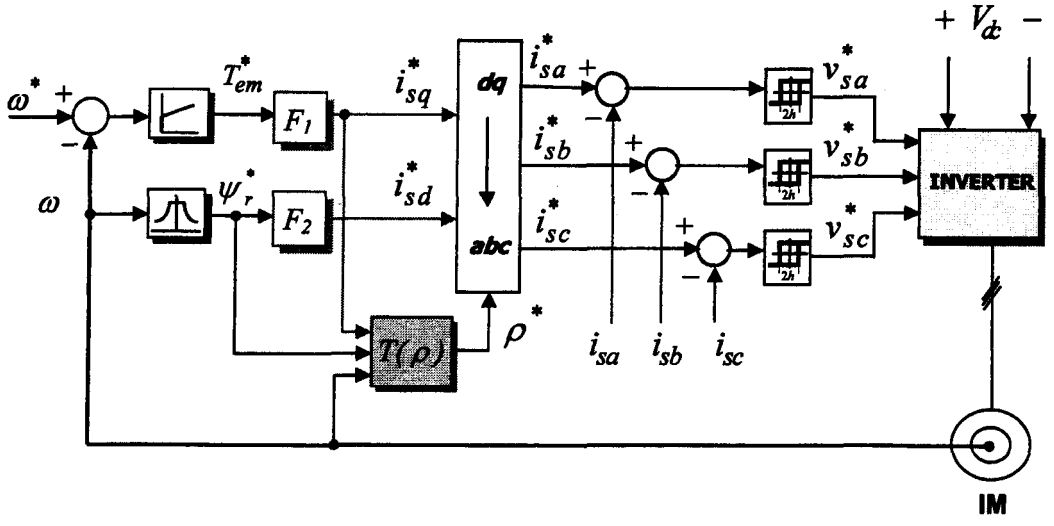


**Figure 3.4** Indirect Vector Control Scheme

In indirect FOC the rotor flux angle is generated in feedforward manner. Since this method relies on knowledge of the machine parameters such as $L_m$ and $L_r / R_r$ the real values of which may be changing with change in operating condition so care should be given during design to take the effects of parameter variations.

The speed control in the indirect VC in Figure 3.4 is achieved using a Proportional-Integral (PI) regulator. The design of PI speed controller is discussed below. The block diagram of speed control loop is shown in Figure 3.5.

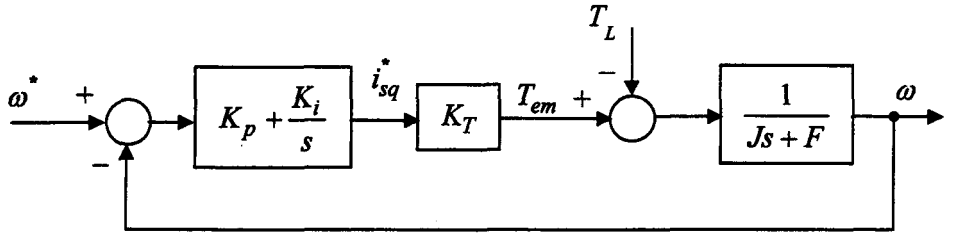


**Figure 3.5** Block Diagram of Speed Control Loop

From Figure 3.5,

$$T_{em} = K_T i_{sq}^* \tag{3.22}$$

$$i_{sq}^* = \frac{2L_r T_{em}}{3pL_m \psi_r^*} \tag{3.23}$$

$$\psi_r^* = L_m i_{sd}^* \tag{3.24}$$

From (3.27)-(3.29) $K_T$ is given by

$$K_T = \left(\frac{3pL_m^2}{2L_r}\right) i_{sd}^* \tag{3.30}$$

Closed-loop transfer function with respect to the reference input is

$$\frac{\omega}{\omega^*} = \frac{K_i K_T}{Js^2 + (F + K_p K_T)s + K_i K_T} = \frac{\omega_n^2}{s^2 + 2\xi\omega_n s + \omega_n^2} \tag{3.31}$$

where $\xi = \dfrac{F + K_p K_T}{2\sqrt{JK_i K_T}}$ and $\omega_n = \sqrt{\dfrac{K_i K_T}{J}}$

Then, for a unit step input the response is

$$\omega = \omega^* \frac{\omega_n^2}{s^2 + 2\xi\omega_n s + \omega_n^2} = \frac{1}{s}\frac{\omega_n^2}{s^2 + 2\xi\omega_n s + \omega_n^2} = \frac{1}{s}\frac{\omega_n^2}{(s + p_1)(s + p_2)} \tag{3.32}$$

In order to obtain a fast response without overshoot, the system should be critically damped, i.e. $\xi = 1$ and $p_1 = p_2 = -\omega_n$; then, the above equation becomes

$$\omega = \frac{1}{s}\frac{\omega_n^2}{(s+\omega_n)^2} = \frac{1}{s} - \frac{\omega_n}{(s+\omega_n)^2} - \frac{1}{(s+\omega_n)} \tag{3.33}$$

The transient response of the system is given by

$$\omega(t) = 1 - \omega_n t e^{-\omega_n t} - e^{-\omega_n t} \tag{3.34}$$

The response time of the system is when the controlled variable attains 90% of the set value

$$0.9 = 1 - \omega_n t e^{-\omega_n t} - e^{-\omega_n t} \tag{3.35}$$

From the solution of the above nonlinear equation we obtain the value of proper frequency using which parameters of the controller can be computed from the equation given below:

$$\begin{cases} 1 = \dfrac{F + K_p K_T}{2\sqrt{J K_i K_T}} \\ \omega_n = \sqrt{\dfrac{K_i K_T}{J}} \end{cases} \tag{3.36}$$

### 3.2.2.2 Direct Vector Control

Direct vector control usually indicates that the rotor flux is directly evaluated, either by using direct flux measurement with Hall Effect sensors or search coils installed in the machine, or by utilising a flux observer. The flux observer could be the stator voltage model, a Kalman filter or a Gopinath observer amongst several others. The modification of the machine to insert sensors is usually undesirable and there may be accuracy issues associated with sensors. In general the observers used for direct VC are susceptible to errors in current and voltage measurements and to thermal variations in stator resistance. These problem means that direct VC is usually applied above 10% of rated speed [50].

Determining this rotor flux angle could be either from the measurement from the air gap flux or from terminal currents and voltages. In the latter case, angle and magnitude of the rotor flux can be calculated by

$$\vec{\psi}_s = \int \left( \vec{v}_s - R_s \vec{i}_s \right) dt \tag{3.22}$$

$$\vec{\psi}_r = \frac{L_m}{L_r} \left( \vec{\psi}_s - \sigma L_s \vec{i}_s \right) \tag{3.23}$$

The principal scheme of the direct vector control is given in figure 3.6 in which the function blocks $F_1$ and $F_2$ are presented by

$$i_{sd}^{*} = \left(\psi_r^{*} - \psi_r\right)\left(k_{p\psi} + \frac{k_{i\psi}}{s}\right) \tag{3.34}$$

$$i_{sq}^{*} = \frac{2}{3p}\frac{L_r}{L_m}\frac{T_{em}}{\psi_r} \tag{3.35}$$

and the rotor flux position $\rho$ is given by

$$\rho = \tan^{-1}\left(\psi_{r\beta} / \psi_{r\alpha}\right) \tag{3.36}$$

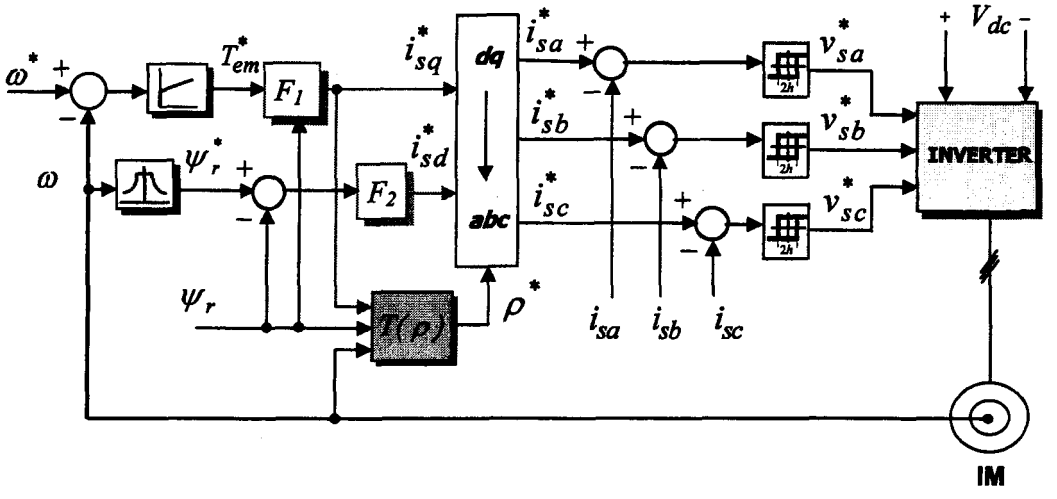


**Figure 3.6** Direct Vector Control scheme

Although Direct Vector Control may be relatively insensitive to the variations (depending on the actual implementation) of the rotor parameters, its performance may be

sluggish at low speed operations due to inaccurate knowledge of the stator resistance, integration drift, etc. [57].

Through the decoupling of the flux and torque control loops a fast dynamic torque response can be achieved similar to those achievable with a D.C. machine. As with the current/slip scalar scheme, vector control requires the use of both current and speed/position transducers.

### 3.2.3 Direct Torque Control

High bandwidth torque control can also be obtained by employing the direct torque control (DTC) method as an alternative to the vector control scheme. The idea of DTC was originally proposed by Takahashi et al [54]. Figure 3.7 show a DTC induction motor drive schematic, which uses the stator flux linkages [50]. Some other schematics based on rotor flux linkages or magnetizing flux linkages are also possible. In Figure 3.7 the induction motor is supplied by a VSI inverter and the stator flux linkage and electromagnetic torque are controlled directly and independently by the selection of inverter switching modes. The selection is made to restrict the flux linkage and torque errors within their hysteresis bands to obtain a fast torque response. The outputs of the flux and torque comparators ($H_{\psi_s}$, $H_{T_{em}}$) are used in the optimal inverter switching table, which also uses information about the sector *S(k)* in which stator flux space vector is located.

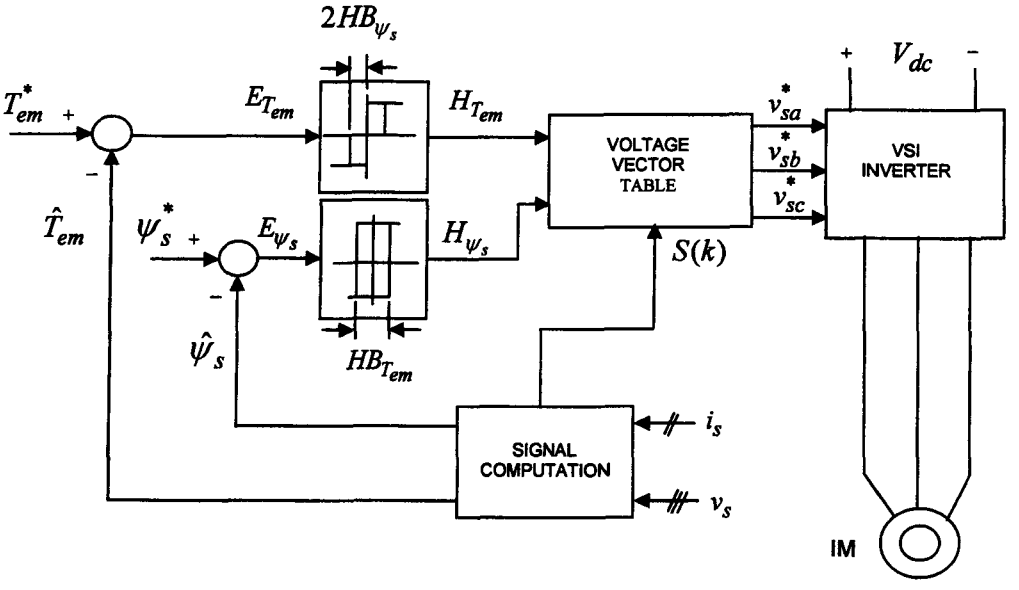


**Figure 3.7** Direct torque controlled induction motor drive.

It can be seen that the drive scheme requires stator flux and electromagnetic torque estimators. The stator flux can be estimated using the voltage model of the machine. However, at low frequencies large errors can occur due to variation in stator resistance. Therefore, some other estimation techniques need to be used to provide the stator flux information.

### 3.2.3.1 DTC Control Strategy

The command stator flux and torque magnitudes are compared with the respective estimated values, and the errors are processed through hysteresis band controllers.

The flux loop has two levels of digital output according to the following relations:

$$H_{\psi_s} = 1 \text{ for } E_{\psi_s} > +HB_{\psi_s} \tag{3.37}$$

$$H_{\psi_s} = -1 \text{ for } E_{\psi_s} < -HB_{\psi_s} \tag{3.38}$$

The torque control loop has three levels of digital output, which have the following relations:

$$H_{T_{em}} = 1 \text{ for } E_{T_{em}} > +HB_{T_{em}} \tag{3.39}$$

$$H_{T_{em}} = -1 \text{ for } E_{T_{em}} < -HB_{T_{em}} \tag{3.40}$$

$$H_{T_{em}} = 0 \text{ for } -HB_{T_{em}} < E_{T_{em}} < +HB_{T_{em}} \tag{3.41}$$

The feedback flux and torque are calculated from the machine terminal voltages and currents. Torque and flux computation block also computes the sector number *S(k)* in which flux vector lies. There are six sectors (each of $\pi/3$ radian wide) as indicated in Figure 3.8. Voltage vector table block in Figure 3.7 generates appropriate control voltage vector (switching states) for the inverter by a look up table, which is shown in Table 3.1. Neglecting stator resistance, we can write

$$\vec{V}_s = \frac{d}{dt}\vec{\psi}_s \tag{3.42}$$

or

$$\Delta\vec{\psi}_s = \vec{V}_s.\Delta t \tag{3.43}$$

which means that stator flux can be changed incrementally by applying stator voltage vector for time increment $\Delta t$.

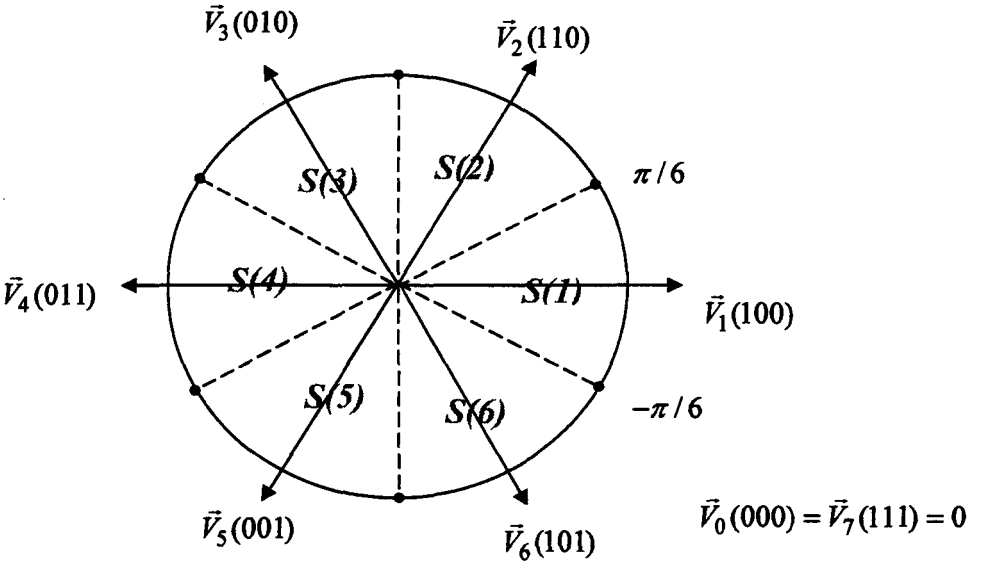


**Figure 3.8** Inverter voltage vectors

**Table 3.1** Switching table of inverter voltage vectors

| $H_{\psi_s}$ | $H_{T_{em}}$ | *S(1)* | *S(2)* | *S(3)* | *S(4)* | *S(5)* | *S(6)* |
|---|---|---|---|---|---|---|---|
| 1 | 1 | $V_2$ | $V_3$ | $V_4$ | $V_5$ | $V_6$ | $V_1$ |
| 1 | 0 | $V_0$ | $V_7$ | $V_0$ | $V_7$ | $V_0$ | $V_7$ |
| 1 | -1 | $V_6$ | $V_1$ | $V_2$ | $V_3$ | $V_4$ | $V_5$ |
| -1 | 1 | $V_3$ | $V_4$ | $V_5$ | $V_6$ | $V_1$ | $V_2$ |
| -1 | 0 | $V_7$ | $V_0$ | $V_7$ | $V_0$ | $V_7$ | $V_0$ |
| -1 | -1 | $V_5$ | $V_6$ | $V_1$ | $V_2$ | $V_3$ | $V_4$ |

Either the hysteresis band will decide the timing of each voltage vector or, if the timing is constant, the switching frequency will be constant. The hysteresis band may be adapted to keep constant the average switching frequency. DTC looks simple; however, the stator flux has to be estimated. Once the stator flux is known, the torque is simply

$$\hat{T}_{em} = \frac{3p}{2}\hat{\vec{\psi}}_s \times \vec{i}_s \tag{3.42}$$

The torque response is quick like that of vector control. The torque pulsations are directly controlled and the core losses and noise may be controlled through the stator flux level selection.

### 3.2.4 Feedback Linearized Control

Vector control was invented to produce separate flux and torque control as it is implicitly possible with d.c. motors.

It is also known that, with constant flux, the torque is proportional to torque current and linear speed-torque characteristics can be obtained. Such decoupling and linearization of induction motor equations may in principle be done with some other nonlinear transformations. Feedback linearization control [55] is such a method. The basic block diagram [58] is shown in Figure 3.9.

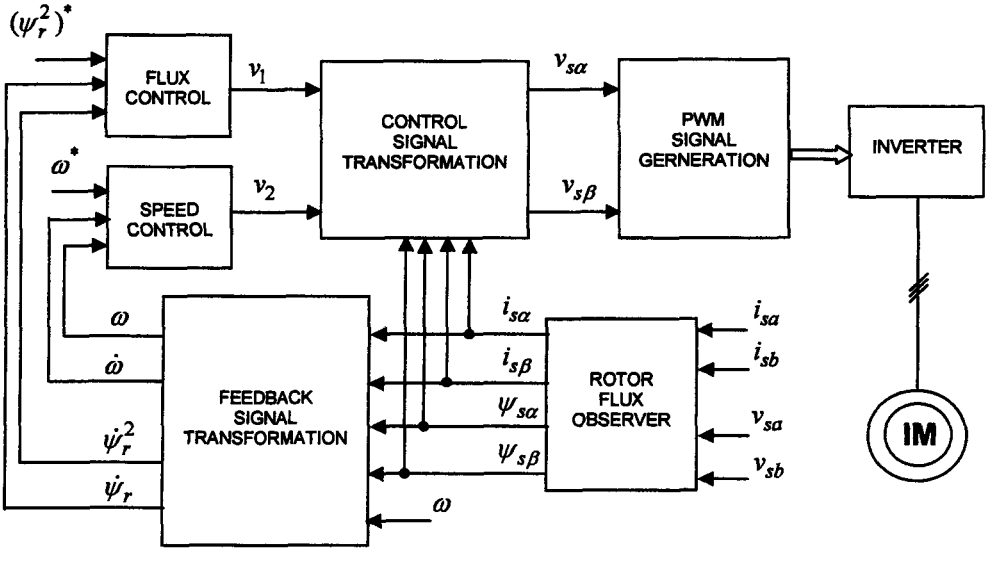


**Figure 3.9** Feedback Linearization Control

The computational effort for FLC is greater than that of vector control or DTC and thorough knowledge of motor parameters is necessary. The dynamic performance of FLC similar to both advanced vector control or DTC could be obtained.

### 3.3 Conclusion

In this chapter some of the important methods of induction motor control have been discussed. The chapter starts with how the speed of the machine was controlled traditionally. Then, scalar control method which is based on the steady state model of the machine was presented. Under the scalar control, voltage/frequency control and current/slip control were discussed. Then, the advanced control methods for induction motor drives such as vector control, direct torque control and feedback linearized control were presented. Among the advanced control techniques, the vector control method which is considered to be the industry standard for use in high performance drive applications was discussed in more detail than other methods. Direct torque control has the problem of torque chattering and feedback linearized control is complicated to implement even though its performance is not better than that of vector control. As rotor flux orientation allows natural decoupling between the torque producing and flux producing components of the stator current space vector, it is considered to be the best choice for use in high performance drive applications.

# CHAPTER 4

# SENSORLESS VECTOR CONTROL OF INDUCTION MOTOR DRIVE

## 4.1 Introduction

Shaft mounted sensors in conventional VC drives lower the system reliability and require special attention to electrical noise in addition to extra expenses involved. Moreover, rotational transducers cannot be mounted in certain applications, such as drives in hostile environments, high-speed drive applications etc. Therefore, sensorless vector controlled induction motor drive is an active research area. With sensorless vector control we have the decoupled control structure similar to that of a separately excited dc machine, retaining the inherent ruggedness of induction motor at the same time.

A good flux and speed estimation algorithm having the capability of accurate estimation under various operating conditions is essential for realizing a high performance sensorless induction motor drive. In this chapter, the development of the high performance drive system is looked into through the angle of developing accurate flux and speed estimation algorithms.

## 4.2 Speed Estimation

Rotor speed has been considered as a constant by many researchers in speed estimation problem [8-10, 20-23, 67-69]. The idea is that the speed changes slowly compared to electrical variables. Adopting such an approach allowed speed estimation without requiring the knowledge of mechanical parameters of the drive system such as load torque, inertia etc. In [8-10] speed was estimated using MRAS considering it as an unknown constant parameter. In [20-23] the speed was considered as an unknown constant state of the machine and EKF was used to estimate it. Recursive Least Square Estimation method was used in [59-61] for speed estimation considering speed as an unknown constant parameter and found out the value of estimated speed that best fits the measured and calculated data to the dynamic equations of the motor.

In this section we propose a speed estimation algorithm for an indirect VC induction motor drive. The proposed method does not require taking derivative of the measured signals unlike that of [10, 59-61]. The method is also simpler to implement than implementing EKF. In this method the model of the motor used for estimation is derived by introducing a new quantity which is a function of rotor flux and speed assuming that rotor speed varies slowly in comparison to electrical states. The new quantity containing information about the rotor flux and speed is estimated using a reduced order observer. Finally, the rotor speed is computed using the estimated quantity.

### 4.2.1 Induction machine model

The induction motor model in stationary stator reference frame $\alpha$-$\beta$ given by equation (2.20) may be written in vector matrix form as:

$$\frac{d\psi_r}{dt} = A_{11}\psi_r + A_{12}i_s \tag{4.1}$$

$$\frac{di_s}{dt} = A_{21}\psi_r + A_{22}i_s + A_{23}v_s \tag{4.2}$$

where $A_{11} = -(R_r / L_r)I + \omega J$, $A_{12} = (L_m R_r / L_r)I$, $A_{21} = \frac{L_m}{\sigma L_s L_r}\{(R_r / L_r)I - \omega J\}$

$A_{22} = -\left\{R_s / (\sigma L_s) + R_r L_m^2 / (\sigma L_s L_r^2)\right\} I$, $A_{23} = 1/(\sigma L_s) I$, $I = \begin{bmatrix} 1 & 0 \\ 0 & 1 \end{bmatrix}$, $J = \begin{bmatrix} 0 & -1 \\ 1 & 0 \end{bmatrix}$

$\psi_r = \begin{bmatrix} \psi_{r\alpha} & \psi_{r\beta} \end{bmatrix}^T$ : rotor flux,

$i_s = \begin{bmatrix} i_{s\alpha} & i_{s\beta} \end{bmatrix}^T$ : stator current,

$v_s = \begin{bmatrix} v_{s\alpha} & v_{s\beta} \end{bmatrix}^T$ : stator voltage,

$\sigma = 1 - L_m^2 / (L_s L_r)$ : leakage coefficient

Now, we introduce a new quantity into the motor model which when introduced will make the right hand side of conventional motor model given by equations (4.1) and (4.2) independent of the unknowns – the rotor flux and speed. Let's define the new quantity as:

$$Z = -A_{11}\psi_r \tag{4.3}$$

A new motor model is obtained after introducing the new quantity as given below:

$$\frac{d\psi_r}{dt} = A_{12}i_s + A_{14}Z \tag{4.4}$$

$$\frac{di_s}{dt} = A_{22}i_s + A_{23}v_s + A_{24}Z \tag{4.5}$$

$$\frac{dZ}{dt} = A_{32}i_s + A_{34}Z \tag{4.6}$$

where $A_{14} = -I$, $A_{24} = \{L_m/(\sigma L_s L_r)\}I$,

$A_{32} = \left(L_m R_r^2/L_r^2\right)I - \omega\left(L_m R_r/L_r\right)J$ and $A_{34} = A_{11}$

### 4.2.2 Observer Structure and Speed Estimation

The proposed speed estimation algorithm is based on observing the newly defined quantity which is a function of rotor flux and speed. Equation (4.5) and (4.6) are used for constructing a Gopinath's reduced order observer [62] for estimating the newly defined quantity. The observer is as given below:

$$\frac{d\hat{\boldsymbol{Z}}}{dt} = \boldsymbol{A}_{32}\boldsymbol{i}_s + \boldsymbol{A}_{34}\hat{\boldsymbol{Z}} + \boldsymbol{G}\left(\frac{d\boldsymbol{i}_s}{dt} - \frac{d\hat{\boldsymbol{i}}_s}{dt}\right) \tag{4.7}$$

where $\boldsymbol{G} = \begin{bmatrix} g_1 & -g_2 \\ g_2 & g_1 \end{bmatrix}$ is the observer gain.

Using equation (4.5) for $\frac{d\hat{\boldsymbol{i}}_s}{dt}$ the observer equation becomes:

$$\frac{d\hat{\boldsymbol{Z}}}{dt} = \boldsymbol{A}_{32}\boldsymbol{i}_s + \boldsymbol{A}_{34}\hat{\boldsymbol{Z}} + \boldsymbol{G}\left(\frac{d\boldsymbol{i}_s}{dt} - \boldsymbol{A}_{22}\boldsymbol{i}_s - \boldsymbol{A}_{23}\boldsymbol{v}_s - \boldsymbol{A}_{24}\hat{\boldsymbol{Z}}\right) \tag{4.8}$$

The observer poles can be placed at the desired locations in the stable region of the complex plane by properly choosing the values of the elements of the G matrix. In order to avoid taking derivative of the stator current in the algorithm we introduce another new quantity:

$$\boldsymbol{D} = \hat{\boldsymbol{Z}} - \boldsymbol{G}\boldsymbol{i}_s \tag{4.9}$$

Finally, the observer is of the following form:

$$\frac{d}{dt}\boldsymbol{F} = \left(\boldsymbol{A}_{32} + \boldsymbol{A}_{34}\boldsymbol{G} - \boldsymbol{G}\boldsymbol{A}_{22} - \boldsymbol{G}\boldsymbol{A}_{24}\boldsymbol{G}\right)\boldsymbol{i}_s - \boldsymbol{G}\boldsymbol{A}_{23}\boldsymbol{v}_s + \left(\boldsymbol{A}_{34} - \boldsymbol{G}\boldsymbol{A}_{24}\right)\boldsymbol{D} \tag{4.10}$$

$$\hat{\boldsymbol{Z}} = \boldsymbol{D} + \boldsymbol{G}\boldsymbol{i}_s \tag{4.11}$$

The block diagram of the $Z$ observer is shown in Figure 4.1.

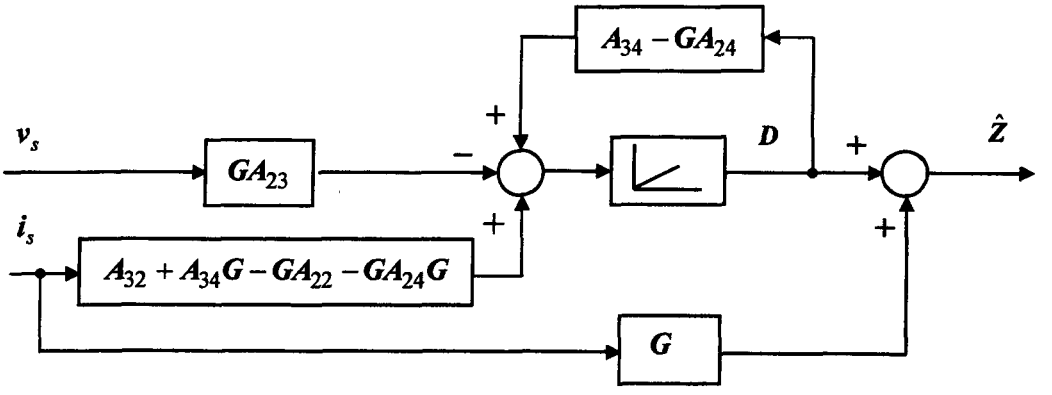


**Figure 4.1** Block diagram of $Z$ observer

Assuming no parameter variation and no speed error, the equation for error dynamics is given by:

$$\frac{d}{dt}\tilde{Z} = \frac{d}{dt}\left(Z - \hat{Z}\right) = \left(A_{34} - A_{24}G\right)\tilde{Z} \tag{4.12}$$

Eigenvalues of $\left(A_{34} - A_{24}G\right)$ are the observer poles which are as given below:

$$P_{obs1,2} = -\left(\frac{R_r}{L_r} + \frac{L_m}{\sigma L_s L_r} g_1\right) \pm j\left(\omega - \frac{L_m}{\sigma L_s L_r} g_2\right) \tag{4.13}$$

The desired observer dynamics can be imposed by proper selection of observer gain G.

Next, let's see how the rotor speed is computed. It can be seen that the observed quantity is a function of rotor flux and speed. Performing matrix multiplication of $\psi_r{}^T J$ with equation (4.3) we have:

$$Z_\alpha \psi_{r\beta} - Z_\beta \psi_{r\alpha} = \left(\psi_{r\alpha}^2 + \psi_{r\beta}^2\right)\omega \tag{4.14}$$

This is a simple equation which does not involve derivative or integration. To use it directly for speed computation we need to know the rotor flux; and as for $Z_\alpha$ and $Z_\beta$ we can use the estimated values. The required flux is obtained from the reference. Rearranging the above equation we have the equation used for rotor speed computation as given below:

$$\hat{\omega} = \frac{\hat{Z}_\alpha \psi_{r\beta}^* - \hat{Z}_\beta \psi_{r\alpha}^*}{\psi_{r\alpha}^{*\,2} + \psi_{r\beta}^{*\,2}} \tag{4.15}$$

The coefficient matrices $A_{32}$ and $A_{34}$ in the observer equation are updated with the estimated values of rotor speed.

It is to be noted here that the model of the motor used in implementing the observer algorithm has been developed assuming that the derivative of the rotor speed is zero. It is valid to make such an assumption since the dynamics of rotor speed is much slower than that of electrical states. Moreover, such an assumption allows estimation without requiring the knowledge of mechanical quantities of the drive such as load torque, inertia etc.

### 4.2.3 Simulation Results

The proposed speed estimation algorithm is validated by simulation. The details of the 3-phase squirrel cage induction motor used in simulation are given in Appendix A. The block diagram of the sensorless indirect vector controlled induction motor drive incorporating the proposed speed estimator shown in Figure 4.2 is simulated. The results of simulation are shown in Fig. 4.3-4.5.

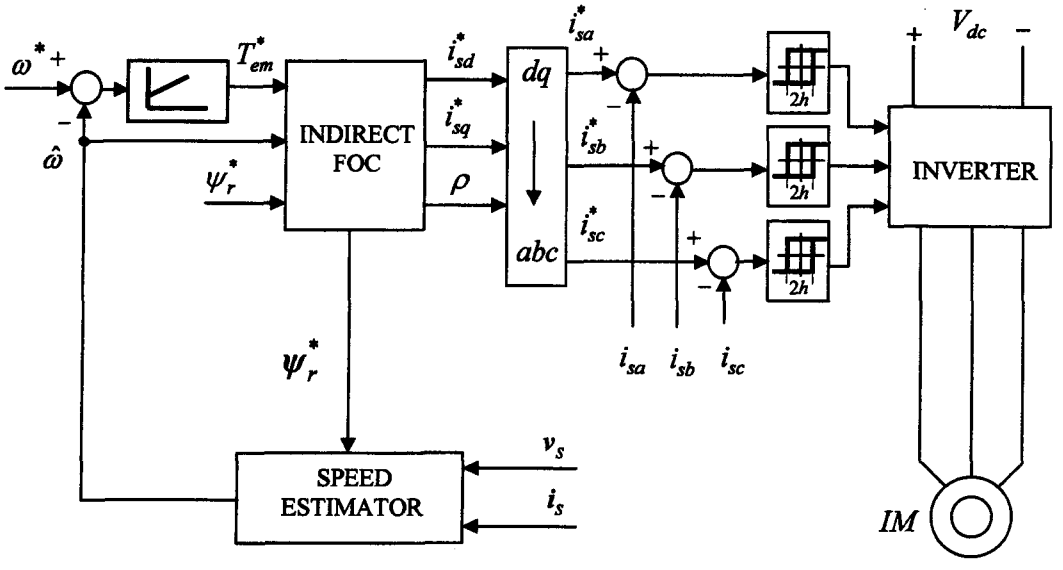


**Figure 4.2** Sensorless indirect VC induction motor drive

Initially, the drive is run at no load. It is accelerated from rest to 150 rad/s at 0.15 sec. and then, the speed is reversed at 2.5 sec. The speed is reversed again at 5.5 sec. The speed

of the motor ($\omega_m$), estimated speed ($\hat{\omega}_m$) and reference speed ($\omega_m^*$) are shown in Figure 4.3 (a). Figure 4.3 (b) shows speed estimation error ($\omega_m - \hat{\omega}_m$). The newly defined quantity ($Z$) and its estimated value ($\hat{Z}$) are shown in Figure 4.3 (c) and its estimation error ($Z - \hat{Z}$) is shown in Figure 4.3 (d).

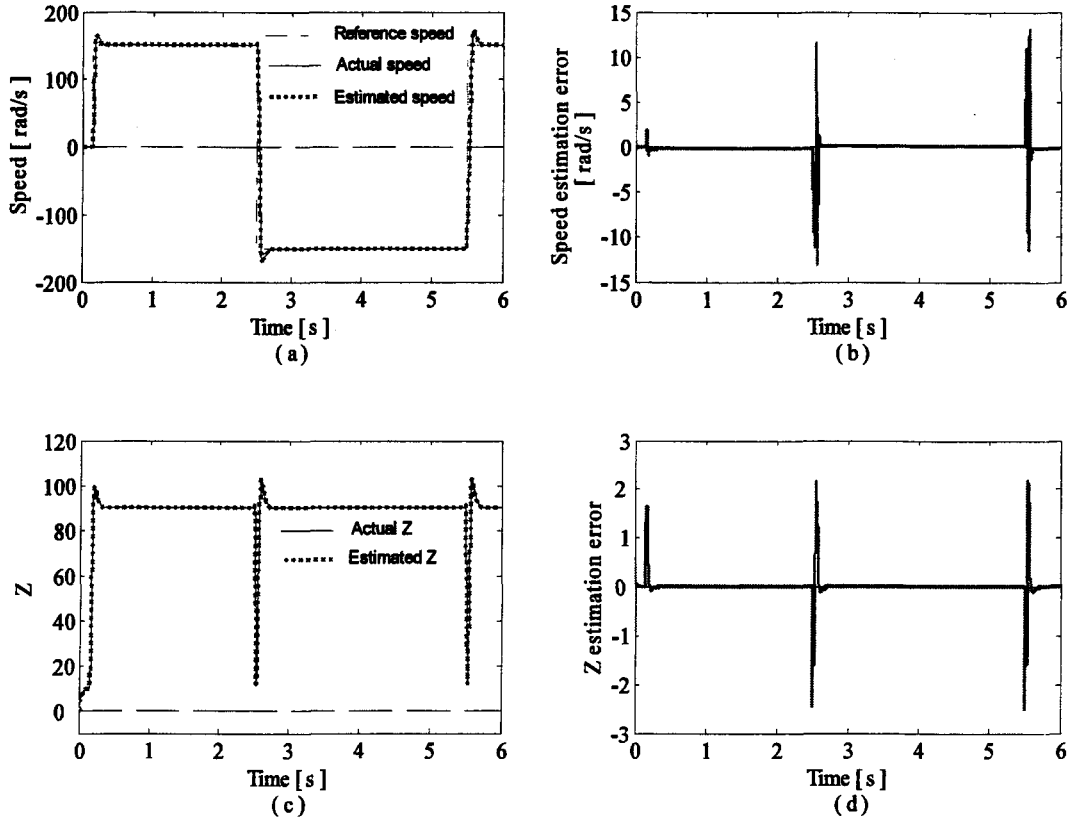


**Figure 4.3** Acceleration and speed reversal at no load; (a) reference, actual and estimated speeds; (b) speed estimation error; (c) actual $Z$ and estimated $Z$ and (d) $Z$ estimation error

The estimation algorithm and the drive response are then verified under loading and unloading conditions. The unloaded drive is started at 0.15 sec and full load is applied at 1 sec; then load is completely removed at 2 s. Later, after speed reversal, full load is applied at 3.5 sec and the load is fully removed at 4.5 sec. The machine is brought to rest at 5.5 sec. Figure 4.4 shows the speed estimation result and response of the sensorless drive system.

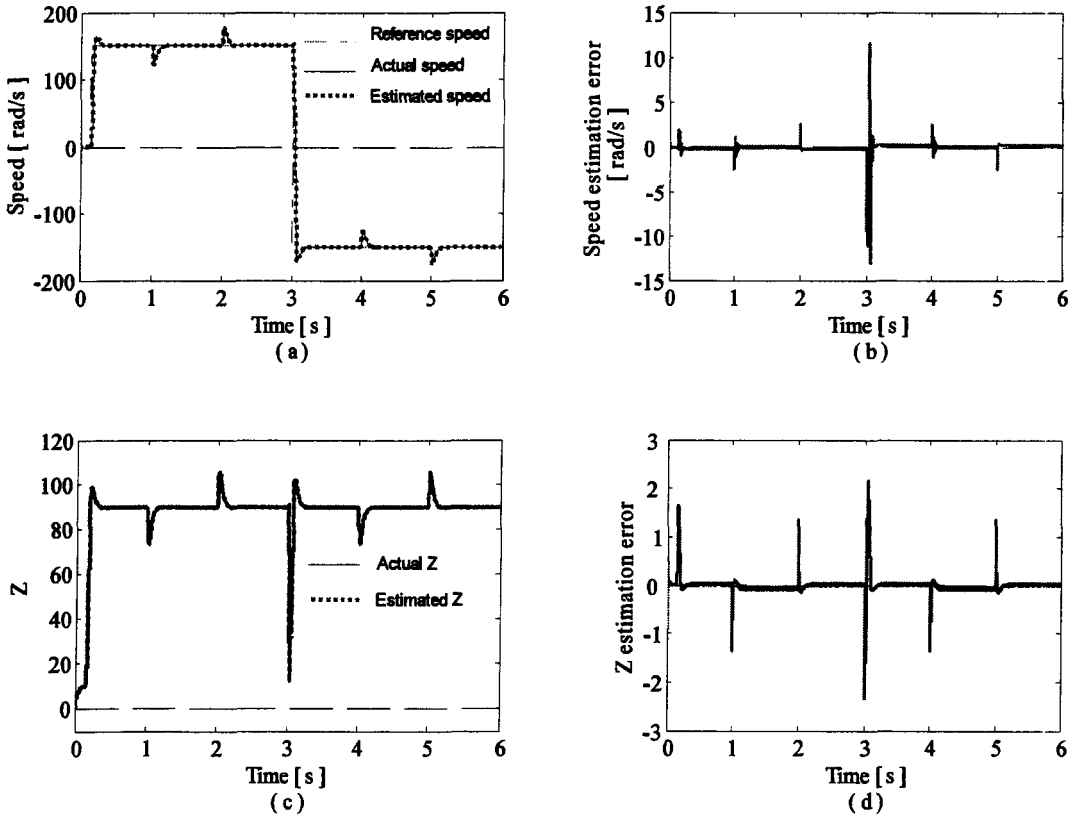


**Figure 4.4** Application and removal of load; (a) reference, actual and estimated speeds; (b) speed estimation error; (c) actual $Z$ and estimated $Z$ and (d) $Z$ estimation error

Then, the accuracy of the estimation algorithm and response of the sensorless induction motor drive is verified under fully loaded condition at various operating speeds. The drive is started at full load to 150 rad/s and the speed is reduced in steps in order to observe the response of the loaded drive at various speeds. Figure 4.5 shows the estimation results and response of the loaded drive.

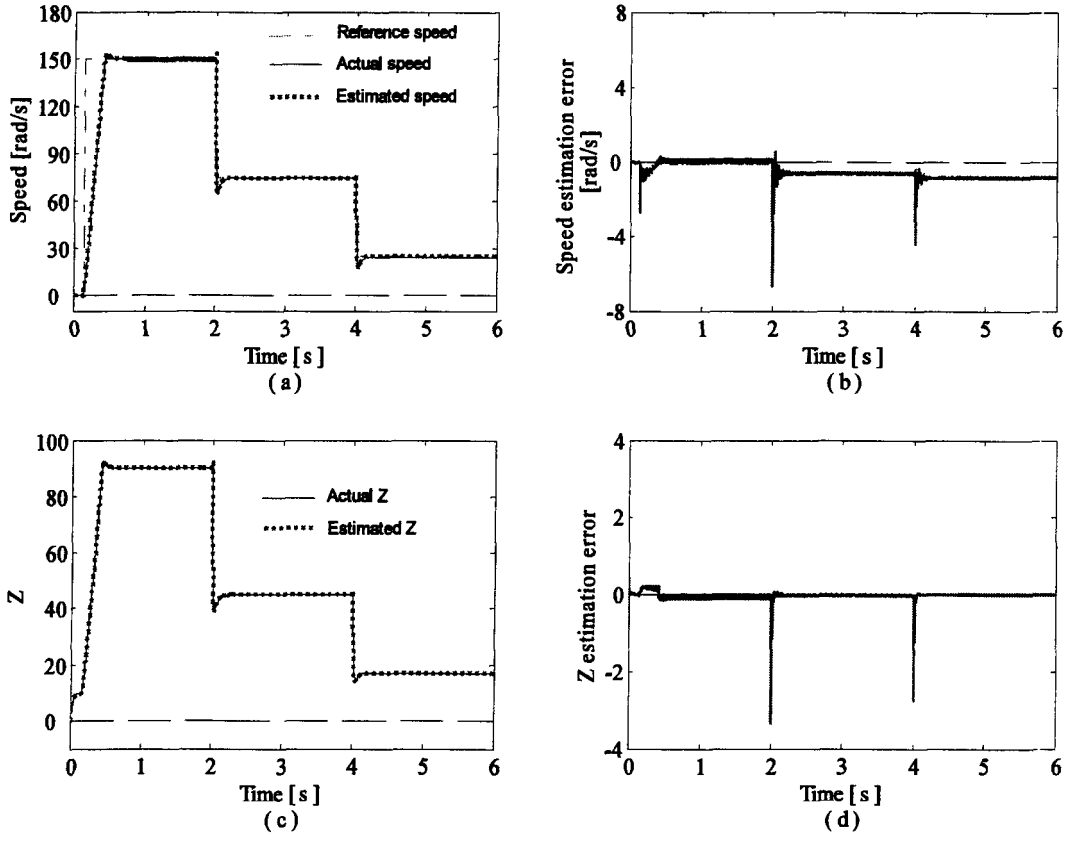


**Figure 4.5** Operation at full load at various speeds; (a) reference, actual and estimated speeds; (b) speed estimation error; (c) actual $Z$ and estimated $Z$ and (d) $Z$ estimation error

### 4.2.4 Discussion

The results of simulation show that the estimation accuracy of the proposed speed estimation algorithm is good; however, it is found that the estimation accuracy decreases with the decrease in speed. This is due to the fact that estimation algorithm uses command flux for speed computation and not the actual rotor flux which however is little bit different from the reference value and the difference becomes more with the decrease in speed. The problem is overcome in the next section by using a rotor flux observer based on the voltage model of the machine along with the observer of the newly defined quantity.

### 4.2.5 Improvement in Speed Estimation

It is observed that the estimation algorithm presented above gives good estimation accuracy under both dynamic and steady state conditions. However, it is found that the estimation accuracy decreases with decrease in speed. This is because of the fact that the estimation algorithm uses the command flux for speed estimation and not the actual rotor flux which however is little bit different from the command value, and the difference becomes more with the decrease in speed. The problem is overcome by using a rotor flux observer based on the voltage model of the machine along with the observer of the newly defined quantity. This allows accurate speed estimation in various operating ranges. The speed is computed using (4.15) after replacing the command flux by the estimated one. Further, due to the obvious advantages of dc current regulators over ac current regulators as regards its robustness, and load and operating point independence [63] the control system uses dc current regulators. The rotor flux estimator and the control scheme are presented in the following subsections.

#### 4.2.5.1 Rotor Flux Estimation

Using (2.11), (2.13) and (2.14) we obtain the equation commonly known as the voltage model of induction motor given below:

$$\psi_r = \frac{L_r}{L_m}\{\int(v_s - R_s i_s)dt - \sigma L_s i_s\} \tag{4.16}$$

The rotor flux can be estimated using (4.16). However, the integration in (4.16) produces a problem of dc off-set and drift component in low speed region. Therefore, a first order low pass filter (LPF) is used instead of integration. The phase error in the low speed region produced due to LPF is approximately compensated by adding low pass filtered reference flux with the same time constant as above, and producing the estimated rotor flux [64]. The estimator equation is given as:

$$\hat{\psi}_r = \frac{L_r}{L_m}\left\{(v_s - R_s i_s)\frac{\tau}{1+\tau s} - \sigma L_s i_s \frac{\tau s}{1+\tau s}\right\} + \Psi_r^* \frac{1}{1+\tau s} \tag{4.17}$$

where $\tau$ is the LPF time constant.

The command rotor flux $\Psi_r^*$ in (4.17) is obtained as follows:

$$\Psi_r^* = \begin{bmatrix} \Psi_{r\alpha}^* \\ \Psi_{r\beta}^* \end{bmatrix} = \begin{bmatrix} \Psi_r^* \cos\rho^* \\ \Psi_r^* \sin\rho^* \end{bmatrix} \tag{4.18}$$

where $\Psi_r^* = L_m i_{sd}^*$ and $\rho^*$ the command rotor flux angle is as given by:

$$\rho^* = \int \omega_e^* dt \tag{4.19}$$

$\omega_e^*$, the command rotor flux speed is computed as given below:

$$\omega_e^* = \omega_{sl}^* + \hat{\omega} \tag{4.20}$$

The command slip speed $\omega_{sl}^*$ is given by:

$$\omega_{sl}^* = \frac{R_r i_{qs}^*}{L_r i_{ds}^*} \tag{4.21}$$

The block diagram of the rotor flux estimator is shown in Figure 4.6.

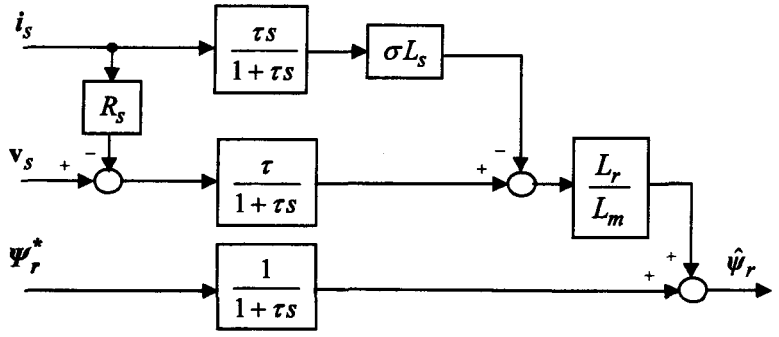


**Figure 4.6** Rotor flux estimator

#### 4.2.5.2 Speed computation

The equation (4.15) after modification is used for speed computation. In place of reference flux, estimated flux is used as given below:

$$\hat{\omega} = \frac{\hat{Z}_\alpha \hat{\psi}_{r\beta} - \hat{Z}_\beta \hat{\psi}_{r\alpha}}{\hat{\psi}_{r\alpha}^{\ 2} + \hat{\psi}_{r\beta}^{\ 2}} \tag{4.22}$$

#### 4.2.5.3 Simulation Results

Simulation is carried out in order to verify the accuracy of the estimation algorithm and to see the response of the sensorless drive system. The block diagram of sensorless vector controlled induction motor drive incorporating the flux and speed estimator is shown in Figure 4.7.

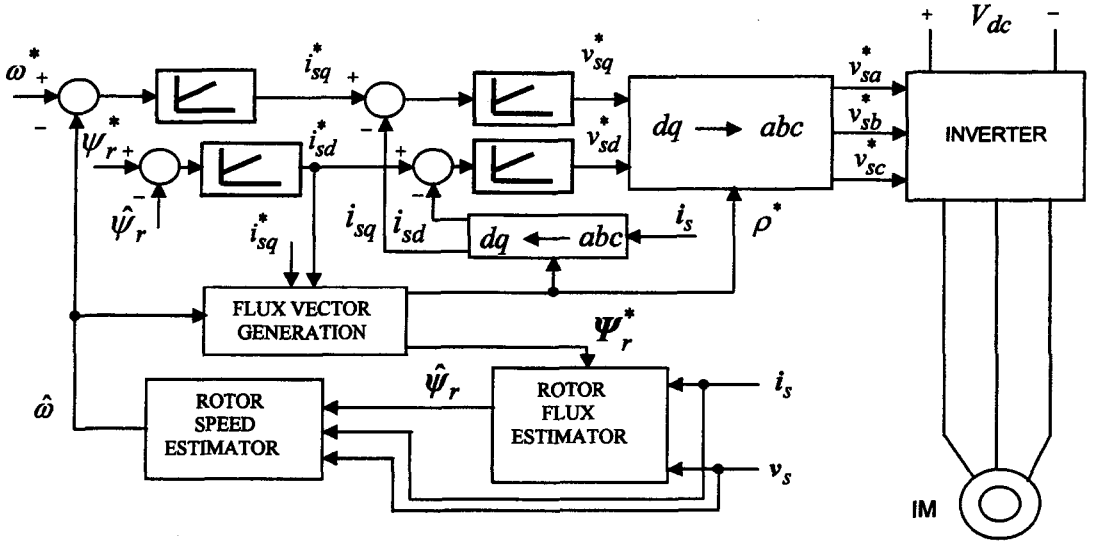


**Figure 4.7** Sensorless vector controlled induction motor drive

First, the sensorless drive is run at no load to verify the performance of the observer under no load condition at various operating speeds. The drive is started at no-load and is run at various speeds by increasing it in steps to 10 rad/s, 50 rad/s, 100 rad/s and 150 rad/s at 0.3 sec, 1.5 sec, 3 sec and 4.5 sec respectively. The speed of the motor ($\omega_m$), estimated

speed ($\hat{\omega}_m$), reference speed ($\omega_m^*$) and speed estimation error ($\omega_m - \hat{\omega}_m$) are shown in Figure 4.8 (a). Figure 4.8 (b) shows the actual Z, estimated Z and Z estimation error ($Z - \hat{Z}$).

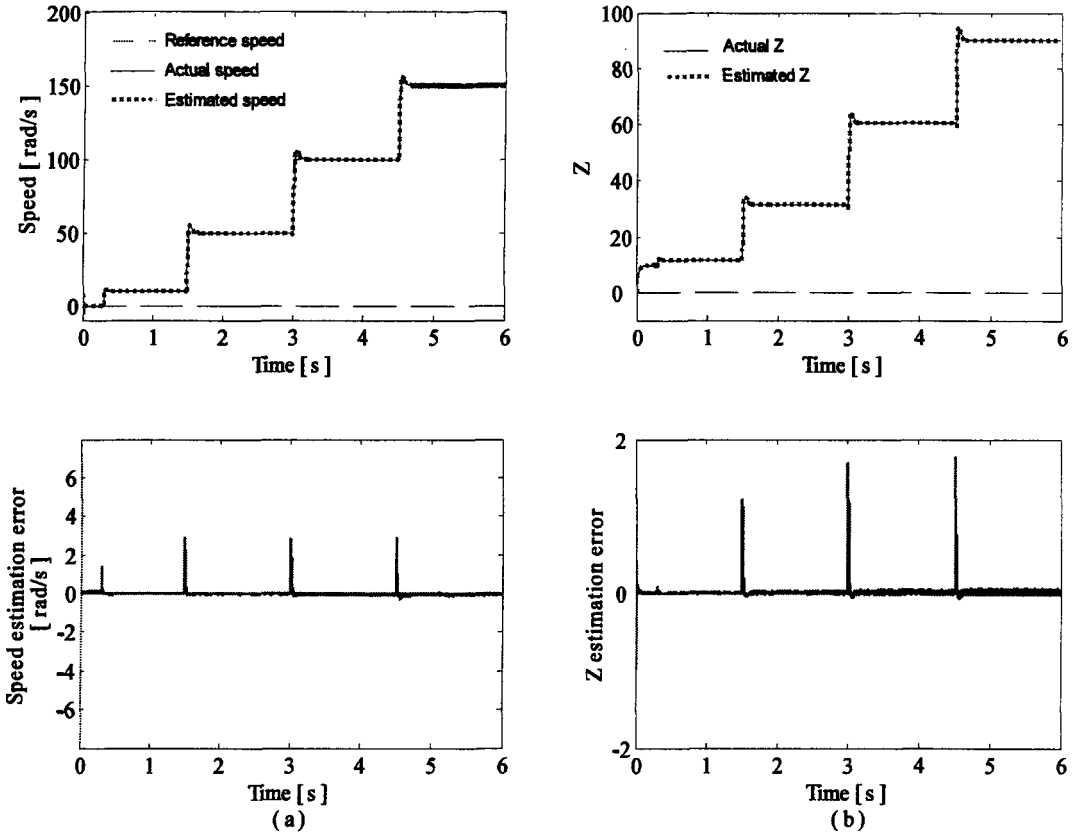


**Figure 4.8** No load operation at various speeds; (a) reference, actual and estimated speed, and speed estimation error; (b) actual $Z$, estimated $Z$, and $Z$ estimation error

Then, the unloaded drive is subjected to a slow change in speed profile (trapezoidal), the results of which are shown in Figure 4.9.

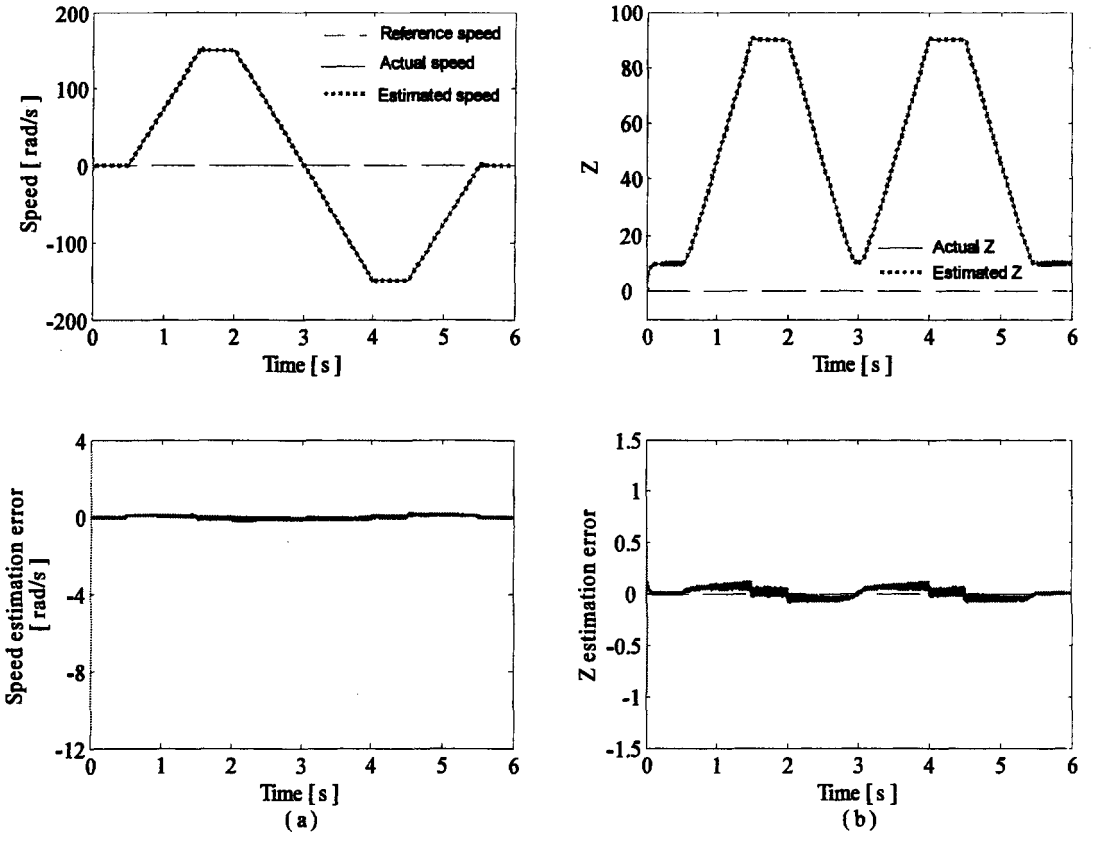


**Figure 4.9** No load operation with trapezoidal speed profile; (a) reference, actual and estimated speed, and speed estimation error; (b) actual $Z$, estimated $Z$, and $Z$ estimation error

Then, the performance of the estimator is verified on loading and unloading. Full load is applied at 1 sec to the machine operating at no load at a speed of 150 rad/s and then the load is removed completely at 2 sec. Later, after speed reversal, full load is applied at 4 s and the load is completely removed at 5 sec. The response of the drive on application and removal of load is shown in Figure 4.10.

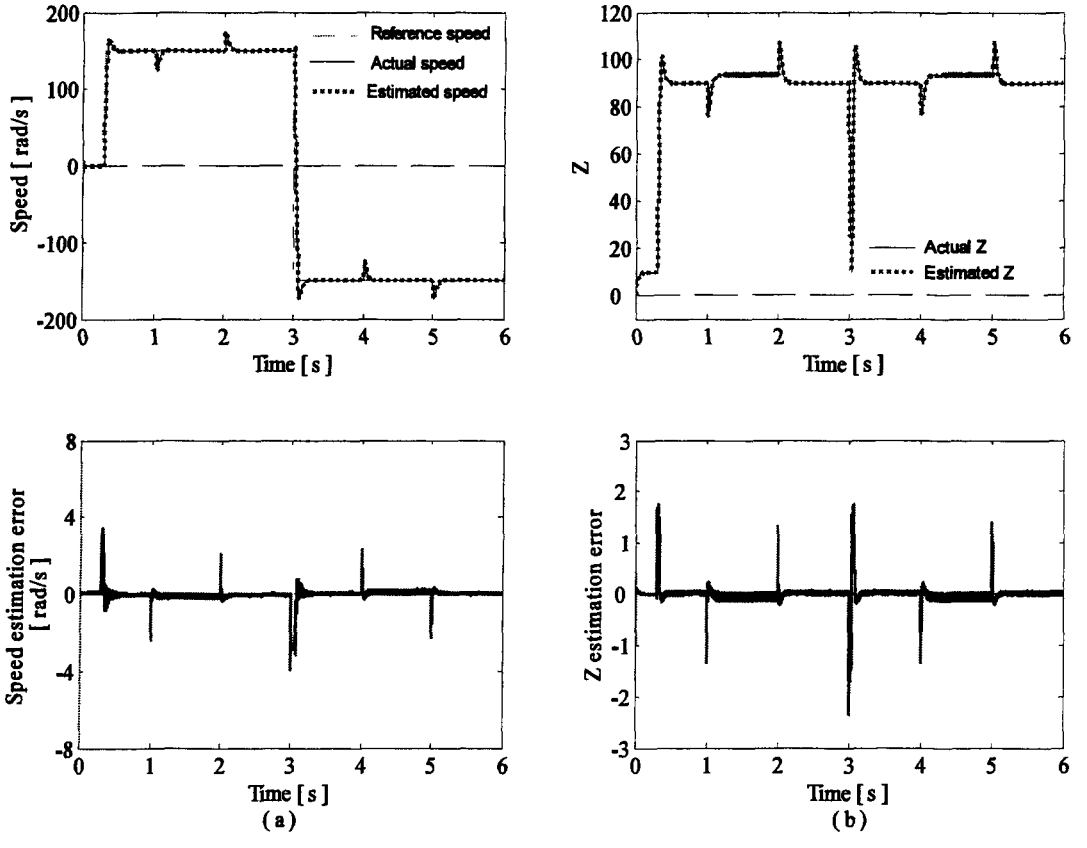


**Figure 4.10** Application and removal of load; (a) reference, actual and estimated speed, and speed estimation error; (b) actual $Z$, estimated $Z$, and $Z$ estimation error.

Then, estimator performance is verified under fully loaded condition of the drive at various operating speeds. The fully loaded machine is accelerated to 150 rad/s at 0.3 s, and then the speed is reduced in steps to 100 rad/s, 50 rad/s and 10 rad/s at 2.5 sec, 3.5 sec and 4.5 sec respectively. Figure 4.11 shows the estimation results and response of the drive during the operation.

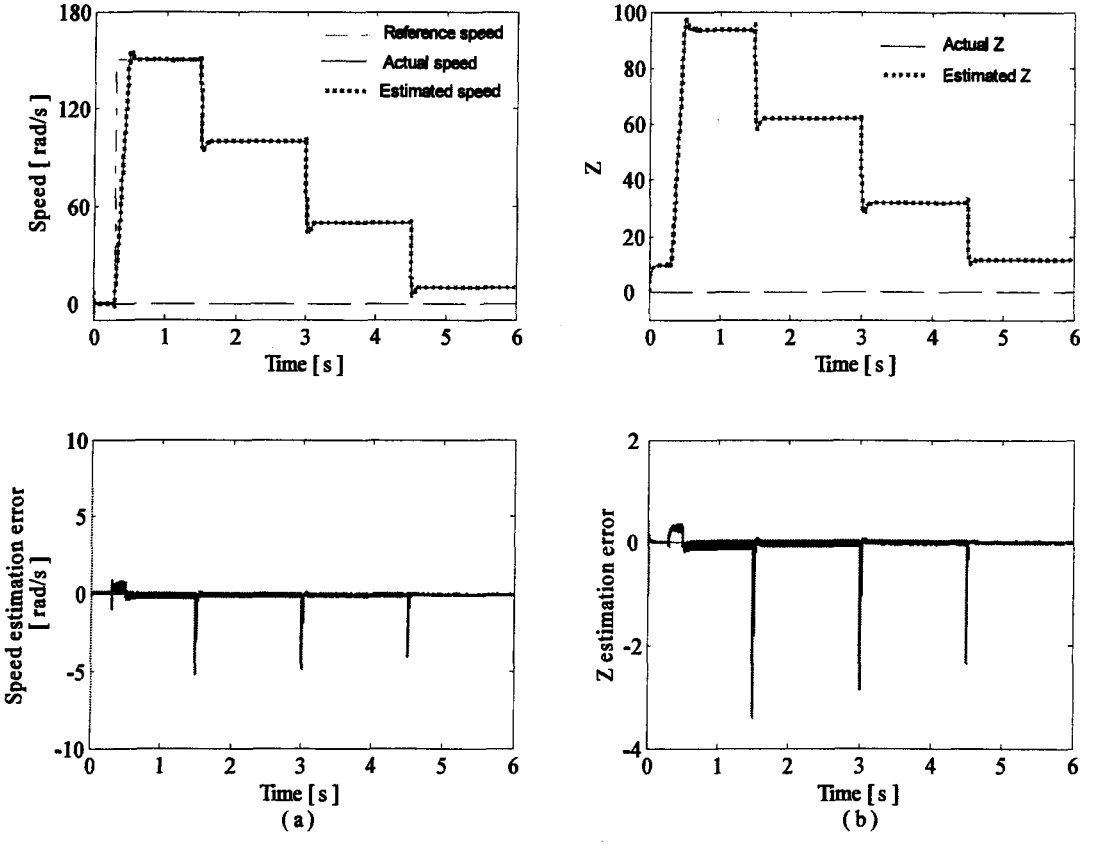


**Figure 4.11** Full load operation at various speeds; (a) reference, actual, estimated speed, and speed estimation error; (b) actual $Z$, estimated $Z$, and $Z$ estimation error.

#### 4.2.5.5 Discussion

Good speed estimation accuracy was obtained under both dynamic and steady state conditions under various operating conditions and response of the VC induction motor drive incorporating the estimation algorithms was found to be good.

The speed estimation algorithm presented in this section depends upon the knowledge of the rotor flux, whereas, the rotor flux estimator is independent of rotor speed and requiring only the measurable stator terminal quantities the stator voltage and current. A new rotor flux estimation algorithm for speed sensorless induction motor drive is presented in the next section where rotor flux and speed are estimated jointly.

## 4.3 Flux Estimation for Speed Sensorless Vector Controlled Induction Motor Drive

Induction machines do not allow rotor flux to be easily measured. The current model and the voltage model are the traditional solutions, and their benefits and drawbacks are well known [65]. Various observers for flux estimation were analyzed in the work by Verghese and Sanders [66] and Jansen and Lorenz [67]. Over the years several other have been presented, many of which include speed estimation [9, 20, 64, 68-70].

Tajima et al [9] proposed MRAS [8] with novel pole allocation method for speed estimation while rotor flux estimation was done using Gopinath's observer. In [20] Extended Kalman Filter was used for estimating the rotor flux and speed using a full order model of the motor assuming that rotor speed is a constant. Ohtani et al [64] used the voltage model for flux estimation overcoming the problem associated with integrator and low pass filter while speed was obtained using a frequency controller. A speed adaptive flux observer was proposed in [68] for estimating rotor flux and speed. In [69] Gopinath style reduced order observer was used for estimating the rotor flux while the speed was computed using an equation derived from the motor model. Yan et al [70] proposed a flux and speed estimator based on the sliding-mode control methodology. In this section, we propose a new flux estimation algorithm for speed sensorless rotor flux oriented controlled induction motor drive. The proposed method is based on observing a newly defined quantity introduced in Section 4.2.1 which when introduced makes the right hand side of the conventional motor model independent of rotor flux and speed. Rotor flux estimation is achieved using a modified Blaschke equation obtained after introduction of the newly

defined quantity into the Blaschke equation or commonly known as the current model; while, speed is computed using a simple equation obtained using this new quantity.

### 4.3.1 Estimation of Rotor Flux and Speed

A new motor model was derived in section 4.2.1 after introducing a newly defined quantity $Z$. Then, a speed estimation algorithm based on observing the newly defined quantity was presented where flux required for speed computation was obtained from the reference flux. Speed estimation accuracy was improved further using a rotor flux estimation algorithm based on the voltage model of the motor. The speed computation equation (4.22) requires the knowledge of rotor flux and $Z$. Here, we propose a joint rotor flux and speed estimation algorithm. The block diagram of the proposed rotor flux and speed estimation algorithm is shown in Figure 4.12.

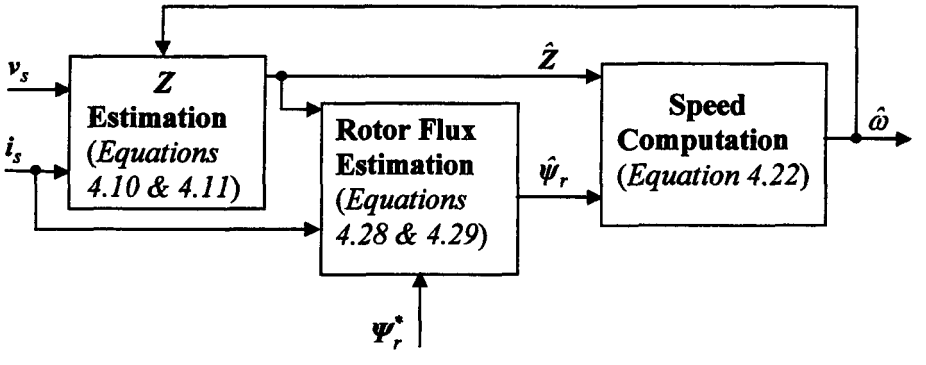


**Figure 4.12** Rotor flux and speed estimator

Rotor flux may be obtained directly using the modified Blaschke equation (4.4) which is obtained after introducing the newly defined quantity $Z$ into the Blaschke equation as:

$$\hat{\psi}_r = \int \left( A_{12} i_s + A_{14} Z \right) dt \tag{4.23}$$

However, rotor flux computation by pure integration suffers from dc offset and drift problems. To overcome the above problems a low pass filter is used instead of pure integrator and the phase error due to low pass filtering is approximately compensated by adding low pass filtered reference flux with the same time constant as used above [64] [80]. The equation of the proposed rotor flux estimator is given below:

$$\hat{\psi}_r = \frac{\tau}{1+\tau s}\left( A_{12} i_s + A_{14} Z \right) + \frac{1}{1+\tau s} \Psi_r^* \tag{4.24}$$

where $\tau$ is the LPF time constant. The command rotor flux $\Psi_r^*$ is obtained as follows:

$$\Psi_r^* = \begin{bmatrix} \Psi_{r\alpha}^* \\ \Psi_{r\beta}^* \end{bmatrix} = \Psi_r^* \begin{bmatrix} cos\,\rho^* \\ sin\,\rho^* \end{bmatrix} = L_m i_{sd}^* \begin{bmatrix} cos\,\rho^* \\ sin\,\rho^* \end{bmatrix} \tag{4.25}$$

The command rotor flux angle $\rho^*$ is obtained by integrating the command rotor flux speed as given below:

$$\rho^* = \int \omega_e^* dt = \int (\omega_{sl}^* + \hat{\omega}) dt \tag{4.26}$$

The command slip speed $\omega_{sl}^*$ is given by:

$$\omega_{sl}^* = \frac{R_r i_{qs}^*}{L_r i_{ds}^*} \tag{4.27}$$

We know that the equation of the back emf is given by:

$$e = \frac{L_m}{L_r}\frac{d\psi_r}{dt} = \frac{L_m}{L_r}\left(A_{12} i_s + A_{14} Z\right) \tag{4.28}$$

Now, equation (4.24) may also be written as:

$$\hat{\psi}_r = \frac{\tau}{1+\tau s}\left(\frac{L_r}{L_m} e\right) + \frac{1}{1+\tau s}\Psi_r^* \tag{4.29}$$

Block diagram of the rotor flux estimator is shown in Figure 4.13.

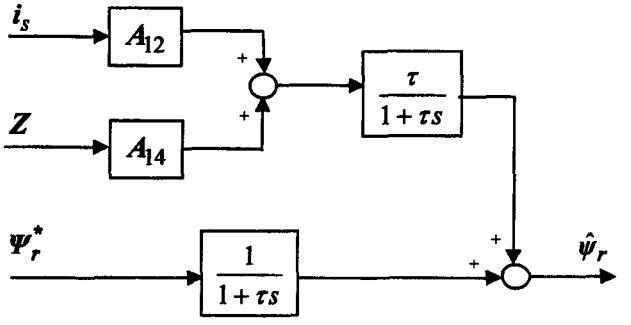


**Figure 4.13** Rotor Flux Estimator

Figure 4.14 explains how estimated flux is obtained using equation (4.29).

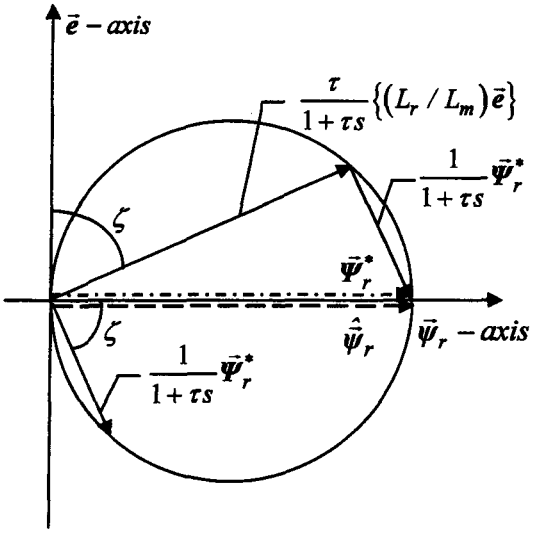


**Figure 4.14** Obtaining estimated rotor flux

### 4.3.2 Simulation Results

The proposed rotor flux and speed estimation algorithm is incorporated into a vector controlled induction motor drive. The block diagram of the sensorless VC induction motor drive is shown in Figure 4.15.

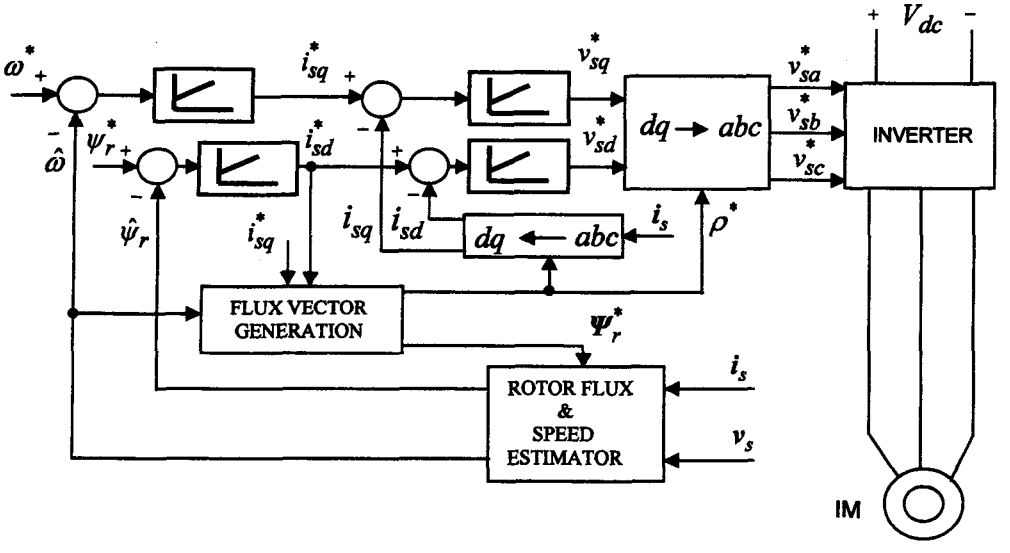


**Figure 4.15** Sensorless VC induction motor drive

First, acceleration and speed reversal at no load is performed. A speed command of 150 rad/s at 0.5 sec is given to the drive system which was initially at rest, and then the speed is reversed at 3 sec. The estimation of rotor flux and speed and the response of the sensorless drive are shown in Figure 4.16. Figure 4.16 (a) shows reference ($\omega_m^*$), actual ($\omega_m$),

estimated ($\hat{\omega}_m$) speed, and speed estimation error ($\omega_m - \hat{\omega}_m$). The module of the actual ($|\psi_r|$), estimated ($|\hat{\psi}_r|$) rotor flux, and rotor flux estimation error ($|\psi_r| - |\hat{\psi}_r|$) are shown in Figure 4.16 (b).

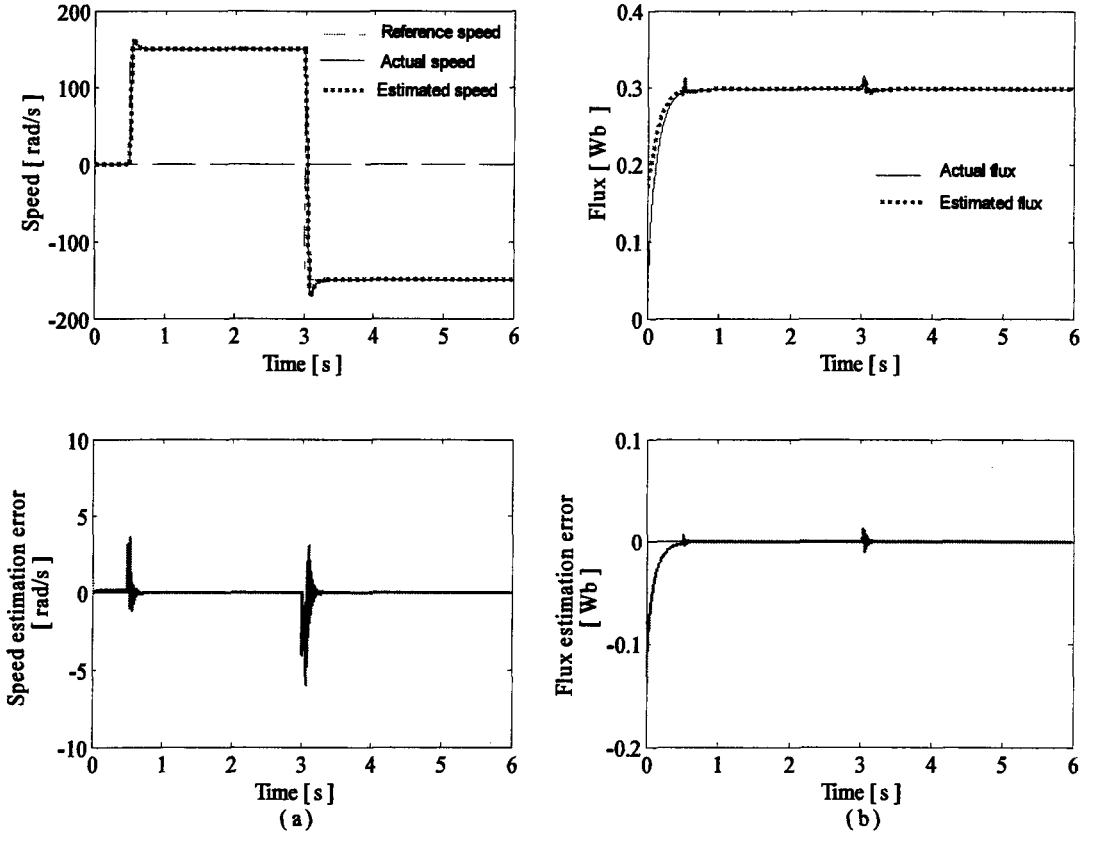


**Figure 4.16** Acceleration and speed reversal at no-load; (a) reference, actual and estimated speed, and speed estimation error; (b) actual and estimated rotor flux, and rotor flux estimation error

The drive is then run at various speeds under no load condition. It is accelerated from rest to 10 rad/s at 0.5 sec, and then accelerated further to 50 rad/s, 100 rad/s and 150 rad/s at 1.5 sec, 3 sec and 4.5 sec respectively. Figure 4.17 shows the estimation of rotor flux and speed, and the response of the sensorless drive system.

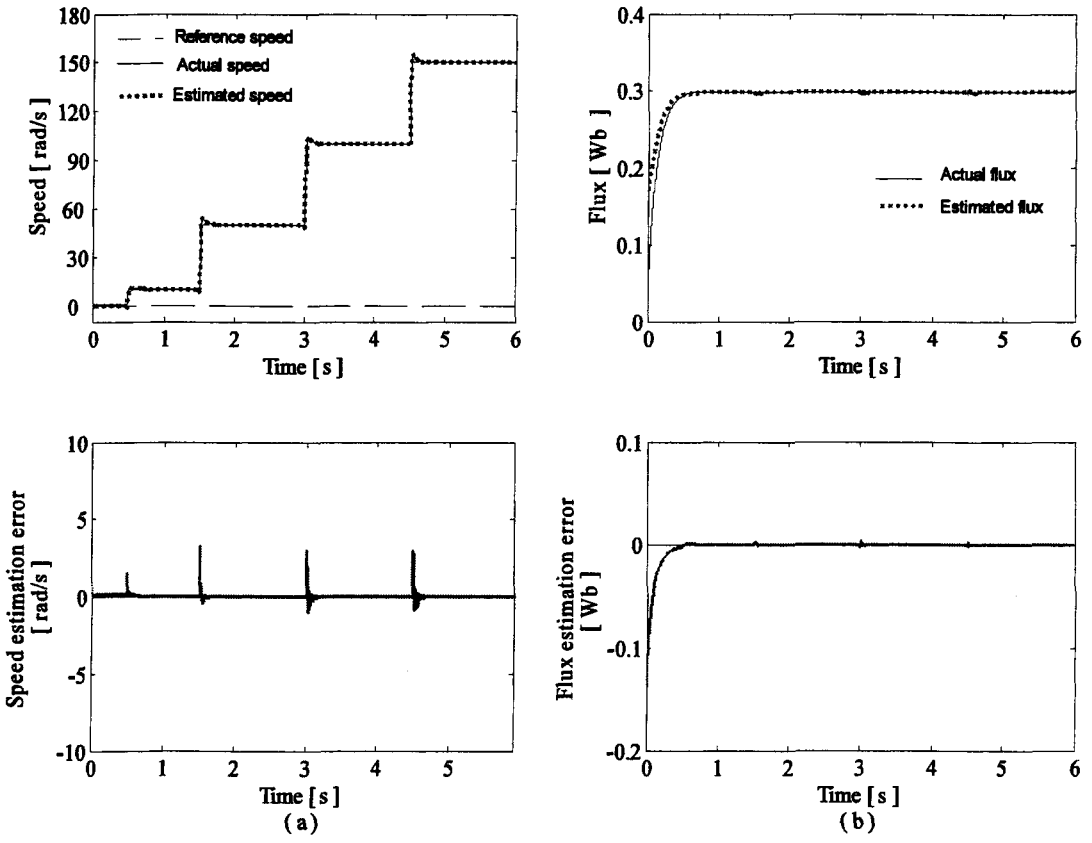


**Figure 4.17** No-load operation at various speeds; (a) reference, actual and estimated speed, and speed estimation error; (b) actual and estimated rotor flux, and rotor flux estimation error

Then, the unloaded drive is subjected to a slow change in reference speed profile (trapezoidal). The estimation results and sensorless drive's response are shown in Figure 4.18.

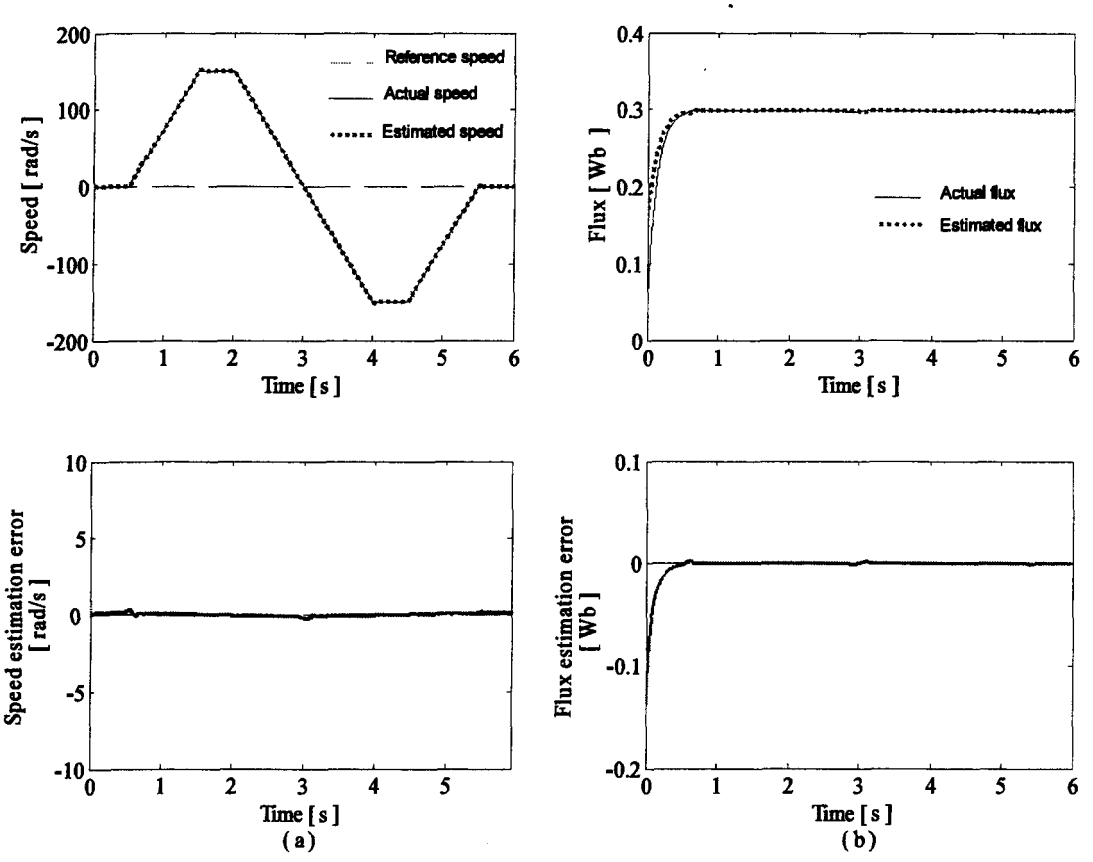


**Figure 4.18** No-load operation with trapezoidal speed profile; (a) reference, actual and estimated speed, and speed estimation error; (b) actual and estimated rotor flux, and rotor flux estimation error

Further, the performance of the estimator and the response of the sensorless drive are verified under loaded conditions at various operating speeds. The fully loaded drive is accelerated to 150 rad/s at 0.5 s and then decelerated in steps to 100 rad/s, 50 rad/s and 10 rad/s at 1.5 sec, 3 sec and 4.5 sec respectively. Figure 4.19 shows the estimation results and response of the loaded drive system.

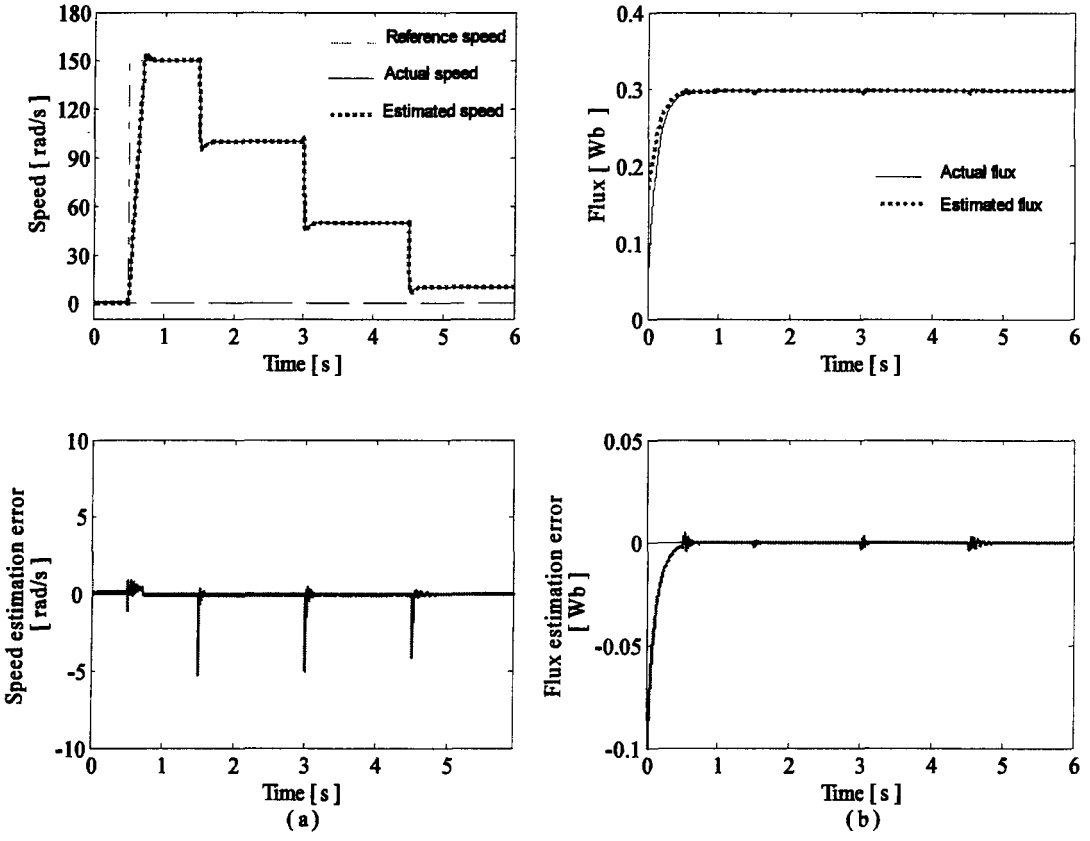


**Figure 4.19** Full load operation at various speeds; (a) reference, actual and estimated speed, and speed estimation error; (b) actual and estimated rotor flux, and rotor flux estimation error

Then, the estimator performance is verified on loading and unloading. The unloaded drive at rest is accelerated to 150 rad/s at 0.5 sec and full load is applied at 1 sec; then, the load completely at 2 s. Later, after speed reversal, full load is applied at 4 s, and, the load is fully removed at 5 s. Figure 4.20 shows the estimation results and the response of the sensorless drive.

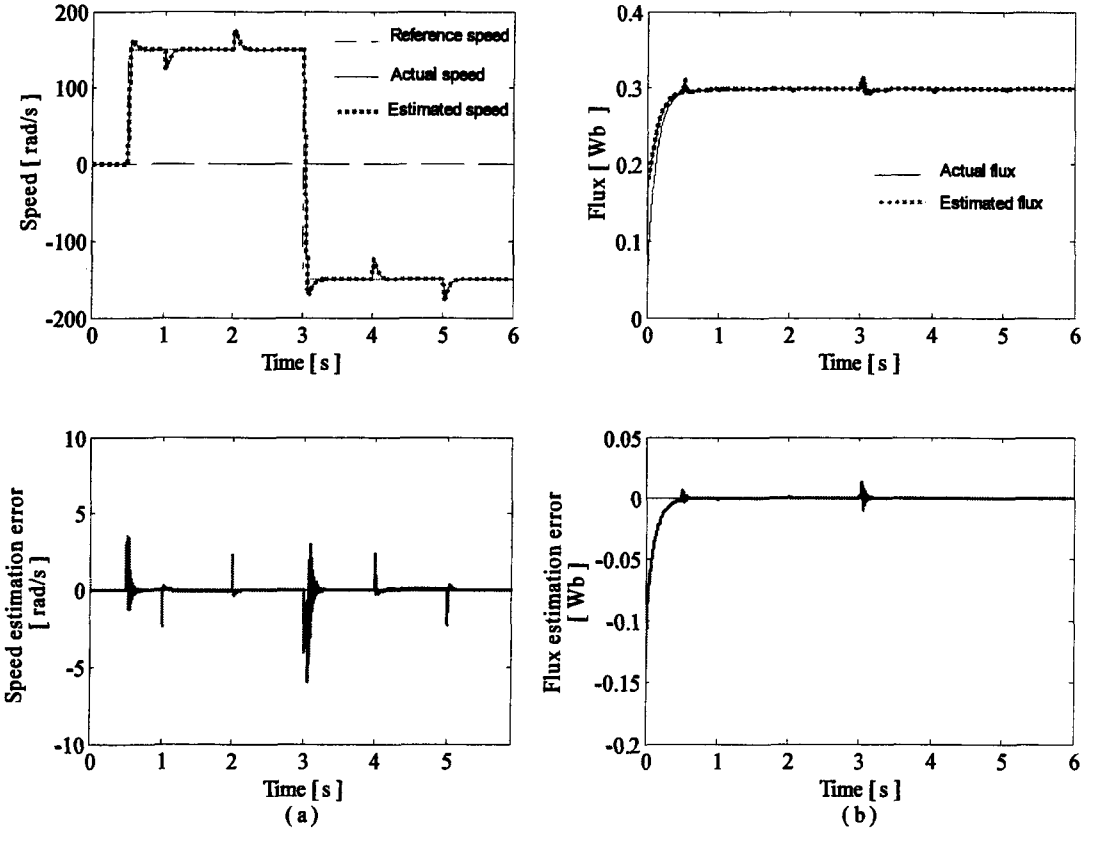


**Figure 4.20** Application and removal of load; (a) reference, actual and estimated speed, and speed estimation error; (b) actual and estimated rotor flux, and rotor flux estimation error

## 4.4 Conclusion

A new speed estimation algorithm in vector controlled induction motor drive has been proposed. The proposed method is based on observing a newly defined quantity which is a function of rotor flux and speed. The algorithm uses command flux for speed computation. The problem of decrease in estimation accuracy with the decrease in speed was overcome using a flux observer based on voltage model of the machine along with the observer of the newly defined quantity, and satisfactory results were obtained.

Finally, a joint rotor flux and speed estimation algorithm has been proposed. The proposed method is based on a modified Blaschke equation and on observing the newly defined quantity mentioned above. Good estimation accuracy was obtained and the response of the sensorless vector controlled drive was found to be satisfactory.

The mathematical model of the motor used for implementing the estimation algorithm was derived with the assumption that the rotor speed dynamics is much slower than that of electrical states. Therefore, increase in estimation accuracy of the proposed algorithms will be observed with the increase in the size of the machine used.

# CHAPTER 5

# SPEED SENSORLESS INDUCTION MOTOR DRIVE ROBUST AGAINST ROTOR RESISTANCE VARIATION

## 5.1 Introduction

A high performance sensorless induction motor drive requires speed estimation in addition to estimating machine parameters most important of which is the rotor resistance which varies during the operation of the motor. However, simultaneous estimation of speed and rotor resistance was considered impossible for a long time. This is because under constant flux operation in rotor flux oriented control, the rotor model is reduced to one equation containing both speed and rotor resistance. So, a change in either rotor speed or rotor resistance has an equal effect on the electrical behaviour of the motor. Recently, few works have been reported on simultaneous estimation of speed and rotor resistance [43-47]. In [43-45] simultaneous estimation was achieved by superimposing ac components on the field current command; however this causes torque ripples and speed oscillations. Adaptive state observer was used in [43] where adaptive schemes for speed and rotor resistance estimation were derived using Lyapunov's stability theorem. In [44] a reduced order model

of the motor was used for implementing estimation algorithm using EKF assuming that the dynamics of speed, taken as a parameter, and rotor resistance are much slower than that of electrical states. In [45] a Lyapunov-like technique was used for designing the estimator with the assumption of constant speed and rotor resistance; however, as the speed was assumed constant during estimator stability proof, rotor resistance estimation was required to be disabled during speed transients to avoid drift errors in the estimate. In [46], it was shown that the outputs of the PWM inverter contain enough high frequency signals which make the injection of external signals unnecessary. A sixth order model of the motor was used for implementing estimation algorithm using EKF. In [47] simultaneous estimation was achieved without injecting any external signal. The rotor resistance was estimated using least mean square algorithm and constant gain algorithm in the transient state and the speed was estimated by subtracting slip speed from the synchronous speed. However, as the simultaneous estimation could be achieved only during speed transients this method is suitable for such applications where speed changes frequently.

This chapter presents a method for simultaneous estimation of speed and rotor resistance in an indirect vector controlled induction motor drive. The proposed method is applicable to a large category of induction motor drives with a gradually varying load torque such as viscous friction, fan/blower and centrifugal pump. Mathematical model of the motor used for implementing estimation algorithm contains electromechanical equation of the drive in order to take coupling between electrical and mechanical modes into consideration, which is especially true for small sized machines. Speed and rotor resistance estimation algorithm is implemented using EKF which is a standard, time-tested algorithm used worldwide for state

and parameter estimation of nonlinear systems. Computational burden for implementing the algorithm is reduced in this work by using reduced order EKF. However, with modern day DSPs and FPGAs having fast computation capabilities, implementing EKF is not considered to be a problem any more. Simultaneous estimation is achieved without injecting any external signal which is believed to be a major contribution in the area of variable speed induction motor drives. The estimated speed and rotor resistance are used for realizing a sensorless indirect VC induction motor drive which is robust against rotor resistance variation.

## 5.2 Induction Machine Model

Load that a motor drives depends upon the particular area of application of the drive. A high percentage of motor applications require driving a gradually varying torque load. Two types of load torques are known to exist under this category and both are considered here in this work: (i) viscous friction load (it produces torque which is proportional to speed; $T_L = K_v\omega$) and (ii) fan/blower or centrifugal pump load (it produces a torque which is proportional to square of the speed; $T_L = K_b\omega^2$).

The state and output equations of the reduced order model of the induction motor established in stationary stator reference frame $\alpha$-$\beta$ given by equation 2.20 can be written as given below:

$$\begin{cases} \dot{x} = \dfrac{d}{dt}\begin{bmatrix} \psi_{r\alpha} \\ \psi_{r\beta} \\ \omega \\ R_r \end{bmatrix} = \boldsymbol{A}\begin{bmatrix} \psi_{r\alpha} \\ \psi_{r\beta} \\ \omega \\ R_r \end{bmatrix} + \boldsymbol{B}\begin{bmatrix} i_{s\alpha} \\ i_{s\beta} \\ T_{em} \end{bmatrix} \\ y = \begin{bmatrix} v_{s\alpha} - R_s i_{s\alpha} - \sigma L_s \dfrac{di_{s\alpha}}{dt} \\ v_{s\beta} - R_s i_{s\beta} - \sigma L_s \dfrac{di_{s\beta}}{dt} \end{bmatrix} = \boldsymbol{C}\begin{bmatrix} \psi_{r\alpha} \\ \psi_{r\beta} \\ \omega \\ R_r \end{bmatrix} \end{cases} \tag{5.1}$$

where $\boldsymbol{A} = \begin{bmatrix} -\dfrac{R_r}{L_r} & -\omega & 0 & 0 \\ \omega & -\dfrac{R_r}{L_r} & 0 & 0 \\ 0 & 0 & -\dfrac{\gamma}{J} & 0 \\ 0 & 0 & 0 & 0 \end{bmatrix}$, $\boldsymbol{B} = \begin{bmatrix} \dfrac{L_m R_r}{L_r} & 0 & 0 \\ 0 & \dfrac{L_m R_r}{L_r} & 0 \\ 0 & 0 & \dfrac{1}{J} \\ 0 & 0 & 0 \end{bmatrix}$,

$$\boldsymbol{C} = \begin{bmatrix} -\dfrac{R_r L_m}{L_r^2} & -\dfrac{L_m \omega}{L_r} & 0 & \dfrac{L_m^2}{L_r^2} i_{s\alpha} \\ \dfrac{L_m \omega}{L_r} & -\dfrac{R_r L_m}{L_r^2} & 0 & \dfrac{L_m^2}{L_r^2} i_{s\beta} \end{bmatrix}$$

$\gamma = F + K_v$ for viscous friction load, and $\gamma = F + K_b \omega$ for fan/blower or centrifugal pump load.

In the model of the motor, the rotor resistance $R_r$ has been introduced as the fourth state. It is assumed that its dynamics is slow in comparison to that of other states and hence its derivative is equated to zero.

The model of the motor, after discretization is written as follows:

$$\begin{cases} \boldsymbol{x}(k+1) = \begin{bmatrix} \psi_{r\alpha} \\ \psi_{r\beta} \\ \omega \\ R_r \end{bmatrix}_{(k+1)} = \boldsymbol{A}(k) \begin{bmatrix} \psi_{r\alpha} \\ \psi_{r\beta} \\ \omega \\ R_r \end{bmatrix}_{(k)} + \boldsymbol{B}(k) \begin{bmatrix} i_{s\alpha} \\ i_{s\beta} \\ T_{em} \end{bmatrix}_{(k)} \\ \boldsymbol{y}(k) = \begin{bmatrix} v_{s\alpha} - R_s i_{s\alpha} - \sigma L_s \delta i_{s\alpha} \\ v_{s\beta} - R_s i_{s\beta} - \sigma L_s \delta i_{s\beta} \end{bmatrix}_{(k)} = \boldsymbol{C}(k) \begin{bmatrix} \psi_{r\alpha} \\ \psi_{r\beta} \\ \omega \\ R_r \end{bmatrix}_{(k)} \end{cases} \tag{5.2}$$

where $\boldsymbol{A}(k) = \begin{bmatrix} \left(1 - \frac{R_r}{L_r} T\right) & -\omega T & 0 & 0 \\ \omega T & \left(1 - \frac{R_r}{L_r} T\right) & 0 & 0 \\ 0 & 0 & \left(1 - \gamma \frac{T}{J}\right) & 0 \\ 0 & 0 & 0 & 1 \end{bmatrix}_{(k)}$,

$$\boldsymbol{B}(k) = \begin{bmatrix} \frac{L_m R_r}{L_r} T & 0 & 0 \\ 0 & \frac{L_m R_r}{L_r} T & 0 \\ 0 & 0 & \frac{T}{J} \\ 0 & 0 & 0 \end{bmatrix}_{(k)}, \quad \boldsymbol{C}(k) = \begin{bmatrix} -\frac{R_r L_m}{L_r^2} & -\frac{\omega L_m}{L_r} & 0 & \frac{L_m^2}{L_r^2} i_{s\alpha} \\ \frac{\omega L_m}{L_r} & -\frac{R_r L_m}{L_r^2} & 0 & \frac{L_m^2}{L_r^2} i_{s\beta} \end{bmatrix}_{(k)},$$

$$\delta i_{s\alpha}(k) = \frac{i_{s\alpha}(k) - i_{s\alpha}(k-1)}{T} \quad \text{and} \quad \delta i_{s\beta}(k) = \frac{i_{s\beta}(k) - i_{s\beta}(k-1)}{T}.$$

$T$ represents the sampling period. Equation (5.2) is used for implementing the speed and rotor resistance estimation algorithm using EKF. The motor torque command $T_{em}^{*}$ which is the output of the speed controller is used in place of $T_{em}$ in the input (command) vector.

## 5.3 Extended Kalman Filter Algorithm

Extended Kalman Filter is one of the most effective algorithms used for online estimation of states and parameters in induction motor drives. The main disadvantage of this well-known method is its computational complexity, which however is no more a problem with modern DSPs. In the case of FOC-Controlled Induction Motor presented in this thesis, in order to reduce the computational requirements and since the stator currents are available for measurement, a reduced order model of the motor is used for implementing the estimation algorithm.

Kalman Filter is a recursive mean squared estimator. It is capable of producing optimal estimates of system states that are not measured. The elements of the covariance matrices $Q$ and $R$ serve as design parameters for convergence of the system. The Kalman Filter approach assumes that the deterministic model of the motor is disturbed by centred white noise viz. the state noise and measurement noise. The discrete time-varying nonlinear model of the induction motor is of the following form:

$$x(k+1) = f(x(k), u(k), k) + W(k) \tag{5.3}$$

$$y(k) = h(x(k), k) + V(k) \tag{5.4}$$

where $f(x(k), u(k), k) = A(k)x(k) + B(k)u(k)$, $h(x(k), k) = C(k)x(k)$; and $W(k)$ and $V(k)$ are the system and measurement noises respectively. These noises are supposed to be white with zero mean and characterized by:

$$E\{W(k)\} = 0, E\{W(k), W^T(k)\} = Q(k) > 0 \tag{5.5}$$

$$E\{V(k)\} = 0, E\{V(k), V^T(k)\} = R(k) > 0 \tag{5.6}$$

The process covariance matrix $Q(k)$ and measurement covariance matrix $R(k)$ are symmetric and semi-definite. The EKF algorithm is as follows:

- ***Step 1: Prediction***

$$\hat{x}(k+1/k) = f\{\hat{x}(k/k), u(k)\} \tag{5.7}$$

$$P(k+1/k) = F(k)P(k/k)F(k)^T + Q(k) \tag{5.8}$$

where $\hat{x}(k)$ is the state estimate, $P(k)$ is the estimation error covariance matrix and

$$\boldsymbol{F}(k)=\frac{\partial}{\partial x}f\{\boldsymbol{x}(k),\boldsymbol{u}(k)\}\Big|_{x(k)=\hat{x}(k/k)} \tag{5.9}$$

- ***Step 2: Updating***

$$\hat{\boldsymbol{x}}(k+1/k+1)=\hat{\boldsymbol{x}}(k+1/k)+\boldsymbol{K}(k+1)\{y(k+1)-\boldsymbol{h}(\hat{x}(k+1/k))\} \tag{5.10}$$

$$\boldsymbol{K}(k+1)=\boldsymbol{P}(k+1/k)\boldsymbol{H}^{T}(k+1).\{\boldsymbol{H}(k+1)\boldsymbol{P}(k+1/k)\boldsymbol{H}^{T}(k+1)+R(k+1)\}^{-1} \tag{5.11}$$

$$\boldsymbol{P}(k+1/k+1)=\boldsymbol{P}(k+1/k)-\boldsymbol{K}(k+1)\boldsymbol{H}(k+1)\boldsymbol{P}(k+1/k) \tag{5.12}$$

where $\boldsymbol{K}$ is the Kalman gain matrix, $(k+1/k)$ denotes prediction at time $(k+1)$ based on data up to and including $k$ and

$$\boldsymbol{H}(k+1)=\frac{\partial}{\partial x}h\{x(k+1)\}\Big|_{x(k+1)=\hat{x}(k+1/k)} \tag{5.13}$$

## 5.4 Simulation Results

Simulation is carried out in order to verify the performance of the speed and rotor resistance estimation algorithm in addition to verifying the response of the drive system. The block diagram of the vector controlled induction motor drive system incorporating the estimation algorithm is shown in Figure 5.1.

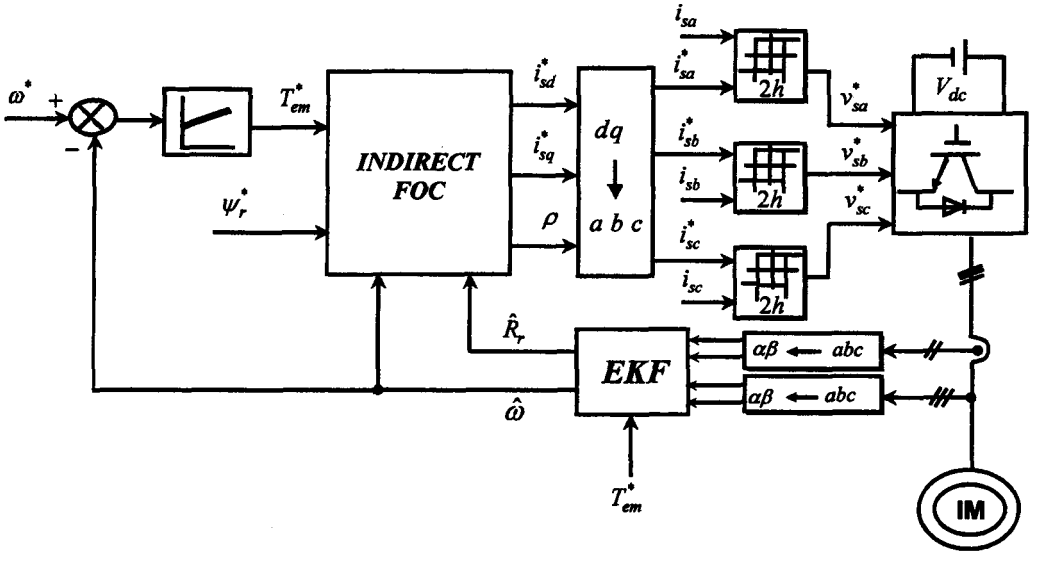


**Figure 5.1** Sensorless indirect FOC induction motor drive

Verification of the performance of the estimation algorithm and the drive system is carried out starting with load torque $T_L = K_v\omega$. First, acceleration and reversal of the drive is carried out in order to observe the performance of the estimator during the operation. The machine is accelerated at 0.12 sec to a command speed of 150 rad/s and then it is reversed at 3 sec. The rotor resistance is changed abruptly during steady state operation of the drive.

Its value is increased from the nominal value of 5.365 Ω to 7 Ω at 0.75 s, and then decreased to original value at 2.25 sec. The resistance is increased again to 7 Ω at 3.75 s, and then decreased to its nominal value at 5.25 sec. The speed ($\omega_m$), estimated speed ($\hat{\omega}_m$) and speed estimation error ($\omega_m - \hat{\omega}_m$) are shown in Figure 5.2 (a). Figure 5.2 (b) shows the rotor resistance ($R_r$), estimated rotor resistance ($\hat{R}_r$) and rotor resistance estimation error ($R_r - \hat{R}_r$).

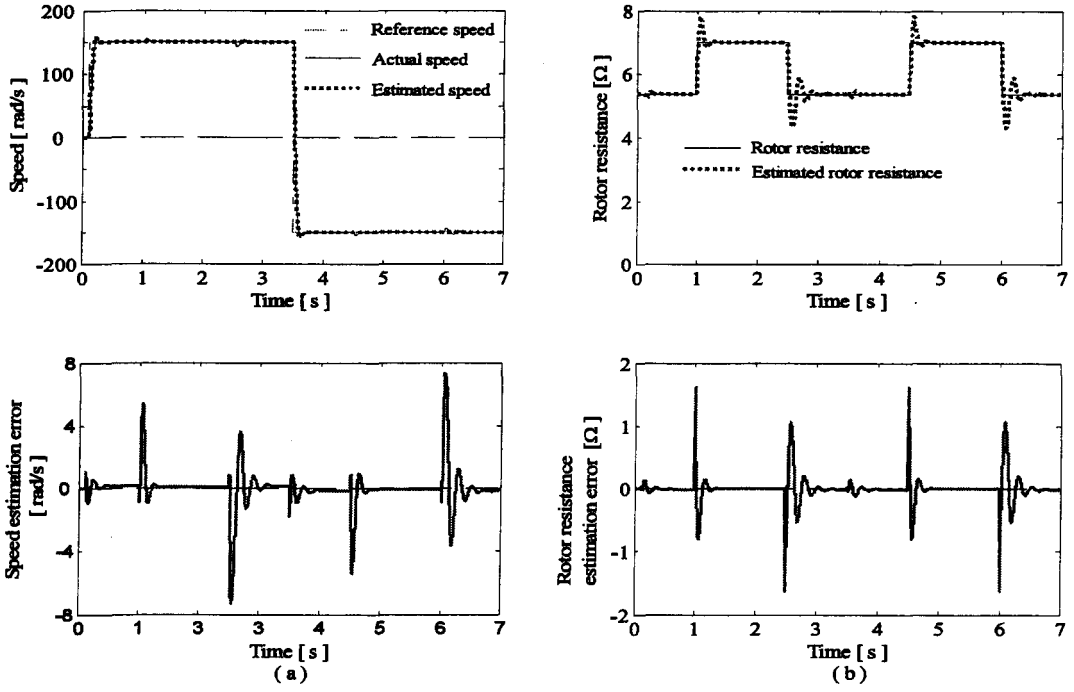


**Figure 5.2** Acceleration and reversal (with $T_L=K_v\omega$); (a) reference, actual and estimated speed, and speed estimation error; (b) rotor resistance, estimated rotor resistance and rotor resistance estimation error

Next, the speed is increased in steps with sudden changes in rotor resistance. The machine is accelerated to 50 rad/s at t=0.12 sec then, the speed is increased in steps to 100 rad/s at 2.5 sec and finally to 150 rad/s at 4.5 s. The rotor resistance is varied with sudden changes in its value in order to observe the performance of the estimator at these speeds. The rotor resistance is increased from its nominal value of 5.365 Ω to 7 Ω at 1.25 sec and then brought down to nominal value at 3 sec. It is increased again to 7 Ω at 4 sec and brought down to nominal value at 5.5 sec. The estimation results and response of the sensorless drive is shown in Figure 5.3.

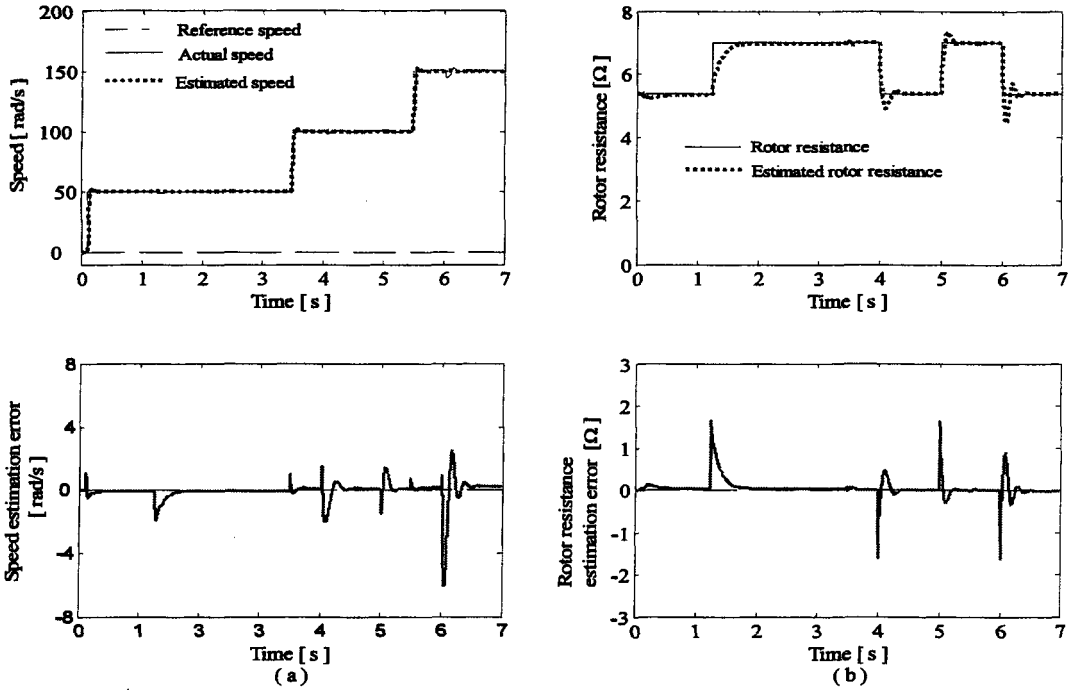


**Figure 5.3** Operation at various speeds (with $T_L=K_v\omega$); (a) reference, actual and estimated speed, and speed estimation error; (b) rotor resistance, estimated rotor resistance and rotor resistance estimation error

Then, the motor load is changed to a blower or centrifugal pump type load. The load torque in this case is proportional to square of the speed ($T_L = K_b\omega^2$). Simulation is carried out with the reference speed and rotor resistance profile similar to previous case when $T_L = K_v\omega$. Estimation results for acceleration and speed reversal, along with sudden changes in rotor resistance is shown in Figure 5.4.

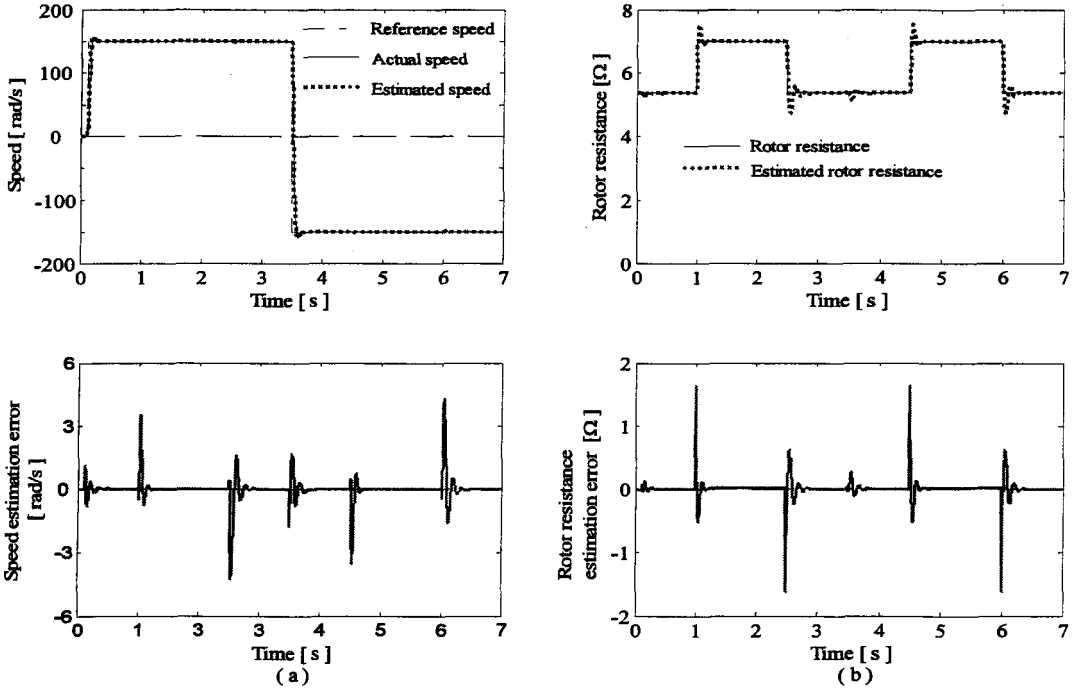


**Figure 5.4** Acceleration and reversal (with $T_L=K_b\omega^2$ ); (a) reference, actual and estimated speed, and speed estimation error; (b) rotor resistance, estimated rotor resistance and rotor resistance estimation error

Then, the performance of the estimation algorithm and response of the drive are verified for step increase in speed along with sudden changes in rotor resistance. The estimation results and response of the drive system are shown in Figure 5.5.

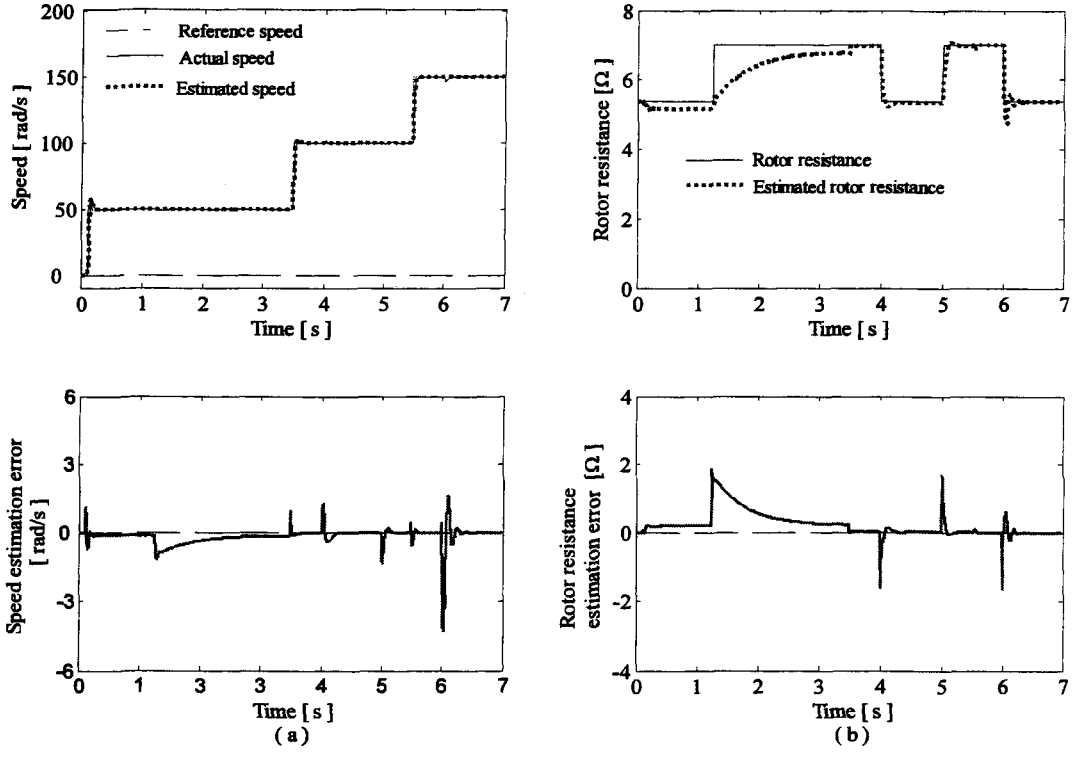


**Figure 5.5** Operation at various speeds (with $T_L=K_b\omega^2$); (a) reference, actual and estimated speed, and speed estimation error; (b) rotor resistance, estimated rotor resistance and rotor resistance estimation error

## 5.5 Conclusion

In this chapter, a new sensorless vector controlled induction motor drive robust against rotor resistance variation has been developed. Mathematical model of the motor used for implementing estimation algorithm contains electromechanical equation of the drive in order to take coupling between electrical and mechanical modes into consideration, which is true especially for small sized machines. Speed and rotor resistance estimation algorithm is implemented using EKF which has established itself as one of the standard algorithms for state and parameter estimation of nonlinear systems. Computational burden for implementing the algorithm is reduced in this work by using reduced order EKF. However, with modern day DSPs and FPGAs having fast computation capabilities, implementing EKF is not considered to be a problem any more. Simultaneous estimation of speed and rotor resistance is achieved without injecting any external signal which is believed to be a major contribution in the area of variable speed induction motor drives. The proposed method is applicable to a large category of induction motor drives with a gradually varying load such as, viscous friction load, fan/blower and centrifugal pump.

# CHAPTER 6

# REAL-TIME DIGITAL SIMULATION

## 6.1 Real-Time Systems

Real-time simulation can refer to the events simulated by a system (for example, a computer) at the same speed they would occur in real life. As an example, in graphic animation, a real-time program would display the objects moving across the screen at the same speed they would actually move. In reference to embedded systems, real-time denotes the required stability of the embedded system. In a real-time system, the embedded device is given a predetermined amount of time, such as 1ms, 5ms, or 20ms to read input signals, such as sensors, to perform all necessary calculations, such as control algorithms, and to write all outputs, such as control actuators, and control fuel flow. Most general–purpose systems are not real-time because they take a few seconds, or even minutes, to react. Thanks to the speed of new processors, it's possible nowadays to implement complex control systems using real-time simulation.

Typically, a real-time system consists of a controlling system and a controlled system. In this type of systems the correctness of the system not only depends on the logical results

of the computations, but also depends on the time at which the results are produced. The controlling system interacting with a real-world plant is based on the information obtained from various sensors and inputs that measure the actual state of the plant. The information presented to the controller must be consistent with the actual state of the environment, or the actions of the controlling system can be disasters.

## 6.2 Real-Time Systems Requirements

In most of the real-time systems, severe consequences result if the timing and logical correctness requirements of the system are not satisfied. The requirements on a real-time-capable system can be attributed to three basic concepts: data throughput, responsiveness and determinism. Data throughput is the speed at which the data is recorded and processed. Responsiveness denotes the time-delay between the occurrence of an event and the availability of the corresponding output data. Deterministic system behaviour requires that the input data occurring at a determined rate can be processed online without any data being lost [71]. The system must react to the events in a predictable manner under all operating conditions and be able to complete the corresponding calculations within the guaranteed response time.

A real-time system must be able to handle time constraints which are commonly divided into two categories: hard real-time systems and soft real-time systems. In soft real-time systems, time correctness is important but not critical while in hard real-time systems it is

critically important and may not be sacrificed for other gains. Computer control in hard real-time systems is becoming common in a wide range of uses, especially in safety critical systems. Timing is no longer a node internal issue since each node has to synchronize its actions with other nodes regarding their time limitations [72].

Therefore, being real-time does not mean for a system, the data is processed as quickly as it's possible according to the used equipments. It rather means that the defined time limits are observed, whereas the absolute limitation values depend on each individual application. The goal of a real-time operation system is to manage the resources of a system in accordance with the above mentioned requirements [73, 74]. Setting the step time very small may make the system behaviour very similar to the real (analog) environment, but the hardware implementation of the system is technologically limited by the hardware (such as CPU time). So, the sampling time can be increased until the results have not been affected by this increase.

## 6.3 Concept of Real-Time Digital Simulation

PC-Cluster based real-time simulation is now widely used by high-tech industries, particularly automotive [75-78] and aeronautics industries (aircraft flight control, satellite control, etc.), as the main tool for rapid prototyping of complex engineering systems in a cost-effective and secure manner, while reducing the time-to-market.

A PC-Cluster is a parallel multiprocessor computer system capable of meeting the real-time performance requirements during simulation. Figure 6.1 shows the concept of digital real-time simulation of an induction motor drive system. Real-time simulation is achieved by running on separate processors (targets) and in parallel the (i) controllers and estimators, (ii) static converter and induction motor, (iii) data acquisition and user interface. These three modules are actually C-codes (numerical modules) obtained by an automatic code generator for real-time execution.

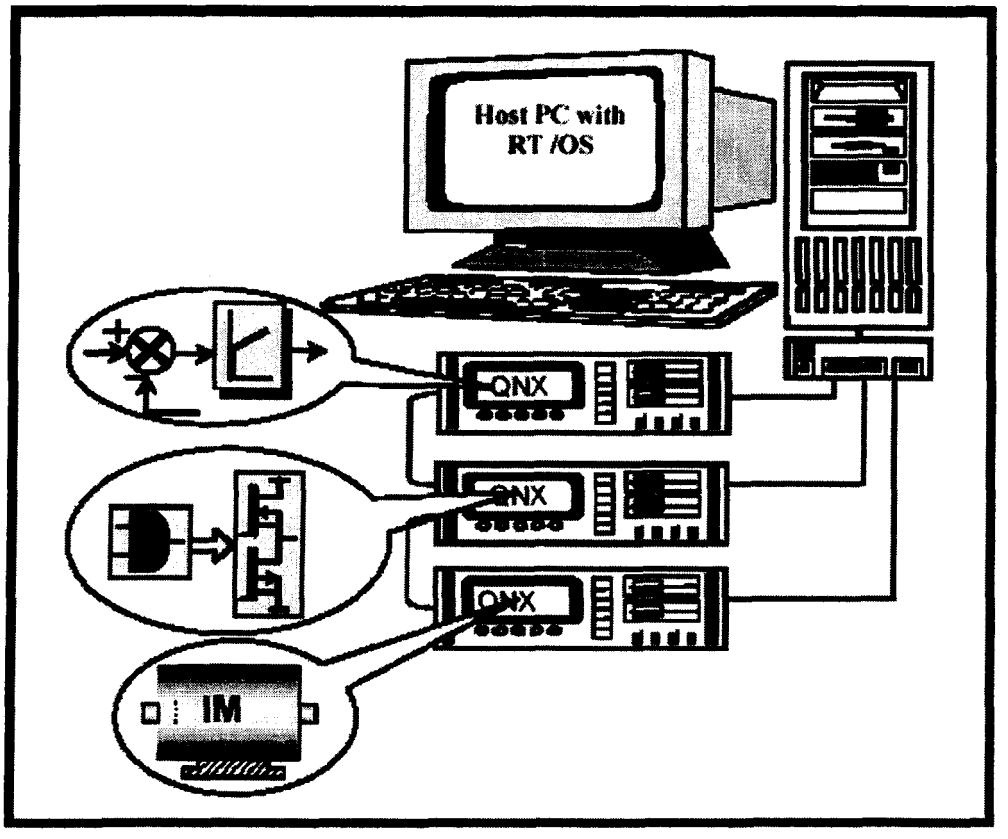


**Figure 6.1** Real-time simulation of induction motor drive system

Real-time simulation is the first step in any rapid control prototyping development project. As soon as the design requirements are fulfilled, the physical process to be controlled may be integrated, via fast I/O interfaces and replace its real-time model, with the simulation environment as shown in Figure 6.2.

Once the Hardware-in-the-Loop simulation has been completed, the automatically generated code of the real-time model of the controller may be used as the actual control system by transferring it into the memory of an embedded controller. This procedure is known as Rapid Control Prototyping.

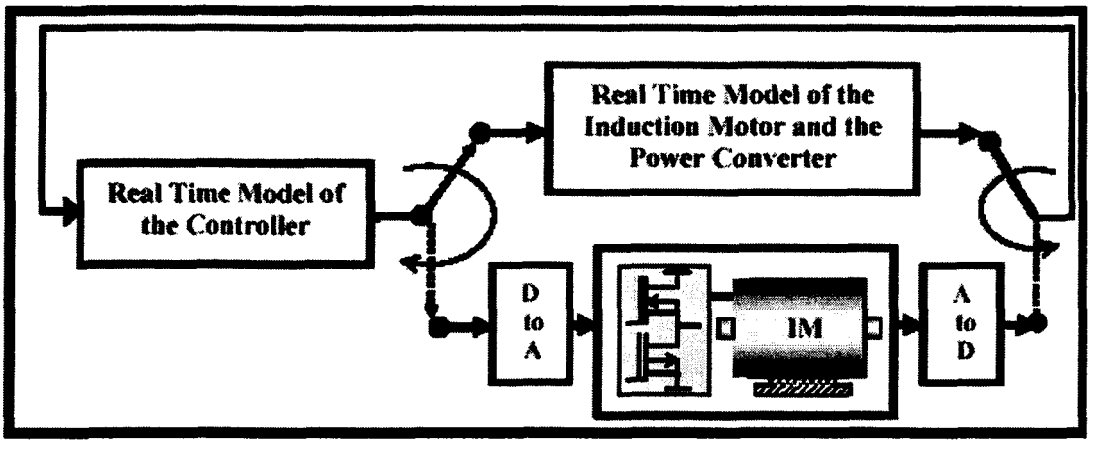


**Figure 6.2** Hardware in the loop simulation of induction motor drive system

## 6.4 Implementation of Real-Time Digital Simulation

The performance of the high performance sensorless vector controlled induction motor drives incorporating the estimation algorithms (as shown in Figure 4.2, 4.7, 4.15 and 5.1) are verified by performing a PC cluster based real-time digital simulation using RT-Lab software package. As shown in Figure 6.3, RT-Lab [79] uses Matlab/Simulink as a front-end interface for editing graphic models in block-diagram format, which are afterwards used by this real-time simulator to generate the necessary C-codes for real-time simulations on a single or more target processors running QNX.

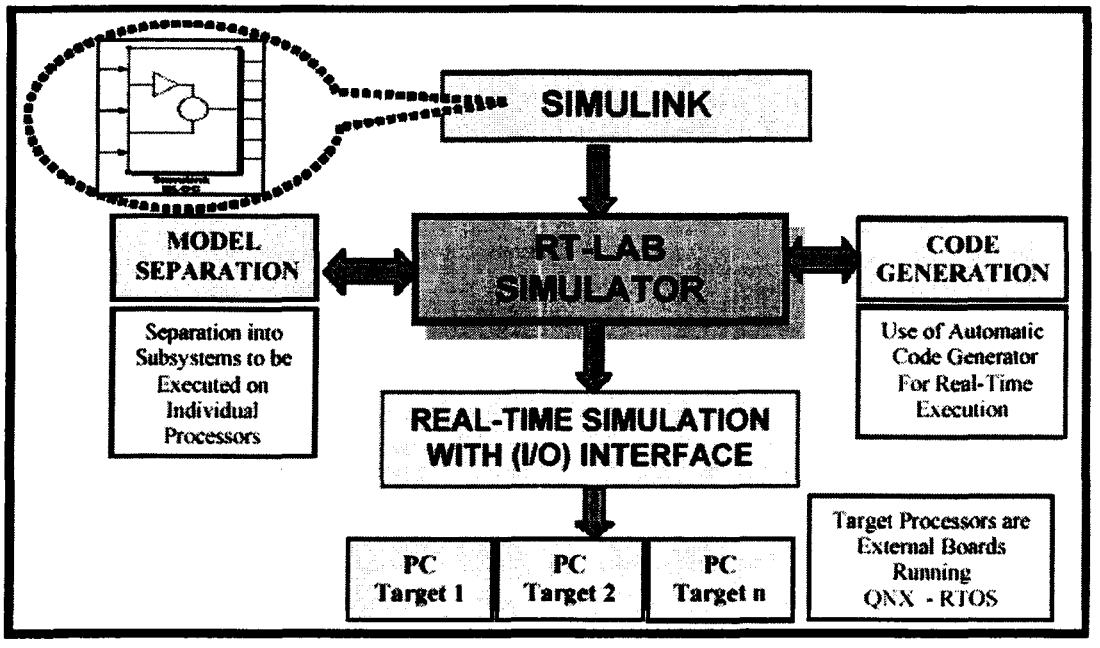


Figure 6.3 Principle of real-time simulation using RT Lab

The sensorless drive systems are taken one by one and real time digital simulation is carried out in order to verify the accuracy of the estimation algorithms in addition to verifying the response of the drive systems. Each drive system in its turn is distributed over three target processors. The first two target processors are Pentium III running at 480 MHz, installed on a dual-CPU motherboard with shared memory of 512 MB. The third one, connected to the others through a fast Fire Wire real-time link, is a Pentium III running at 400 MHz with 128 Mbytes of memory. The first CPU of the dual-CPU unit, acting as slave #1: **ss_controller_estimator**, computes in real-time the estimator algorithms, the controllers, the rotor flux decoupling unit and the coordinate transformation unit. The second one, acting as slave # 2: **ss_inv_motor**, computes in realtime the induction motor, the PWM signal generator and the voltage source inverter. The third processor, acting as master: **sm_data_aquisition,** is dedicated to data acquisition. **sc_user_interface** is the console used for input reference and command signals and for signal visualisation. These block diagrams are actually Simulink models grouped to form a subsystem. Once the models are grouped into console (**sc_**), data acquisition (**sm_**) and computation (**ss_**) subsystems, special blocks called OpComm blocks must be inserted into the subsystems. These are simple feed-through blocks that intercept all incoming signals before sending them to computation blocks and provide information to RT-Lab concerning the type and size of these intercepted signals. This signal interception is mandatory because when a simulation model runs in the RT-Lab environment; all connections between the main subsystems are replaced by hardware communication links. Opcomm also controls the speed of data flow between the subsystems in addition to controlling the subsystem

sampling time. In this work the sampling time for the slaves are set to 50 μs while the sampling time for the master is set to 1 ms. The drive control system in RT Lab environment is as shown in Figure 6.4.

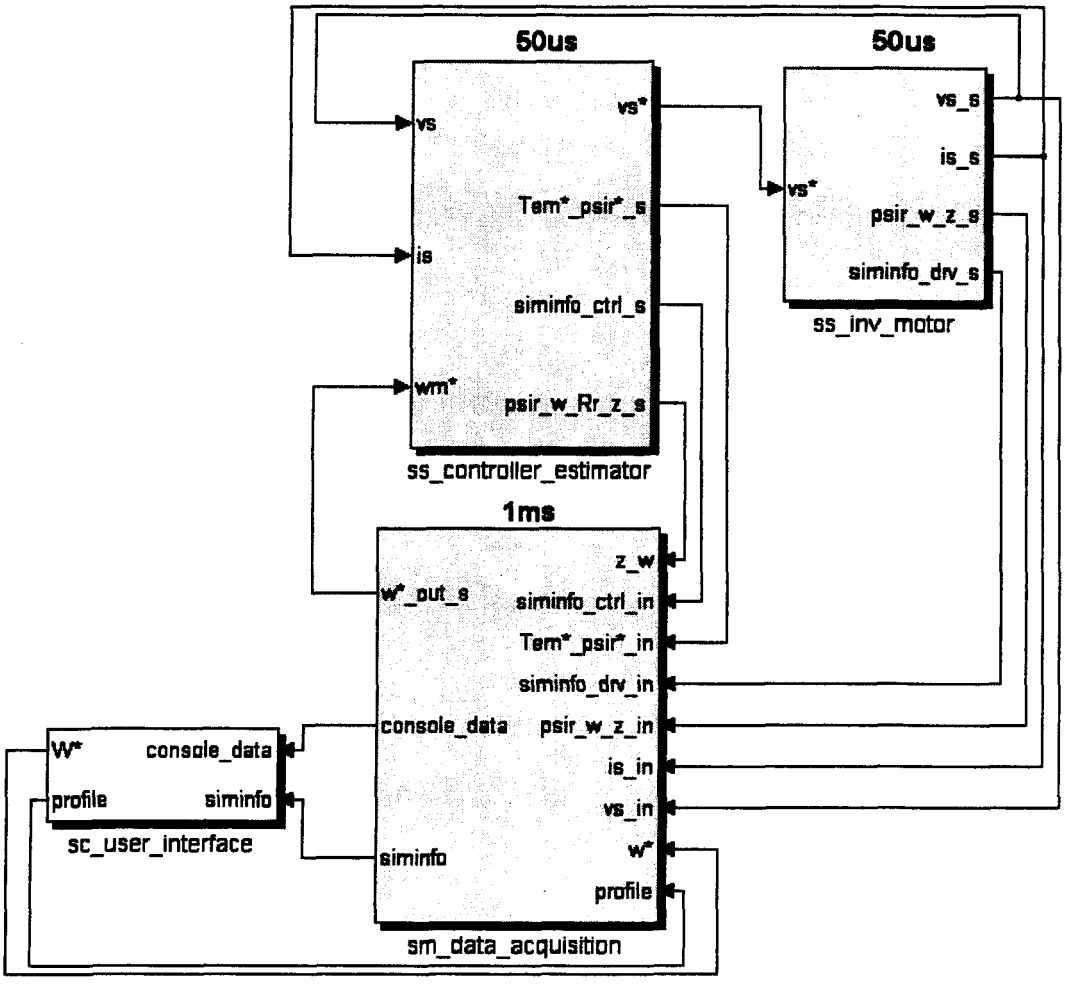


**Figure 6.4** RT Lab model of the induction machine sensorless drive

### 6.4.1 Speed Estimation in Vector Controlled Induction Motor Drive

The sensorless drive control scheme shown in figure 4.2 is distributed over three processors as shown in Figure 6.4. The slave #1: **ss_controller_estimator** subsystem computes in real-time the speed estimation algorithm, the speed controller, the rotor flux decoupling unit, the coordinate transformation and the current controllers, whereas, the slave #2: **ss_inv_motor** computes the induction motor, the PWM signal generator and the voltage source inverter. The master: **sm_data_aquisition,** is dedicated to data acquisition, and **sc_user_interface** is the console used for input reference and command signals and for signal visualisation.

Performance of the sensorless drive is verified under various operating conditions. Initially, the drive is run at no load. Figure 6.5 shows the response of the unloaded drive system during starting and speed reversal. The speed of the motor $(\omega_m)$, estimated speed $(\hat{\omega}_m)$ and reference speed $(\omega_m^*)$ are shown in Figure 6.5 (a). Actual speed is the speed obtained from the simulated model of the motor. Figure 6.5 (b) shows speed estimation error $(\omega_m - \hat{\omega}_m)$. The newly defined quantity $(Z)$ and its estimated value $(\hat{Z})$ are shown in Figure 6.5 (c) and their estimation error $(Z - \hat{Z})$ is shown in Figure 6.5 (d).

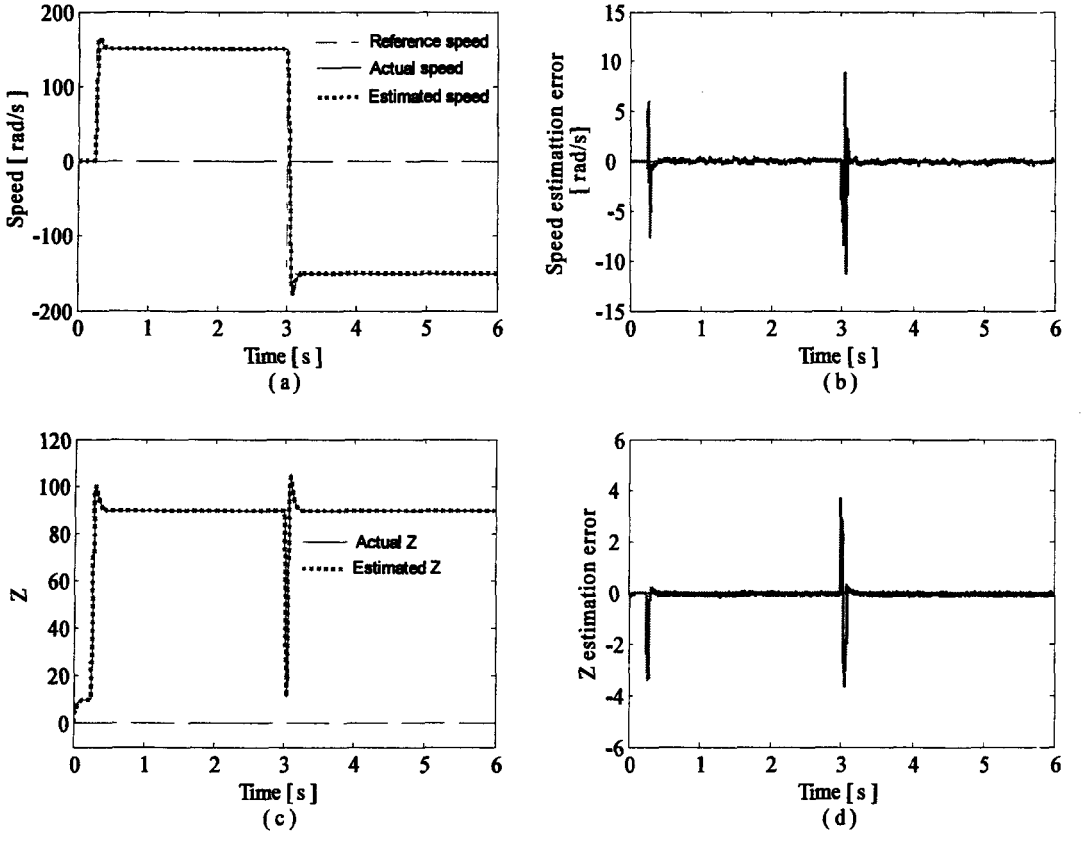


**Figure 6.5** No load operation; (a) reference, actual and estimated speed, (b) speed estimation error, (c) actual *Z* and estimated *Z*, and (d) Z estimation error

Then, the drive system is subjected to loading and unloading conditions. The machine is started at no load at 0.25 sec then, full load is applied at 1 sec and the load is completely removed at 2 sec. Later, after speed reversal, full load is applied at 4 sec and the load is fully removed at 5 sec. The response of the sensorless drive on application and removal of load is shown in Figure 6.6 (a - d).

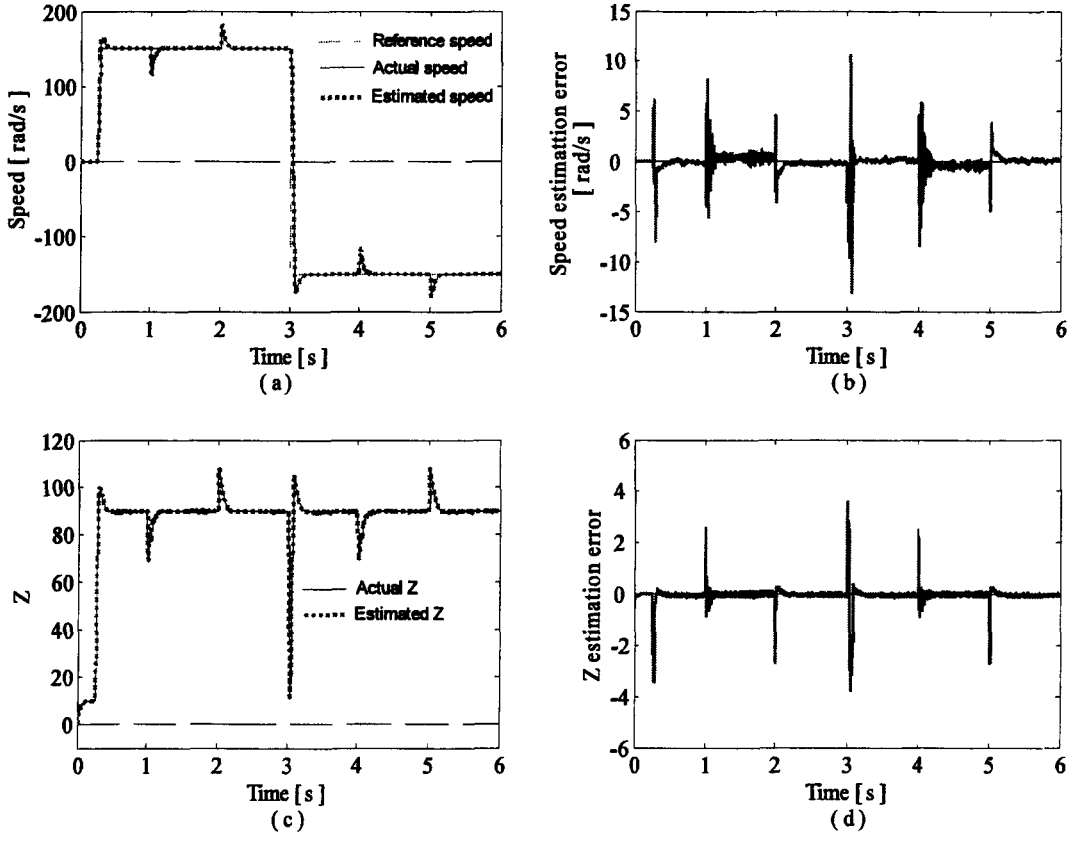


**Figure 6.6** Loading and unloading; (a) reference, actual and estimated speed, (b) speed estimation error, (c) actual *Z* and estimated *Z*, and (d) Z estimation error

The drive is then, operated under full load conditon at various speeds. The fully loaded drive is started at 0.25 sec to 150 rad/s and the speed is reduced in steps to 75 rad/s at 2 sec and then to 25 rad/s at 4 sec in order to observe the speed estimation accuracy and response of the loaded drive at various speeds. Figure 6.7 shows results of operation under under above-mentioned conditions.

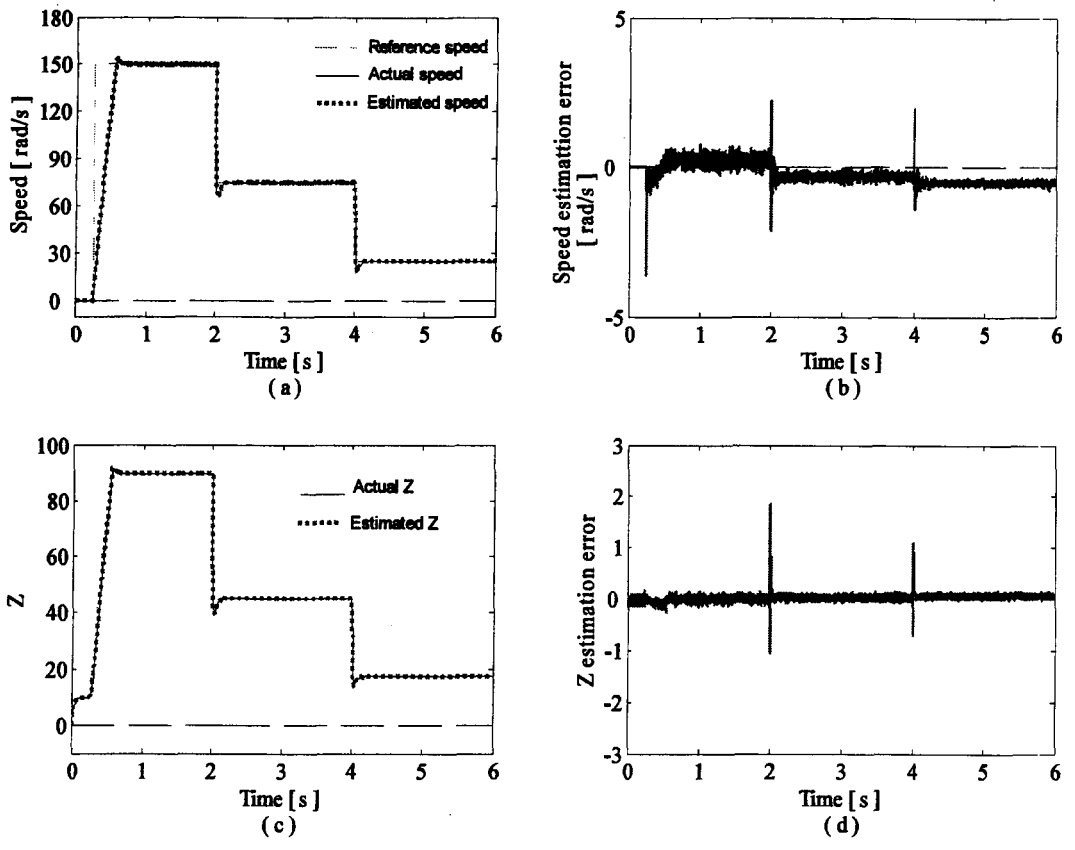


Figure 6.7 Full load operation at various speeds; (a) reference, actual and estimated speed, (b) speed estimation error, (c) actual *Z* and estimated *Z*, and (d) Z estimation error

### 6.4.2 Improvement in Speed Estimation

Improvement in speed estimation and drive dynamics was suggested in section 4.2.4. The sensorless drive control scheme shown in figure 4.7 is distributed over three processors as shown in Figure 6.4. In this case, the slave #1: **ss_controller_estimator** subsystem computes in real-time the speed estimation algorithm, flux estimation algorithm, the speed controller, the flux controller, the current controllers and the coordinate transformation, whereas, the slave #2: **ss_inv_motor** computes the induction motor, the PWM signal generator and the voltage source inverter. The master: **sm_data_aquisition,** is dedicated to data acquisition, and **sc_user_interface** is the console used for input reference and command signals and for signal visualisation.

The accuracy of the estimation algorithm and performance of the drive system incorporporating the estimation algorithms are verified under various operating conditions. First, the sensorless drive is run without load to verify the performance of the observer under no-load condition. The drive is run at various operating speeds by increasing the speed in steps to 10 rad/s, 50 rad/s, 100 rad/s and 150 rad/s at 0.5 sec, 1.5 sec, 3 sec and 4.5 sec respectively. The speed of the motor ($\omega_m$), estimated speed ($\hat{\omega}_m$), reference speed ($\omega_m^*$) and speed estimation error ($\omega_m - \hat{\omega}_m$) are shown in Figure 6.8 (a). Figure 6.8 (b) shows the actual Z, estimated Z and Z estimation error ($Z - \hat{Z}$).

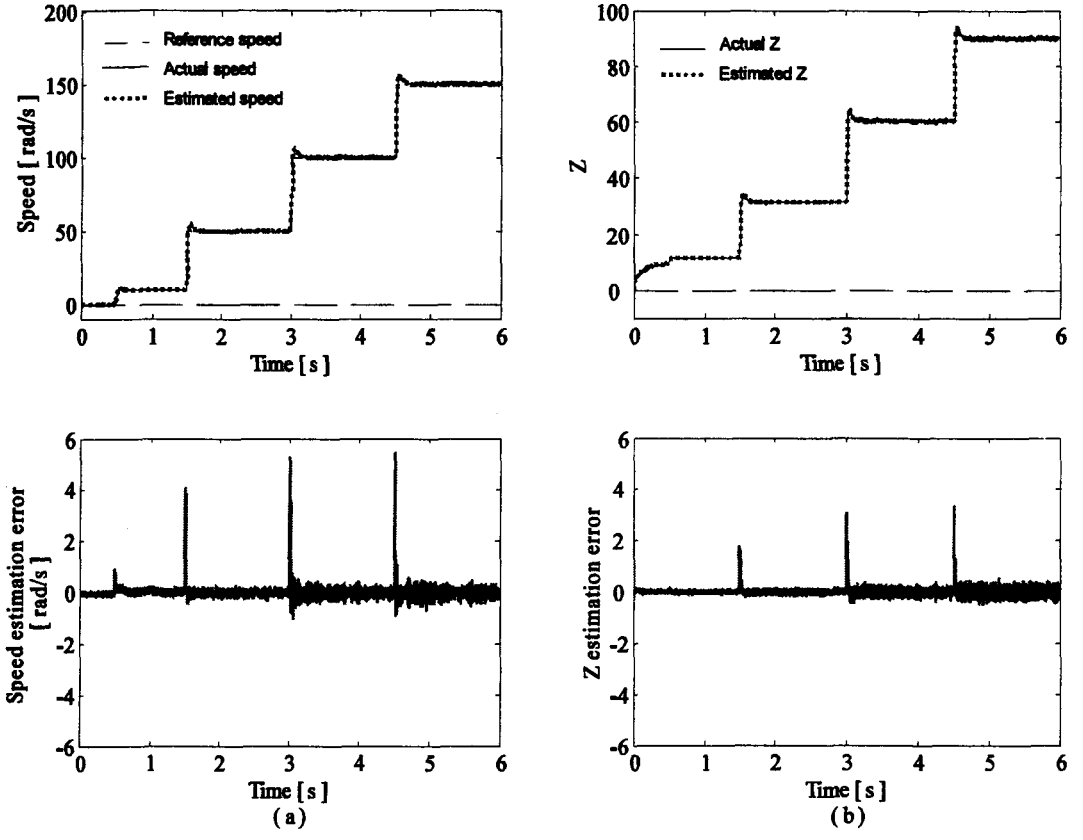


**Figure 6.8** No load operation at various speeds; (a) reference, actual and estimated speed, and speed estimation error, (b) actual *Z*, estimated *Z* and *Z* estimation error

The sensorless drive system is then subjected to a slow change in speed profile (trapezoidal) without applying any load during the whole operation. The results of real-time digital simulation during this operation are shown in Figure 6.9.

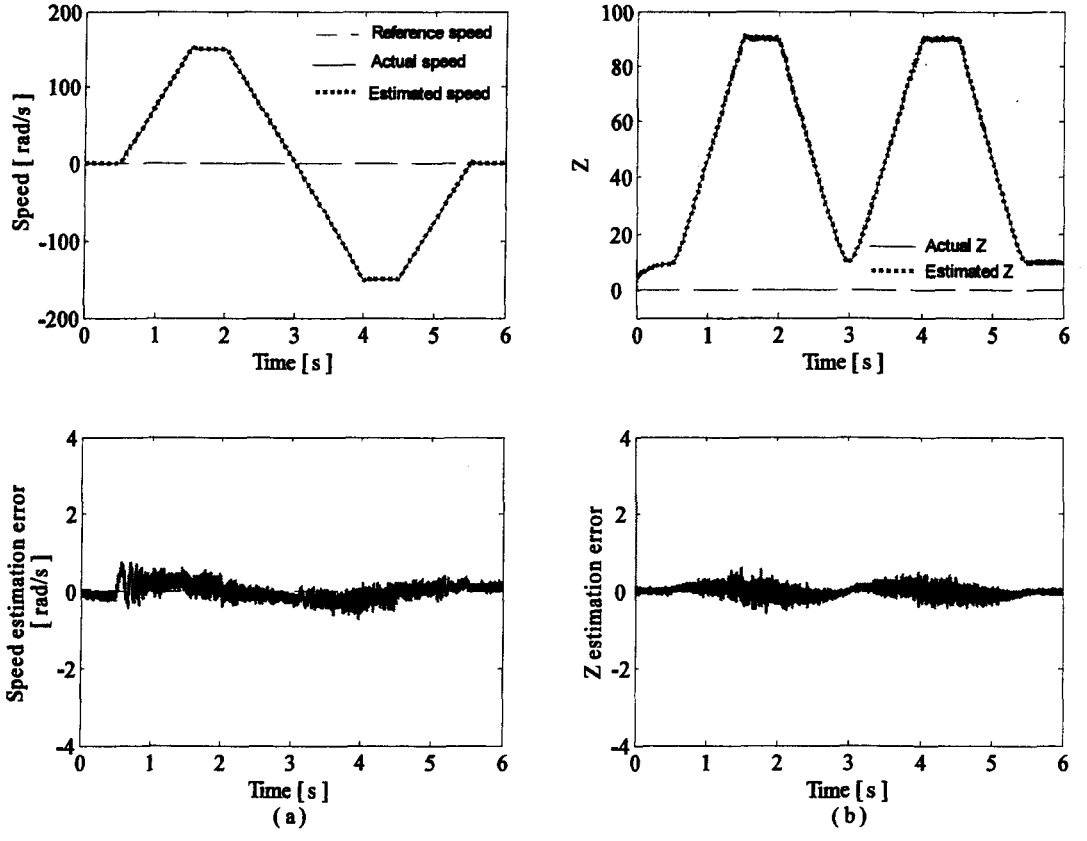


**Figure 6.9** No load operation with trapezoidal speed profile; (a) reference, actual and estimated speed, and speed estimation error, (b) actual *Z*, estimated *Z* and *Z* estimation error

Next, the performance of the estimator is verified on loading and unloading. The drive is started at 0.5 sec without any load to a speed of 150 rad/s and full load is applied at 1 sec; then, the load is removed completely at 2 sec. Later, after speed reversal at no load, full load is applied at 4 s and the load is fully removed at 5 s. The response of the drive on application and removal of load is shown in Figure 6.10.

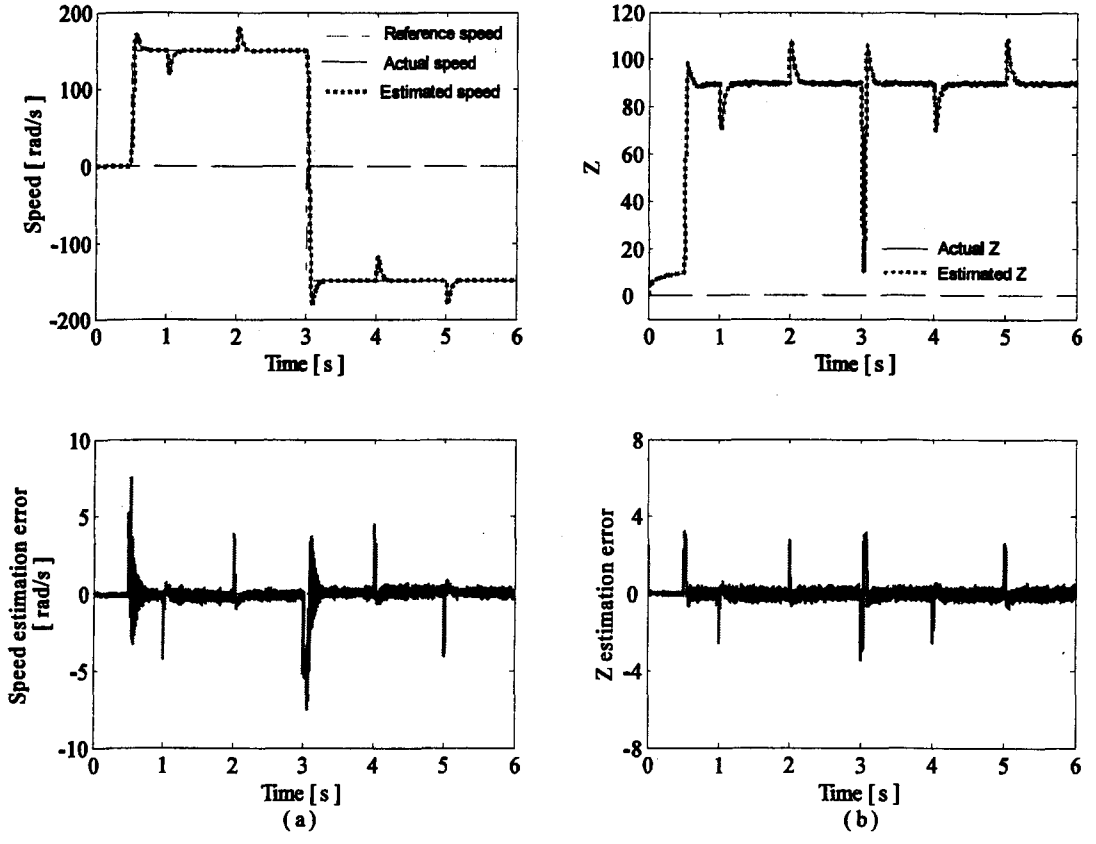


**Figure 6.10** Application and removal of load; (a) reference, actual and estimated speed, and speed estimation error, (b) actual *Z*, estimated *Z* and *Z* estimation error

Then, the performance of the estimator is verified under fully loaded condition of the drive at various operating speeds. The fully loaded drive is accelerated to 150 rad/s at 0.3 s, and then, the speed is reduced in steps to 100 rad/s, 50 rad/s and 10 rad/s at 1.5 sec, 3 sec and 4.5 sec respectively. Figure 6.11 shows the real-time simulation results during the operation of the drive.

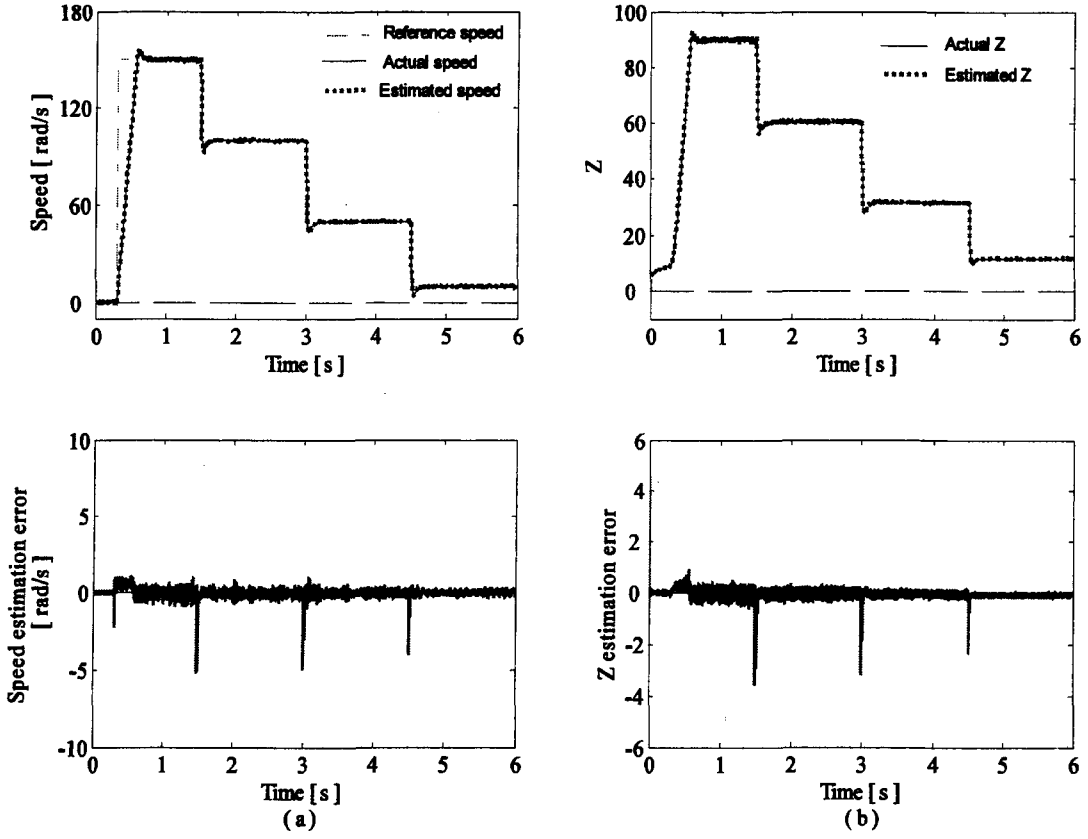


**Figure 6.11** Full load operation at various reference speeds; (a) reference, actual and estimated speed, and speed estimation error, (b) actual *Z*, estimated *Z* and *Z* estimation error

### 6.4.3 Flux Estimation for Speed Sensorless Induction Motor Drive

In this section the results of real-time digital simulation of the joint estimation algorithm for rotor flux and speed proposed in section 4.3.1 is presented. The vector controlled drive scheme incorporating the estimation algorithm shown in figure 4.15 is distributed over three processors as shown in Figure 6.4. In this case, the slave #1: **ss_controller_estimator** subsystem computes in real-time the rotor flux and speed estimation algorithm, the speed controller, the current controllers and the coordinate transformation; whereas, the slave #2: **ss_inv_motor** computes the induction motor, the PWM signal generator and the voltage source inverter. The master: **sm_data_aquisition,** is dedicated to data acquisition, and **sc_user_interface** is the console used for giving command signals and for signal visualisation.

The accuracy of the flux and speed estimation algorithm and performance of the drive system incorporporating the estimation algorithm are verified under various operating conditions. First, acceleration and speed reversal at no load is performed. A speed command of 150 rad/s at 0.5 sec is given to the drive system which was initially at rest, and then the speed is reversed at 3 sec. The response of the drive is shown in Figure 6.12. Figure 6.12 (a) shows reference ($\omega_m^*$), actual ($\omega_m$), estimated ($\hat{\omega}_m$) speed, and speed estimation error ($\omega_m - \hat{\omega}_m$). The module of the actual ($|\Psi_r|$), estimated ($|\hat{\Psi}_r|$) rotor flux, and rotor flux estimation error ($|\Psi_r| - |\hat{\Psi}_r|$) are shown in Figure 6.12 (b).

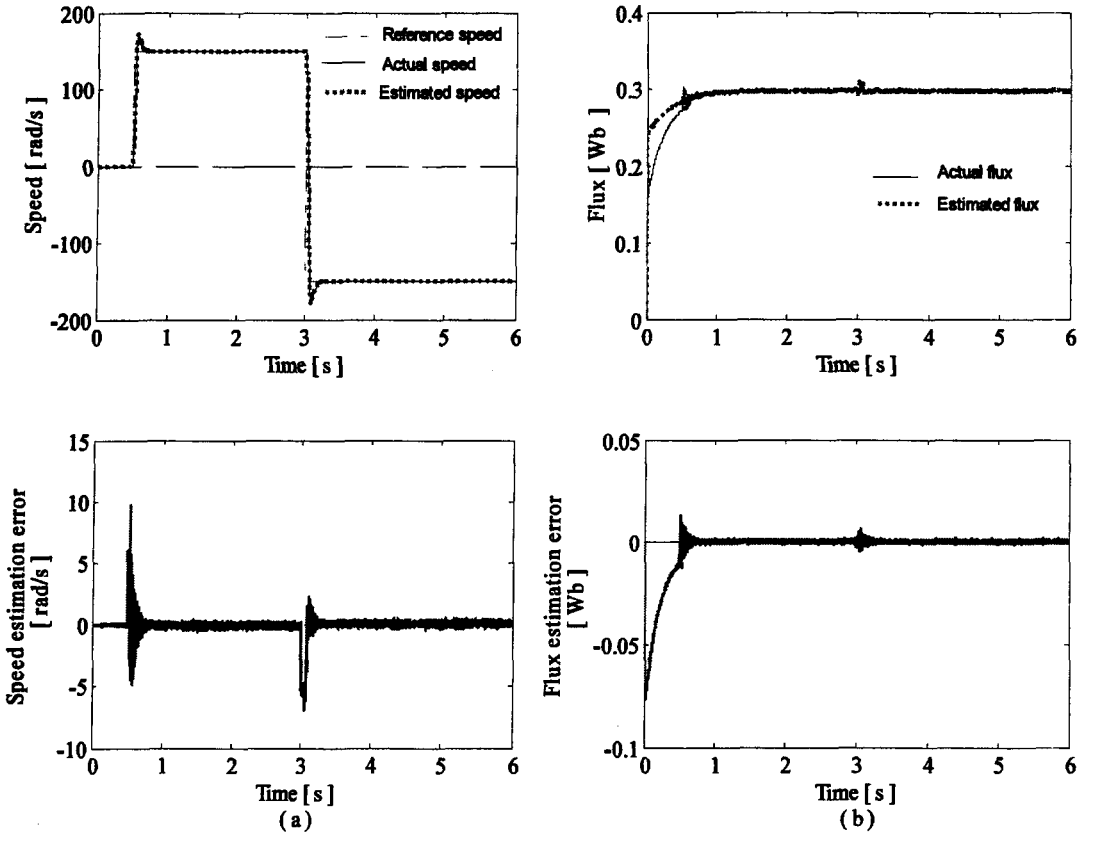


**Figure 6.12** Acceleration and speed reversal at no-load; (a) reference, actual and estimated speed, and speed estimation error; (b) actual and estimated rotor flux, and rotor flux estimation error

The drive is then run at various speeds under no load condition. It is accelerated from rest to 10 rad/s at 0.5 sec, then accelerated further to 50 rad/s, 100 rad/s and 150 rad/s at 1.5 sec, 3 sec and 4.5 sec respectively. Figure 6.13 shows the results of estimation of rotor flux and speed, and the response of the sensorless drive system.

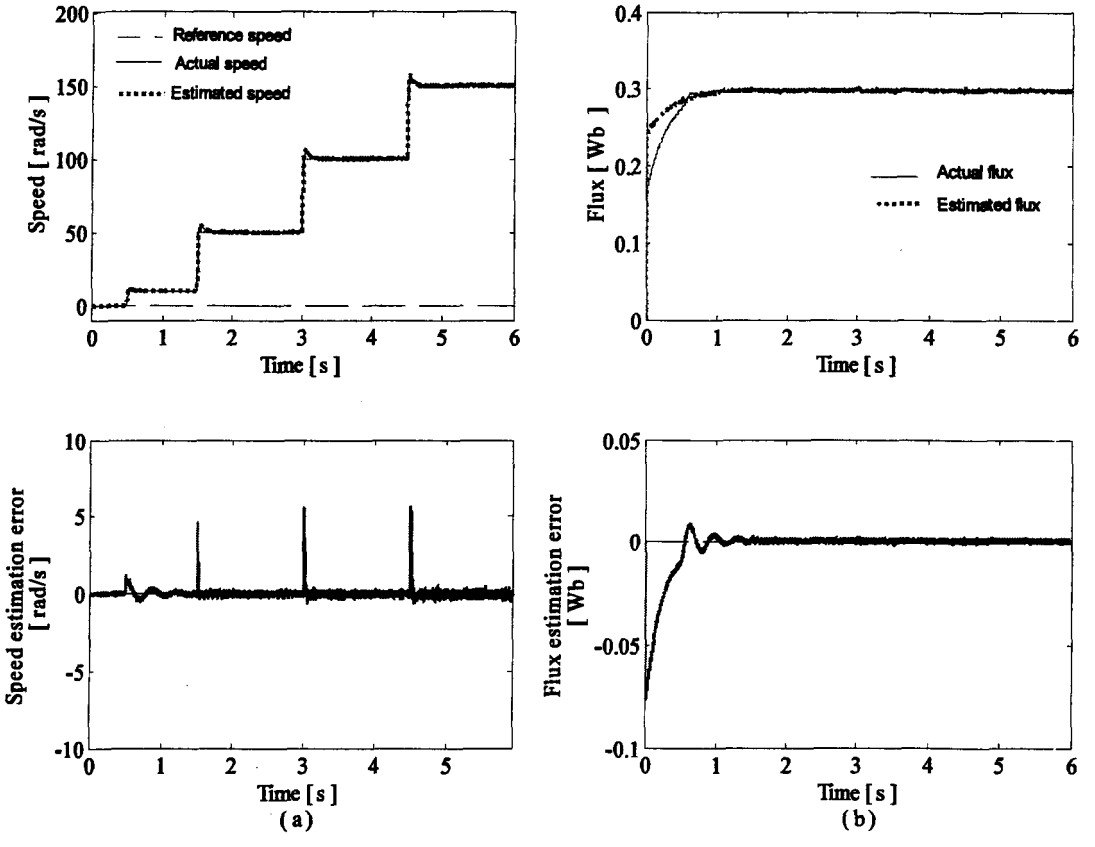


**Figure 6.13** No-load operation at various speeds; (a) reference, actual and estimated speed, and speed estimation error; (b) actual and estimated rotor flux, and rotor flux estimation error.

Then, the drive is subjected to a slow change in reference speed profile (trapezoidal), the results of which are shown in Figure 6.14.

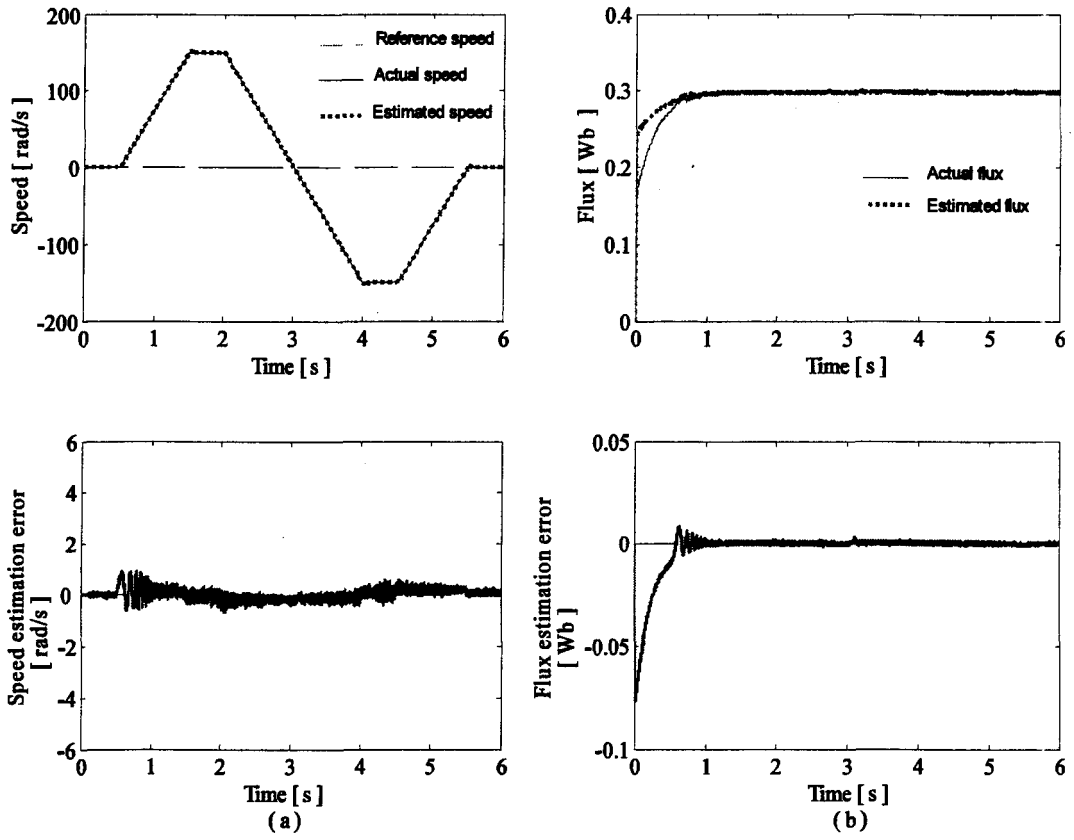


**Figure 6.14** No-load operation with trapezoidal speed profile; (a) reference, actual and estimated speed, and speed estimation error; (b) actual and estimated rotor flux, and rotor flux estimation error.

Further, the performance of the estimator is verified under loaded conditions at various operating speeds. The fully loaded drive is accelerated to 150 rad/s at 0.5 sec and then decelerated in steps to 100 rad/s, 50 rad/s and 10 rad/s at 1.5 sec, 3 sec and 4.5 sec respectively. Figure 6.15 shows the estimation results and response of the loaded drive system.

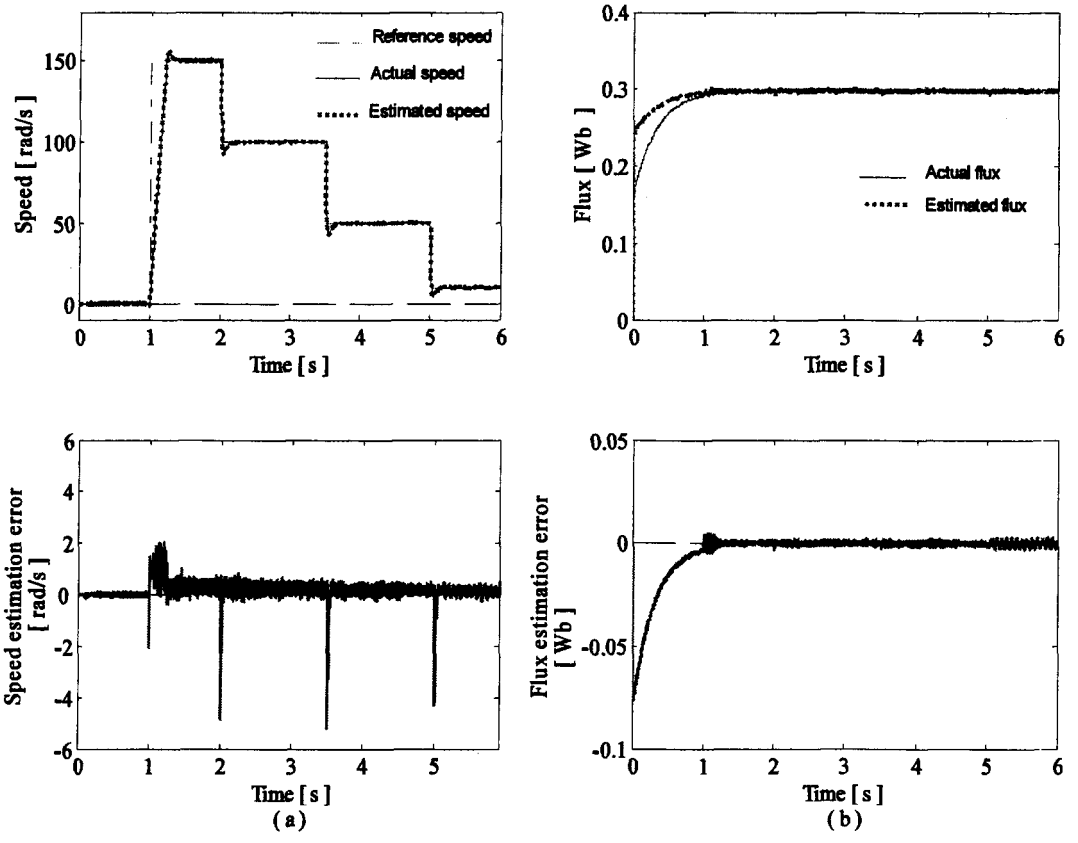


**Figure 6.15** Full load operation at various speeds; (a) reference, actual and estimated speed, and speed estimation error; (b) actual and estimated rotor flux, and rotor flux estimation error

The performance of the estimator is then verified on loading and unloading. The drive at rest is accelerated at no-load to 150 rad/s at 0.5 sec and full load is applied at 1 sec; the load is then removed completely at 2 sec. Later, after speed reversal, full load is applied at 4 sec, then, the load is fully removed at 5 sec. Figure 6.16 shows the estimation results and the response of the sensorless drive.

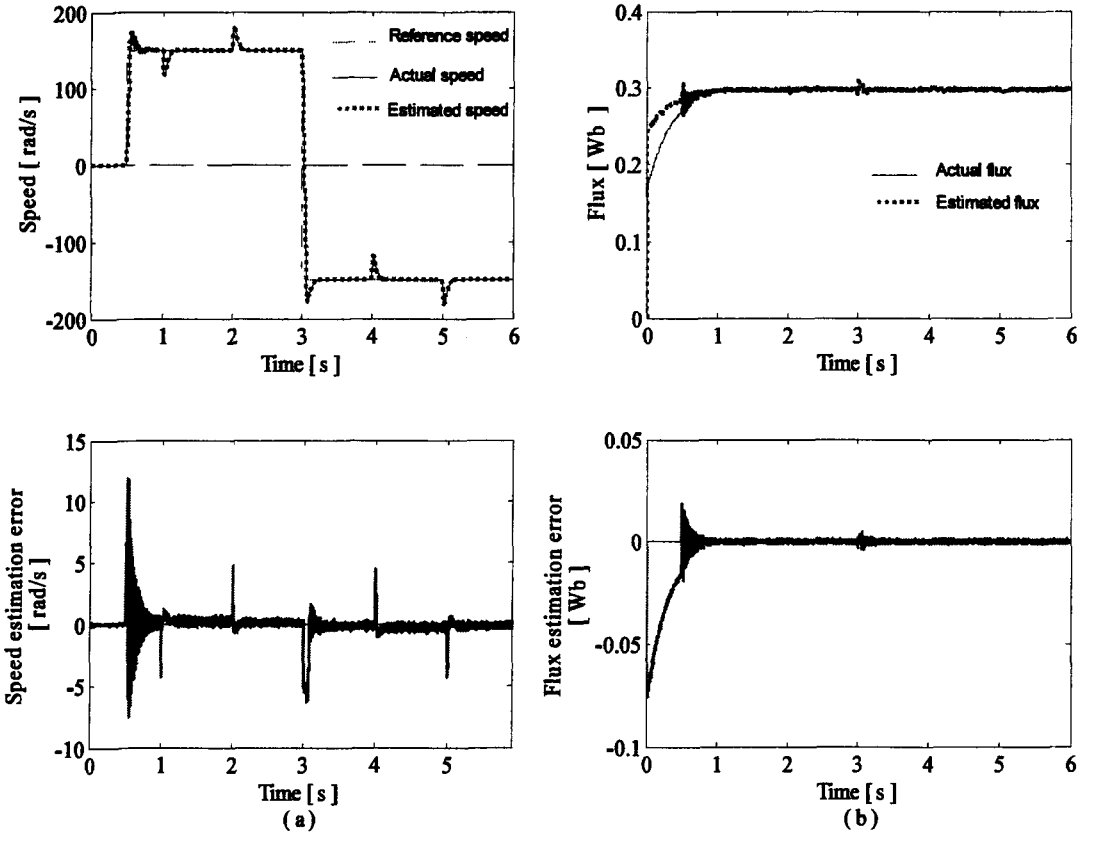


**Figure 6.16** Drive response on application and removal of load; (a) reference, actual and estimated speed, and speed estimation error; (b) actual and estimated rotor flux, and rotor flux estimation error

### 6.4.4 Speed Sensorless Induction Motor Drive Robust Against Rotor Resistance Variation

The results of real-time digital simulation of the simultaneous speed and rotor resistance estimation algorithm proposed in Chapter 5 are presented in this section. The vector controlled drive scheme incorporating the estimation algorithm shown in Figure 5.1 is distributed over the three processors as shown in Figure 6.4. The slave #1: **ss_controller_estimator** subsystem computes in real-time the speed and rotor resistance estimation algorithm, the speed controller, rotor flux decoupling module, the coordinate transformation and the current controllers; whereas, the slave #2: **ss_inv_motor** computes the induction motor, the PWM signal generator and the voltage source inverter. The master: **sm_data_aquisition,** is dedicated to data acquisition, and **sc_user_interface** is the console used for giving command signals and for signal visualisation.

We start with the induction motor drive with load torque $T_L=K_v\omega$. First, acceleration and reversal of the drive is carried out in order to observe the performance of the estimator during the operation. The machine is accelerated at 0.12 sec to a command speed of 150 rad/s and then it is reversed at 5 sec. The rotor resistance is changed abruptly during steady state operation of the drive. Its value is increased from the nominal value of 5.365 Ω to 7 Ω at 1.5 sec, and then decreased to original value at 4 sec. The resistance is increased again to 7 Ω at 6 sec, and then decreased to its nominal value at 9 sec. Figure 6.17 (a) shows reference ($\omega_m^*$), actual ($\omega_m$), estimated ($\hat{\omega}_m$) speed, and speed estimation error

($\omega_m - \hat{\omega}_m$). The actual rotor resistance ($R_r$), estimated rotor resistance ($\hat{R}_r$) and rotor resistance estimation error ($R_r - \hat{R}_r$) are shown in Figure 6.17 (b).

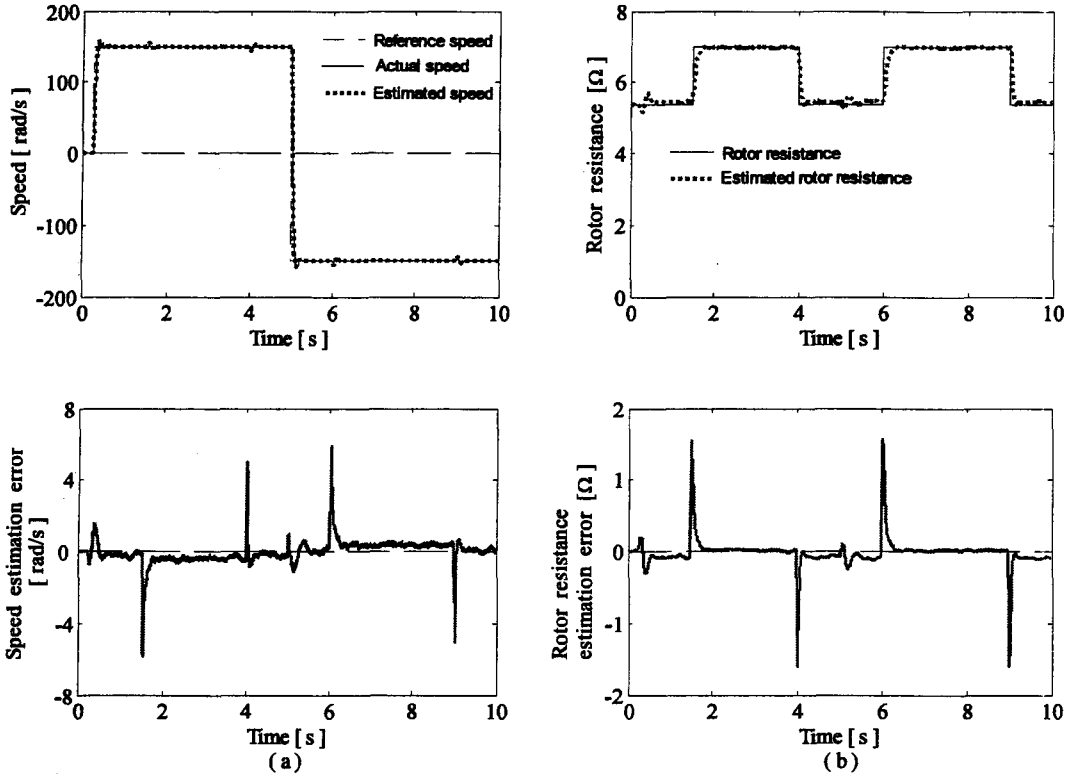


**Figure 6.17** Acceleration and speed reversal (with $T_L=K_r\omega$); (a) reference, actual and estimated speed, and speed estimation error; (b) rotor resistance, estimated rotor resistance and rotor resistance estimation error

Next, the drive is accelerated to 50 rad/s at t=0.12 sec then, the speed is increased in steps to 100 rad/s at 4 sec and finally to 150 rad/s at 8 sec. The rotor resistance is varied with sudden changes in its value in order to observe the performance of the estimator at

these speeds. The rotor resistance is increased from its nominal value of 5.365 Ω to 7 Ω at 2 sec and then brought down to nominal value at 5.5 sec. It is increased again to 7 Ω at 6.5 sec and brought down to nominal value at 9 sec. Figure 6.18 shows the results of estimation and response of the drive system.

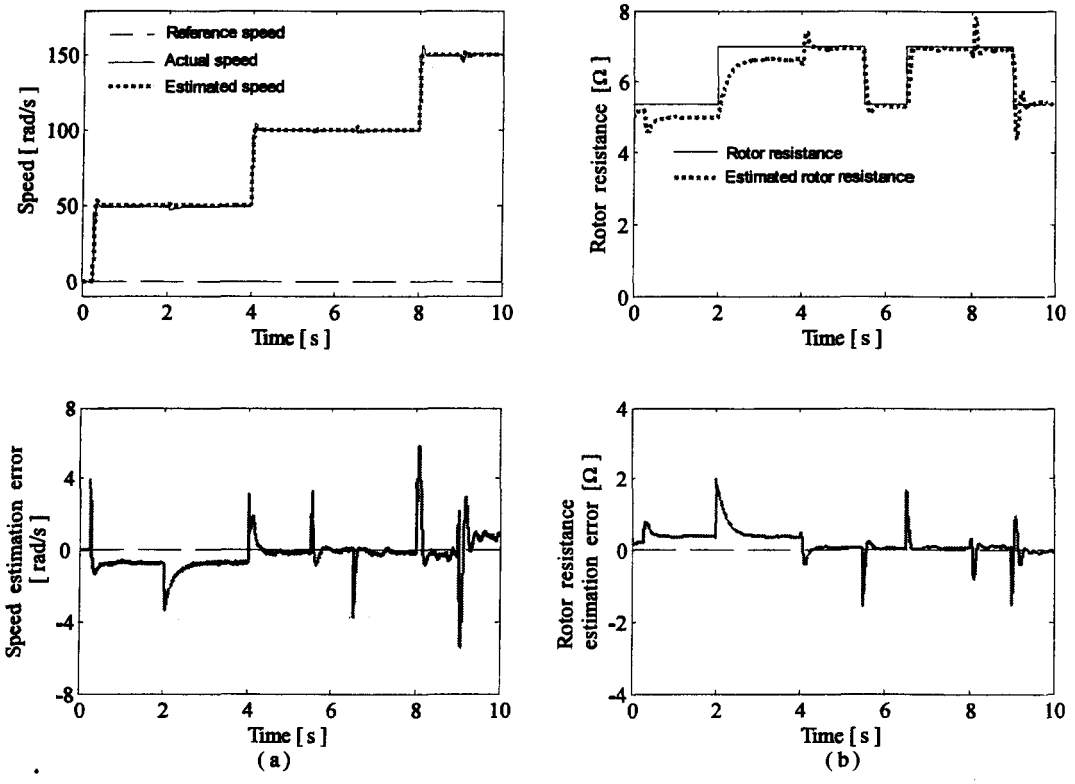


**Figure 6.18** Operation at various speeds (with $T_L=K_v\omega$); (a) reference, actual and estimated speed, and speed estimation error; (b) rotor resistance, estimated rotor resistance and rotor resistance estimation error

Now, we change the motor load to a blower or centrifugal pump type load. The load torque in this case is proportional to square of the speed ($T_L = K_b\omega^2$). Real-time digital

simulation is carried out to verify the performance of the observer and the response of the drive system. First, acceleration and reversal is carried out with sudden rotor resistance changes similar to the speed and rotor resistance presented above (for $T_L=K_v\omega$). The estimation results and drive response are shown in Figure 6.19.

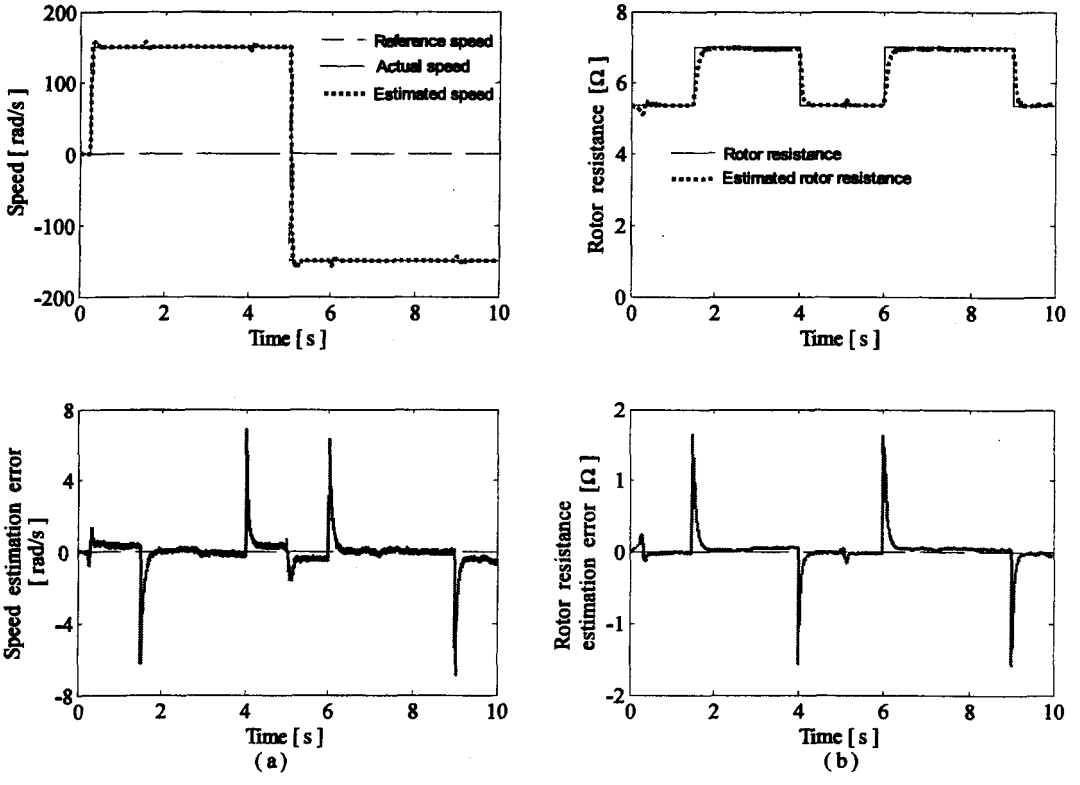


**Figure 6.19** Acceleration and reversal (with $T_L=K_b\omega^2$); (a) reference, actual and estimated speed, and speed estimation error; (b) rotor resistance, estimated rotor resistance and rotor resistance estimation error

Then, the drive is run at various speeds to see the performance of the observer at different speeds. The machine is accelerated to 50 rad/s at t=0.12 sec then, the speed is

increased in steps to 100 rad/s at 5 sec and finally to 150 rad/s at 8 sec. The rotor resistance is varied with sudden changes in its value in order to observe the performance of the estimator at these speeds. The rotor resistance is increased from its nominal value of 5.365 Ω to 7 Ω at 2 sec and then brought down to nominal value at 6 sec. It is increased again to 7 Ω at 7 sec and brought down to nominal value at 9 sec. Figure 6.20 shows the estimation results of estimation and drive response.

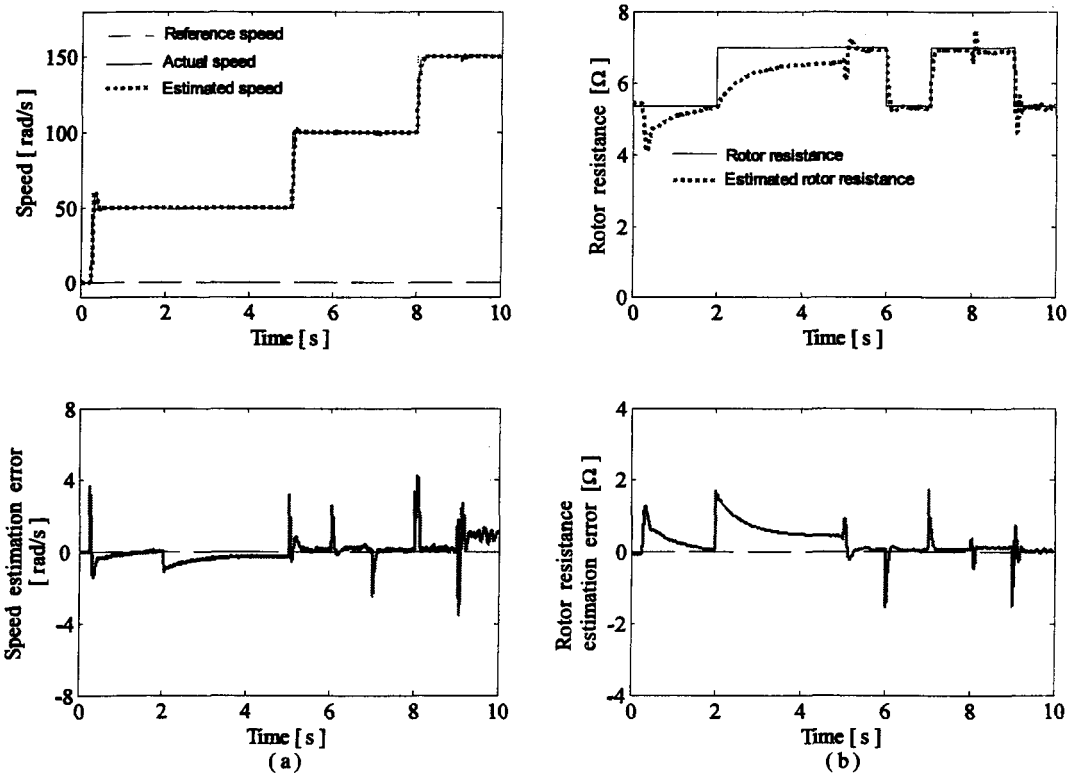


**Figure 6.20** Operation at various speeds (with $T_L=K_b\omega^2$); (a) reference, actual and estimated speed, and speed estimation error; (b) rotor resistance, estimated rotor resistance and rotor resistance estimation error

## 6.5 Conclusion

In this chapter, real-time digital simulation, a powerful tool for rapid prototyping of complex control system has been carried out in order to further validate the estimation algorithms proposed earlier in addition to verifying the response of the drive systems incorporating the estimation algorithms

The drive systems presented in chapter 4 and 5 were taken one by one and real-time digital simulations were carried out. The parts of each drive system were grouped into three modules: (i) subsystem one (controllers and estimators), (ii) subsystem two (static converter and induction motor) and (iii) subsystem three (data acquisition and user interface). Then, these three modules were distributed over three CPUs and real-time digital simulation is carried out where the CPUs work in parallel. Therefore, communication between these modules is only through hardware. Real-time digital simulations were carried out taking realistic sampling time for each part of the drive system so that realistic results were obtained just like that of any drive control system in real-time. Results obtained with Real-time digital simulation agree with what were obtained earlier using Simulink. Good estimation accuracies were obtained and responses of the sensorless drives were found to be satisfactory.

# CHAPTER 7

# CONCLUSIONS AND SUGGESTIONS FOR FUTURE WORK

## 7.1 Conclusions

The development of a high performance sensorless induction motor drive has been addressed in this thesis. Drive control has been done in rotor flux coordinates in order to allow natural decoupling of flux and torque producing components of the stator current space vector. Problem associated with sensored drives has been removed by developing new rotor flux and speed estimation algorithms which uses only the measurable stator terminal quantities: the voltage and current. The state and parameter estimation problem has been looked into as a question of proper mathematical modeling of the machine in an appropriate reference frame, which, along with proper choice of states enables us to develop a new estimation algorithm capable of accurate estimation.

The research objective of developing a high performance sensorless induction motor drive has been achieved by adopting a two directional strategy while developing estimation algorithms. In the first approach, the dynamics of rotor speed was considered much slower than that of electrical states and hence its time derivative was equated to zero in the motor model used for estimation. A new quantity, which is a function of rotor flux and speed, was

defined, introducing which a new motor model was derived. A new rotor speed estimation algorithm in an indirect VC induction motor drive based on observing the newly defined quantity has been proposed. The proposed method is simple and involves no derivative. It has been demonstrated that the method has good estimation accuracy under various operating conditions. The problem of decrease in estimation accuracy at low speed with the proposed observer was overcome using a flux observer, based on voltage model of the machine along with the observer of the newly defined quantity. Finally, a new rotor flux estimation algorithm for speed sensorless rotor flux oriented controlled induction motor drive has been developed. The proposed algorithm is based on a modified Blaschke equation and on observing the newly defined quantity. It was observed that estimation accuracy of the proposed estimator was good under both transient and steady state conditions, and response of the sensorless vector controlled induction motor drive system was found to be satisfactory. As the mathematical model of the motor used for implementing the estimation algorithm was derived with the assumption that the rotor speed dynamics is much slower than that of electrical states, increase in estimation accuracy of the proposed algorithms will be observed with the increase in the size of the machine used.

In the second approach electro-mechanical equation of the drive was used in the motor model used for implementing estimation algorithm in order to take the coupling between the electrical and mechanical modes into consideration which is true especially for small sized machines. A new sensorless vector controlled induction motor drive robust against rotor resistance variation has been developed. Speed and rotor resistance estimation

algorithm was implemented using EKF which is a standard, time-tested algorithm used worldwide for state and parameter estimation of nonlinear systems. Computational burden for implementing the algorithm was reduced in this work by using reduced order EKF. However, with modern day DSPs and FPGAs having fast computation capabilities, implementing EKF is not considered to be a problem any more. Simultaneous estimation of speed and rotor resistance could be achieved under both transient and steady state conditions without injecting any external signal. This achievement is believed to be a major contribution in the area of variable speed induction motor drives. Results showed good estimation accuracies, and the performance of the sensorless vector controlled induction motor drive incorporating the estimation algorithm was found to be satisfactory. The proposed method is applicable to a large category of induction motor drives with a gradually varying load such as, viscous friction load, fan/blower and centrifugal pump. Even though a small sized machine was used in this work the algorithm is valid for induction machine of any size.

## 7.2 Suggestions for Future Work

The newly defined quantity introduced in Chapter 4 contains rotor resistance information as well, in addition to that of rotor flux and speed. Therefore, future research efforts may be made towards developing a rotor resistance estimation algorithm using the new motor model. In the proposed algorithms rotor flux was necessary for speed estimation. Future research efforts may also be made towards developing a speed estimation algorithm for which the knowledge of rotor flux is not necessary.

A method for simultaneous estimation of speed and rotor resistance which does not require external signal injection was proposed in Chapter 5. The proposed method is applicable to a large category of induction motor drives with a gradually varying load torque such as viscous friction, fan/blower and centrifugal pump. Research works may be carried out in future in order to develop algorithms for simultaneous speed and rotor resistance estimation for other load types. Further, in the present work speed and rotor resistance estimation algorithm is implemented using EKF which is a standard, time-tested algorithm used worldwide for state and parameter estimation of nonlinear systems. Future estimation work may be done by using the recently developed Unscented Kalman Filter [80-82] which is a derivative-free alternative to the Extended Kalman Filter.

# REFERENCES


[1] F. Blaschke, "The principle of Field Orientation as applied to the new transvector closed-loop control system for rotating field machines", *Siemens review XXXIX*, (5), 1972, pp. 217-219.

[2] K. Hasse, "On the dynamics of speed control of a static ac drive with a squirrel-cage induction machine", *PhD dissertation, Tech. Hochsch. Darmstadt*, 1969

[3] A. Abbondante, M.B. Brennen, "Variable Speed Induction Motor Drives use Electronic Slip Calculator Based on Motor Voltages and Currents", *IEEE Trans. Ind. Appl.*, Vol. 1A-11, No. 5, Sept/Oct 1975, pp. 483-488.

[4] K. Ohyama, G.M. Asher, "Comparative Experimental Assessment for High Performance Sensorless Induction Motor Drives", *IEEE ISIE conf.* 1999, Bled, Slovenia, pp. 386-391.

[5] J. Holtz, "Methods for Speed Sensorless Control of AC Drives", Sensorless Control of AC Motors, *IEEE Press Books*, 1996.

[6] L. Harnefors, "A Comparision Between Directly Parametrised Observers and Extended Kalman Filters for Sensorless Induction Motor Drives", *IEE PEVD*, Pub. No. 456, 1998, pp. 275-280.

[7] K. Rajashekara, A. Kawamura, K. Matsuse, "Speed Sensorless Control of Induction Motors", Sensorless Control of AC Motors, *IEEE press Books*, 1996.

[8] C. Schauder, "Adaptive Speed Identification for Vector Control of Induction Motors without Rotational Transducers", *IEEE Trans. Ind. Appl.*, Vol. 28, No. 5, Sept/Oct 1992, pp. 1054-1061.

[9] H. Tajima and Y. Hori, "Speed Sensorless Field-Orientation Control of the Induction Machine", *IEEE Trans. Ind. Appl.*, 1993, Vol. 29, No. 1, pp. 175-180.

[10] F.Z. Peng and T. Fukao, "Robust Speed Identification for Speed Sensorless Vector Control of Induction Motors", *IEEE Trans. Ind. Appl.*, Vol. 30, No. 5, pp. 1234-1240, Sept/Oct 1994.

[11] I. Choy, S.H. Kwon, J. Lim and S.W. Hong, "Robust Speed Estimation for Tacholess Induction Motor Drives", *IEEE Electronics Letters*, Vol. 32, No. 19, pp. 1836-1838, 1996.

[12] M.G. Simoes and B.K. Bose, "Neural Network Based Estimation of Feedback Signals for a Vector Controlled Induction Motor Drive", *IEEE Trans. Ind. Appl.*, Vol. 31, pp. 620-629, May/June 1995.

[13] D. Fodor, J.P. Six and D. Diana, "Neural Networks Applied for Induction Motor Speed Sensorless Estimation", *In Proc. ISIE' 95*, pp. 181-186.

[14] I.B. Brahim, and T. Kudor, "Implementation of an Induction Motor Speed Estimator using Neural Networks", *In Proc. IPEC 1995*, pp. 52-57.

[15] S.H. Kim, T.S. Park, J.Y. Yoo and G.T. Park, "Speed-Sensorless Vector Control of an Induction Motor Using Neural Network Speed Estimation", *IEEE Trans. Ind. Elec.*, Vol. 48, No. 3, June 2001.

[16] R.S. Toqeer, and N.S. Bayindir, "Speed estimation of an induction motor using Elman neural network", *Neuro Computing,* Volume 55, Issues 3-4, October 2003, pp. 727-730.

[17] F. Haghgoeian, M. Ouhrouche, and J. S. Thongam (2005), "Neural Network Based Real-Time Speed Estimation in Induction Motor Sensorless Drive", *Proc. of IASTED International Conference on Artificial Intelligence and Applications (AIA),* Innsbruck, Austria, 14-16 Febbruary 2005.

[18] F. Haghgoeian, M. Ouhrouche and J. S. Thongam (2005) "Speed Estimation using Neural Network in Vector Controlled Induction Motor Drive", *Proc. of WSEAS International Conf on Dynamical Systems and Control,* Venice (Venezia), Italy, Nov. 2-4, 2005.

[19] F. Haghgoeian, M. Ouhrouche and J.S. Thongam (2005) "MRAS-Based Speed Estimation for an Induction Motor Sensorless Drive Using Neural Networks", *WSEAS Transactions on Systems,* Issue 12, Vol. 4, December 2005, pp. 2346-2352.

[20] Y.R. Kim, S.K. Sul and M.H. Park, "Speed Sensorless Vector Control of Induction Motor Using Extended Kalman Filter", *IEEE Trans. Ind. Appl.*, Vol. 30, No. 5, Sept/Oct 1994, pp. 1225-1233.

[21] V. Comnac, M. Cernat, M. Cotorogea and I. Draghici, "Sensorless Direct Torque and Stator Flux Control of Induction Machines Using an Extended Kalman Filter", *Proc. IEEE Int. Conf. on Control Appl.*, Mexico, Sept. 5-7, 2001, pp. 674-679.

[22] X. Ma and Y. Gui, "Extended Kalman Filter for Speed Sensor-less DTC Based on DSP", *Proc. 4th World Cong. on Intelligent Control and Automation*, Shanghai, China, June 10-14, 2002, pp. 119-122.

[23] T. Du, P. Vas and F. Stronach, "Design and Application of Extended Observers for Joint State and Parameter Estimation in High Performance AC Drives", *IEE Proc. Elec. Power Appl.*, 1995, Vol. 142, No. 2, pp. 71-78.

[24] J. S. Thongam and V. P. S. Thoudam, "Estimation of Stator Flux and Rotor Speed in SFOC of Induction Motor Drive", *National Power Electronics Conference NEPC2003*, 16-17 Oct. 2003, IIT Bombay, India, pp. 39-46.

[25] J. S. Thongam and V.P.S.Thoudam, "Stator Flux based Speed Estimation of Induction Motor Drive using EKF", *IETE Journal of Research*, India, Vol. 50, No. 3 May-June 2004, pp 191-197.

[26] M. Bodson, J. Chiasson and R.T. Novotnak, "Nonlinear Speed Observer for High Performance Induction Motor Control", *IEEE Trans. Ind. Elec.*, Vol. 42, No. 4, Aug. 1995.

[27] J. J. Liu, I. C. Kung and H. C. Chao, "Speed Estimation of Induction Motor Using a Non-Linear Identification Technique", *Proc. Natl. Sci. Counc. ROC(A)*, Vol. 25, No. 2, 2001, pp. 107-114.

[28] V. Pappano and B. Friedland, "Speed Sensorless Observer for an Induction Machine", *Proc. of the American Control Conf.*, Albuquerque, New Mexico, June 1997, pp.3805-3806.

[29] V. Pappano, S.E. Lyshevski and B. Friedland, "Identification of Induction Motor Parameters", *Proc. of the 37th IEEE Conf. on Decision and Control*, Tampa, Florida USA, Dec. 1998, pp. 989-994.

[30] T. M. Rowan, R. J. Kerkman and D. Leggate, "A Simple On-Line Adaptation for Indirect Field Orientation of Induction Machine", *IEEE IAS Annual Mtg. 1989*, pp. 579-587.

[31] M. Boussak, G. A. Capalino and M. Poloujadoff, "Parameter Indentification in Vector Controlled induction Machine with Flux Model reference Adaptive System (MRAS)", *ICEM'92*, (3), 1992, pp. 838-842.

[32] R. Beguenane, M. Ouhrouche, "MRAC-IFO Induction Motor Control With Simultaneous Velocity and Inverse Rotor Time-Constant", *Proceeding of the IASTED International Conference PES'2003*, Palm Springs, California, 2003, 465-470.

[33] D. J. Atkinson, P. P. Arcanley and J.W. Finch, "Application of Estimation Techniques in Vector Controlled Induction Motor Drive", *IEE Conf. PEVD*, 1990, pp. 358-363.

[34] D. J. Atkinson, P. P. Arcanley and J.W. Finch, "Observers for Induction Motor State and Parameter Estimation", *IEEE Trans. Ind. Appl.*, Vol. 27, No. 6, 1991, pp. 1119-1127.

[35] S. Wade, M.W. Dunnigan and B.W. Williams, "Improving the Accuracy of Rotor Resistance Estimate for Vector Controlled Induction Machines", *IEE-Proc. Elec. Power Appl.*, Sept 1997, Vol. 144, No. 5, pp. 285-294.

[36] M. Kai, "Efficient Tr Estimation in Field Coordinates", *IEEE ISIE*, July 12-16, 1999, Bled, Slovenia.

[37] M. A. Ouhrouche, "EKF-Based Estimation of Speed and Rotor Resistance in Cage Induction Motor Sensorless Drive", *Proceedings of the IASTED International Conference MS'2000,* May 15-17, Pittsburgh, Pennsylvania, USA, pp. 114-118.

[38] M. Ouhrouche, R. Beguenane, A. Trzynadlowski, J. S. Thongam and M. Dube-Dallaire, "PC-Cluster Based Fully Digital Real-Time Simulation of a Field-Oriented Speed Controller for an Induction Motor", *International Journal of Modeling and Simulation,* In Press; accepted on Jan 31, 2005.

[39] B. Karanayil, M.F. Rahman and C. Grantham, "On-line rotor resistance identification for induction motor drive with Artificial Neural Networks supported by a simple PI stator resistance estimator", *Proceedings of the Fifth International Conference on Power Electronics and Drive Systems PEDS 2003,* 17-20 November 2003, Singapore, pp. 433-438.

[40] B. Karanayil, M.F. Rahman and C. Grantham, "Rotor Resistance Identification using Artificial Neural Networks for a Speed Sensorless Vector Controlled Induction Motor Drive", *Proceedings of the 29th Annual Conference of the IEEE Industrial Electronics Society,* IECON 2003, November 2-6, 2003, Roanoke, Virginia, USA, pp. 419-424.

[41] M. Ebrahimi, B. Moshiri, "A neural network approach to rotor time constant updating for Vector-controlled induction motor", *Proceedings of the IASTED International Conference Control and Applications*, July 1999.

[42] M. Ebrahimi, A. Shoulaie, H. Seifi, V. Tahani, "Compensation of rotor time constant variations in induction machines using artificial neural networks", *International Journal of Engineering Science*, Vol. 8, No.2a, pp 81-95, 1995.

[43] H. Kubota and K. Matsuse, "Speed Sensorless Field-Oriented Control of Induction Motor with Rotor Resistance Adaptation", *IEEE Trans. Ind. Appl.*, Vol. 30, No. 5, Sept./Oct., 1994, pp. 1219-1224.

[44] C.E. Moucary, G.G. Soto, and E. Mendes, "Robust Rotor Flux, Rotor Resistance and Speed Estimation of an Induction Machine using the Extended Kalman Filter", *IEEE International Symposium on Industrial Electronics, ISIE'99*, July 12-16, 1999, pp. 742-746.

[45] M. Montanari, S. Peresada, A. Tilli, and A. Tonielli, "Speed Sensorless Control of Induction Motor based on Indirect Field-Orientation", *35th Ann. Meeting, IEEE Ind. Appl. Society*, Rome, 2000, pp. 1858-1865.

[46] M. Ouhrouche, "Estimation of Speed, Rotor Flux and Rotor Resistance in Cage Induction Motor Sensorless Drive Using the EKF Algorithm", *International Journal of Power and Energy Systems*, 2002, Vol. 22, No. 2, pp. 103-109.

[47] K. Akatsu and A. Kawamura, "Online Rotor Resistance Estimation Using the Transient State Under the Speed Sensorless Control of Induction Motor", *IEEE Trans. Power Elec.*, Vol. 15, No. 3, May 2000, pp. 553-560.

[48] R. H. Park, "Two-reaction Theory of Synchronous Machines", *Trans. AIEE*, Vol. 48, pp. 716-730, 1929.

[49] W. Leonhard, "Control of Electrical Drives", *Springer-Verlag*, Berlin, 2001.

[50] B. K. Bose, "Modern Power Electronics and AC Drives", *Prentice-Hall*, 2002.

[51] M. G. Say, "Alternating Current Machines", *Pitman Publishing*, 1976.

[52] K. C. Rajaraman and K. G. Betigeri, Optimum Designs of 1:2 Pole-Changing Motor", *IEE Proc.*, Vol. 129, Part B, No. 3, pp. 151-158, 1982.

[53] T. C. Green, "Scalar Controlled Induction Motor Drives", *PhD Thesis, Heriot-Watt University*, August 1990.

[54] I. Takahashi and T. Noguchi, "A new quick response and high efficiency control strategy of an induction motor", *Record of IEEE-IAS-1985*, Annual Meeting, pp.496-502.

[55] M. Bodson, J. Chiasson and P. Valigi, "Adaptive partial feedback linearization of induction motors", *Proc. 29th Conf. on decision and control*, Honululu, Hawaii, 1990, pp.3313-3318.

[56] S. Sathiakumar, S.K. Biswas and J. Vithayathil, "Microprocessor-based field-oriented control of a CSI-fed induction motor drive", *IEEE Transactions on Industrial Electronics*, vol.IE-33, no.1, pp 39 – 43, Feb. 1986.

[57] R. D. Doncker and D. W. Novotny, "The Universal Field Oriented controller", *IEEE Trans. Ind. Appl.*, vol. 30, no.1, Jan. 1994, pp. 92-100.

[58] D. L. Sobczuk, "Nonlinear Control of PWM Inverter Fed Induction Motor Drives", Record of ISIE' 96, Warsaw, Poland, vol. 2, pp. 958-962.

[59] K. Minami, M. Veley-Reyez, D. Elten, G. C.Verghese, and D. Filbert, "Multi-stage Speed and Parameter Estimation for Induction Machines", *IEEE Power Electronics Specialists Conf.*, Boston MA, 1991, pp. 596-604.

[60] M. Veleyez-Reyes and G. C. Verghese, "Decomposed Algorithms for Speed and Parameter Estimation in Induction Machines", *IFAC Symposium on Nonlinear Control System Design*, Bordeaux, France, 1992, pp. 77-82.

[61] M. Velez-Reyes, K. Minami and G. C. Verghese, "Recursive Speed and Parameter Estimation for Induction Machines", *IEEE/IAS Ann. Meet. Conf. Rec.*, San Diego, 1989, pp. 607-611.

[62] B. Gopinath, "On the Control of Linear Multiple Input-Output Systems", *Bell Sys. Tech. J.*, 50, March 1971.

[63] T. M. Rowan and R. J. Kerkman, "A New Synchronous Current Regulator and an analysis of Current-Regulated PWM Inverters", *IEEE Trans. Ind. Appl.*, Vol. IA-22, No. 4, July/Aug. 1986, pp. 678-690.

[64] T. Ohtani, N. Takada and K. Tanaka, "Vector Control of Induction Motor without Shaft Encoder", *IEEE Trans. Ind. Appl.*, Vol. 28, No. 1, Jan/Feb 1992, pp. 157-164.

[65] B. K. Bose, Power Electronics and Variable Frequency Drives, Piscataway, NJ: *IEEE Press*, 1996.

[66] G. C. Verghese and S. R. Sanders, "Observers for Flux Estimation in Induction Machines", *IEEE Trans. Ind. Elec.*, Vol. 35, No. 1, Feb. 1988, pp. 85-94.

[67] P. L. Jansen and R. D. Lorenz, "A Physically Insightful Approach to the Design and Accuracy Assessment of Flux Observers for Field Oriented Induction Machine Drives", *IEEE Trans. Ind. App.,* Vol. 30, No.1, Jan./Feb. 1994, pp. 101-110.

[68] H. Kubota, K. Matsuse and T. Nakano, "DSP-Based Speed Adaptative Flux Observer of Induction Motor", *IEEE Trans. Ind. Appl.,* Vol. 29, No. 2, March/April 1993, pp. 344-348.

[69] S. Sathiakumar, "Dynamic Flux Observer for Induction Motor Speed Control", *Proc. Australian Universities Power Engineering Conf. AUPEC 2000*, Brisbane, Australia, 24-27 Sept. 2000, pp. 108-113.

[70] Z. Yan, C. Jin and V. I. Utkin, "Sensorless Sliding-Mode Control of Induction Motors", *IEEE Trans. Ind. Elec.*, Vol. 47, No. 6, Dec. 2000, pp. 1286-1297.

[71] R. Otterbach and R. Leinfellner, "Real-Time Simulation", *Translation from "Virtuelles Ausprobieren", Elektronik 8,* 1999, pp. 1-4.

[72] T. P. Backer, "Stack-Baased Scheduling of Real-time Process", *The Journal of Real-Time Systems,* No. 3, 1991, pp. 67-99.

[73] P. Laplante, "Real-Time Systems Design and analysis", *Willey-IEEE Press*, 2004.

[74] W. Stallings, "Operating Systems," *Prentice Hall*, Englewood Cliffs, 1995.

[75] P. Baracos, G. Murere, C.A. Rabbath and W. Jin, "Enabling PC-Based HIL simulation for Automotive Applications", *Proceedings of the IEEE International Electric Machines and Drives Conference* (IEMDC'01), *Cambridge, MA, USA,* 2001.

[76] M. Glesner, A., Kirschbaum, F.M., Renner and B., Voss, State-of-the-Art in Rapid Prototyping for Mechatronic Systems, *Pergamon, Mechatronics (12), 2002, pp. 987-998.*

[77] M. Linjama, T. Virvalo, J. Gustafsson, J. Lintula, V. Aaltonen, M. Kivikoski, Hardware-in-the-Loop Environment for Servo System Controller Design Tuning and Testing, *Elsevier, Microprocessors and Microsystems (24), 2000, pp. 13-21.*

[78] J. Chiasson and L. Tolbert, "A Library of Simulink Blocks for Real-Time Control of HEV Traction Drives", *Proceedings of the Future Car Congress, june3-5, 2002, Arlington, Virginia, USA.*

[79] Opal RT Technologies, RT Lab 8 User's Manual.

[80] S. J. Julier and J. K. Uhlmann, "A New Extension of the Kalman Filter to Nonlinear Systems", Proc. of AeroSense: The 11th Int. Symp. On Aerospace/Defence Sensing, Simulation and Controls, Orlando, FL, USA, 1997.

[81] E. A. Wan and R. Van Der Merwe, "The Unscented Kalman Filter for Nonlinear Estimation", Proc. of IEEE Symp. 2000 (AS-SPCC), Lake Luise, Alberta, Canada, Oct. 2000.

[82] R. Van Der Merwe and E. A. Wan, "The Square Root Unscented Kalman Filter for State and Parameter Estimation", Proc. of IEEE Int. Conf. on Acoustics, Speech, and Signal Processing, (ICASSP '01), 7-11 May, 2001, vol. 6, pp. 3461 – 3464.

# APPENDICES

## APPENDIX A: INDUCTION MACHINE DETAILS

| | | |
|---|---|---|
| Rated Power | Pr | 500 $W$ |
| Rated Line-Line Voltage | Vr | 220 $V$ |
| Rated Torque | T | 3.33 $N.m$ |
| Number of Poles | P | 4 |
| Stator Resistance | Rs | 4.495 $\Omega$ |
| Stator Inductance | Ls | 0.165 $H$ |
| Magnetising Inductance | Lm | 0.149 $H$ |
| Rotor Resistance | Rr | 5.365 $\Omega$ |
| Rotor Inductance | Lr | 0.162 $H$ |
| Rotor Moment of Inertia | J | 0.00095 $Kg.m^2$ |
| Damping Coefficient | F | 0.0004 $N.m.s$ |

# APPENDIX B: RELEVANT WORKS PUBLISHED BY AUTHOR

## APPENDIX B.1: Journal Papers

[1] **J. S. Thongam**, M. Ouhrouche, F. Haghgoeian and H. Ezzaidi, "Simultaneous Estimation of Speed and Rotor Resistance in Sensorless Induction Motor Vector Controlled Drive", International Journal of Modeling and Simulation, In Press; accepted on November 23, 2005.

**Abstract:** In this paper a new sensorless indirect vector controlled induction motor drive robust against rotor resistance variation is presented. The speed and rotor resistance are estimated simultaneously, which is reported in many papers as impossible. The estimation is achieved using a reduced order Kalman filter to reduce the computational burden. This algorithm uses a reduced order model of the motor. The model takes into account the coupling between the electrical and mechanical modes, which is true for small size machines. The method proposed in this paper is applicable to a large category of induction motor drives with a gradually varying load torque such as viscous friction, fan/blower and centrifugal pump. A fully real-time digital simulation, a new powerful tool for rapid control prototyping, is carried out to verify the effectiveness of the proposed method. Results show that accurate estimation is achieved under both transient and steady state conditions without injecting any external signal. This

achievement is, to the best of authors' knowledge, reported for the first time and is believed to be of great importance for induction machine sensorless control.

[2] **J. S. Thongam** and M. Ouhrouche, "A Novel Speed Estimation Algorithm in Indirect Vector Controlled Induction Motor Drive," International Journal of Power and Energy Systems, In Press; accepted on September 21, 2005.

**Abstract:** A rotor speed estimation algorithm in an indirect vector controlled (VC) induction motor drive is proposed. The proposed method is based on observing a newly defined quantity which is a function of rotor flux and speed. A reduced order observer is used to estimate the new quantity from which the rotor speed is computed. The method is simple to implement and does not require taking derivative of the measured signals. Simulation is carried out to verify the accuracy of the estimation algorithm.

[3] **J. S. Thongam** and M. Ouhrouche, "Flux Estimation for Speed Sensorless Rotor Flux Oriented Controlled Induction Motor Drive", WSEAS Transactions on Systems , Issue 1, Vol. 5, January 2006, pp. 63-69.

**Abstract:** A new flux estimation algorithm for speed sensorless rotor flux oriented controlled induction motor drive is proposed. In the proposed method, a new state is defined which when

introduced makes the right hand side of the conventional motor model independant of the unknown terms containing rotor flux and speed. A new motor model is derived after introducing the newly defined state assuming zero time derivative of rotor speed which allows speed estimation without requiring the knowledge of mechanical parameters of the drive system. The estimation algorithm is based on observing this newly defined state which is used for estimating both the rotor flux and the speed. Rotor flux estimation is achieved using a modified Blaschke equation obtained after introduction of the new state into the Blaschke equation or commonly known as the current model; while, speed is computed using a simple equation obtained using this new state.

[4] **J. S. Thongam** and M. Ouhrouche, "A New Speed Estimation Algorithm in Rotor Flux Oriented Controlled Induction Motor Drive", WSEAS Transactions on Systems, Issue 5, Vol. 4, May 2005, pp. 585-592.

**Abstract:** A speed estimation algorithm capable of accurate estimation is desirable for a high performance sensorless induction motor drive. In this paper, we propose a new speed estimation algorithm for speed sensorless rotor field oriented control of induction motor drive capable of accurate estimation under both transient and steady state conditions. The proposed method is based on observing a newly defined quantity which is function of rotor flux and speed. The mathematical model of the motor obtained after introducing the new quantity assumes rotor speed to be a constant parameter of the machine, and this allows speed estimation without

requiring the knowledge of mechanical parameters of the drive. A simple equation is obtained from the new quantity for speed estimation which does not involve integration or differentiation. The proposed algorithm is validated using a fully digital real-time simulation: a new powerful tool for rapid prototyping of complex control systems.

**APPENDIX B.2 Conference Proceedings**


[1] **J. S. Thongam** and M. Ouhrouche, "Speed Sensorless Rotor Flux Estimation in Vector Controlled Induction Motor Drive", *Proc. of WSEAS International Conf. on Dynamical Systems and Control,* Venice (Venezia), Italy, Nov. 2-4, 2005.

[2] **J. S.Thongam** and M.Ouhrouche, "Speed Sensorless Rotor Field Oriented Control of Induction Motor Drive", *Proc. of 9th International Conf. of WSEAS on Systems,* Vouliagmeni, Athens, Greece, 11-13 July, 2005.

[3] **J. S. Thongam**, M. Ouhrouche and R. Beguenane, "Sensorless Indirect Vector Control of Induction Motor Drive Robust Against Rotor Resistance Variation," *Proceedings of 7th IASTED International Conf. on Power and Energy Systems,* November 28 – December 1, 2004, Clearwater Beach, Florida, USA.